NASA Contractor Report 172384

Application of Stiffened Cylinder Analysis to ATP Interior Noise Studies

E.G. Wilby and J.F. Wilby

Bolt Beranek and Newman Inc.
Canoga Park, CA 91303

NASA
National Aeronautics and
Space Administration

Langley Research Center
Hampton, Virginia 23665

Application of Stiffened Cylinder Analysis to ATP Interior Noise Studies

E.G. Wilby and J.F. Wilby

Bolt Beranek and Newman Inc.
Canoga Park, CA 91303

TABLE OF CONTENTS

TABLE OF CONTENTS
(Continued)

TABLE OF CONTENTS
(Continued)

LIST OF FIGURES

LIST OF FIGURES
(Continued)

LIST OF TABLES

1.0 INTRODUCTION

The transmission of propeller noise into an airplane fuselage has a direct influence on the design of General Aviation and Advanced Turboprop (ATP) aircraft. For this reason NASA has undertaken several analytical or experimental studies which consider different aspects of the overall problem. In one analytical study [1-4] a method was developed to predict sound levels in a stiffened cylindrical fuselage when the exterior of the fuselage was exposed to a propeller noise field. The analytical model was compared with experimental results obtained from a small test cylinder. Under a separate investigation [5], noise transmission measurements were made in the laboratory using the fuselage of a Fairchild Metro II airplane. This experimental investigation provided validation data for ATP noise control studies.

The present study has two objectives. The first is to adapt the stiffened cylinder analytical model [1-4] to the test conditions associated with the Metro II experiment [5] and to compare predicted and measured results for the noise reduction provided by the fuselage structure and treatment. The second objective is to extend the analytical model to include turbulent boundary layer excitation so that comparative noise reduction predictions can be performed for different types of excitation.

The first part of this report (Section 2) describes the analytical model [1] and the changes made to it in order to accomplish the objectives of the study. Section 3 presents an outline of the Metro II test with emphasis being placed on the information relevant to the current study. Analytical representations of the Metro II test structure and the test excitation field are given in Sections 4 and 5. Then the predicted and measured noise reductions for the test fuselage are compared in Section 6. The effect of type of excitation on the noise reduction is discussed in Section 7 and final conclusions are presented in Section 8.

2.0 ANALYTICAL MODEL

2.1 Outline

An analytical model for aircraft interior noise prediction was developed under a program sponsored by NASA Langley Research Center, (NASA Contract NAS1-15782), and is described in [1-4]. The model calculates space-average sound pressure levels inside a cylindrical fuselage with a floor and sidewall treatment, when the exterior pressure field is generated by a propeller. In addition the model derives the noise reduction for an exterior reverberant (diffuse) acoustic field.

For this report, the analytical model has been extended to calculate the noise reduction associated with turbulent boundary layer excitation. In addition, the sidewall treatment has been modified so that it may consist of 1 to 4 trim elements. Modifications have also been made to the noise transmitted from the cabin floor to the interior, to allow variation of the floor treatment transmission loss.

2.2 Tone Transmission

The band-limited, space-average mean-square pressure in the interior of the fuselage, for harmonic H at frequency ω_H, is given by Equations (3), (8) and (10) in [1]. If τ_{ML}^H is written in terms of its component parts, $\tau_{ML}^H = \left(\dfrac{2\rho_I c_{oI}}{\omega_H m}\right)^2$, then

$$\langle p_i^2 \rangle_{s,t}^H = \frac{\rho_I^2 c_{oI}^4}{V^2} \cdot \omega_H^4 \cdot \sum_n \frac{\varepsilon_n}{\omega_n^4} \cdot \sum_r \frac{A^2 \bar{F'}^2(n,r)}{M^2 \omega_r^4} \cdot \Psi_G(r,H)$$

$$\times \frac{1}{\left[\left(1 - \dfrac{\omega_H^2}{\omega_n^2}\right)^2 + \eta_n^2\right]\left[\left(1 - \dfrac{\omega_H^2}{\omega_r^2}\right)^2 + (\eta_r' + \eta_r'')^2\right]} \cdot \quad (1)$$

where A = interior (cylinder + floor) surface area associated with interior coupling factor $\bar{F}'(n,r)$

$$= L \left[L_p + 2a(\pi - \theta_o) \right] \quad , \tag{2}$$

and ρ_I and c_{oI} are the interior density and speed of sound, respectively. Other symbols are defined in Appendix A.

The interior coupling factor, $\bar{F}'(n,r)$, between a fuselage structural mode and a cabin acoustic mode is defined in Equation (52) Ref.[1] for a bare cabin floor. The $\bar{F}'(n,r)$ includes a sidewall trim transmission coefficient τ_t, and, in a similar way, a transmission coefficient, τ_F, could be included for the treatment on the floor.* If the floor treatment transmission loss is known and is defined as

Floor treatment transmission loss = $-10 \log (\tau_F)$ dB

Equation (52) Ref.[1] becomes

$$\bar{F}'(n,r) = \bar{F}'(qi,r) = \frac{1}{L} \int_o^L \cos \frac{q z}{L} \sin \frac{M z}{L} dz \tag{3}$$

$$\times \frac{1}{L_p + 2a(\pi - \theta_o)} \left[\sqrt{\tau_t^H} \int_{\theta_o}^{2\pi - \theta_o} a\psi_s^r(\theta)\phi_i(\theta)d\theta - \sqrt{\tau_F^H} \int_{-L_p/2}^{L_p/2} \psi_p^r(x)\phi_i(x)dx \right] .$$

The sidewall trim is assumed to cover all the curved surface of the fuselage above the floor, and the trim transmission coefficient τ_t is defined in Appendix A [1].

The analytical model divides the frequency range into "low" and "high" regimes. At low frequencies acoustic coupling between structural and cavity modes is calculated on a mode-by-mode basis. As frequency increases the number of acoustic modes in a given frequency band becomes very large and the coupling between structural and acoustic modes is calculated on a band-average basis (as is done in the statistical energy analysis method).

---

* τ_F can be used to represent vibration isolation mounts supporting the floor.

An estimate of the change-over frequency from low freqency to high frequency regimes is based on the volume of the cavity. The change-over frequency is the center frequency of the one-third octave band in which the following empirical values lies

$$f_V = \frac{4.1\ c_{oI}}{\sqrt[3]{V}}\ Hz$$

where c_{oI} is the speed of sound (m/s) in the cavity of volume $V(m^3)$.

For high frequencies, the expected value of the space average mean-square interior pressure for harmonic H is given by equation (16) in [1]. Without using the approximation for g_r developed in Section 3.2 of [1], this becomes

$$E\left[<p_i^2>_{s,t}^H\right] = \frac{\rho_I^2 c_{oI}}{2\pi V} \cdot \frac{\omega_H^3}{\bar{n}_n} \sum_{r\epsilon\Delta\omega} \frac{\Psi_G(r,H)}{M_r^2\omega_r^4\left[\left(1-\frac{\omega_H^2}{\omega_r^2}\right)^2 + \eta_r'^2\right]} \cdot \left[A^2 j_r^2(\omega_H)\right]_{interior}^{rev} \quad (4)$$

The bandwidth $\Delta\omega$, containing ω_H, should be wide enough to ensure smoothness and may be selected to include a sufficiently large number of modes for computational accuracy. The notation $r\epsilon\Delta\omega$ implies that ω_r also lies within the band $\Delta\omega$.

It is now assumed that the modal displacement of the surface which forms the inner boundary of the sidewall trim or floor covering can be given approximately by the function $\sqrt{\tau(\bar{x})}\psi^r(\bar{x})$ where $\tau(\bar{x})$ is a general transmission coefficient

Then the interior joint acceptance (i.e., the joint acceptance coupling the fuselage structure to the interior sound field) can be defined for the interior cavity above the floor as

$$j_r^2(\omega) = \frac{1}{A^2} \iint_{\substack{\text{interior} \\ \text{cavity}}} \sqrt{\tau(\bar{x})\tau(\bar{x}')}\, C(\bar{x}|\bar{x}';\omega)\psi^r(\bar{x})\psi^r d\bar{x}d\bar{x}'$$

$$\simeq \frac{1}{A^2}\left\{ \iint_{\substack{\text{fuselage above} \\ \text{floor}}} \tau_t C(\bar{x}|\bar{x}';\omega)\psi^r(\bar{x})\psi^r(\bar{x}')d\bar{x}d\bar{x}' \right.$$

$$\left. + \iint_{\text{floor}} \tau_F\, C(\bar{x}|\bar{x}';\omega)\psi^r(\bar{x})\psi^r(\bar{x}')d\bar{x}d\bar{x}' \right\}$$

This approximation assumes that the cross terms between the floor and the fuselage above the floor can be neglected. For a reverberant field, the correlation function is of the form

$$C(\bar{x}|\bar{x}';\omega) = \frac{\sin k(\bar{x}-\bar{x}')}{k(\bar{x}-\bar{x}')} \tag{5}$$

The neglect of the cross terms is therefore reasonable at high frequencies, but is only approximate in the mid-frequency range.

Calculation of the joint acceptance of the fuselage above the floor is considerably more complex than that for the whole fuselage, because the integration from floor-to-floor does not cover full modal wavelengths. However some simplifying approximations are possible. In Sections 5.4 and 5.5 of Ref.[6], it was shown that for reverberant field excitation, at high frequencies, $A\langle j_r^2(\omega)^{rev}\rangle$ is essentially independent of area. Thus

$$\left[\bar{A}j_r^{2}{}^{rev}(\omega)\right]_{\substack{\text{whole} \\ \text{cylinder}}} \simeq \left[A_t j_r^{2}{}^{rev}(\omega)\right]_{\substack{\text{cylinder} \\ \text{above floor}}} \tag{6}$$

where $\bar{A}$ = fuselage surface area

$$= L.2\pi a \qquad (7)$$

A_t = fuselage surface area above floor

= Transmitting area of fuselage with trim

$$= L.2a(\pi-\theta_o) \qquad (8)$$

This gives

$$\left[A^2 j_r^2(\omega_H)\right]^{rev}_{interior} = \tau_t A_t \bar{A} \left[j_r^2(\omega_H)\right]^{rev}_{\substack{fuselage \\ interior}} + \tau_F A_f^2 \left[j_r^2(\omega_H)\right]^{rev}_{floor} \qquad (9)$$

The reverberant field joint acceptance for the fuselage is defined in Equations 62-73, Ref.[1], and for the floor is defined in Section 2.7 of this report. The value of the speed of sound, c_{oI}, for the interior volume should be used.

2.3 Noise Reduction due to Reverberant Field Excitation

For a reverberant field, the exterior mean square pressure $\langle p_e^2 \rangle_{s,t}$ is related to the mean square blocked pressure $\langle p_{bl}^2 \rangle_{s,t}$ incident on the fuselage by

$$\langle p_e^2 \rangle_{s,t} = \langle p_{bl}^2 \rangle_{s,t}/2$$

The noise reduction of the fuselage for the one-third octave band at center frequency ω is given by Equation 18 in Ref.[1]. Expanding the expression for τ_{ML} gives

$$\frac{<p_i^2>_{s,t}}{<p_e^2>_{s,t}} = \frac{2\rho_I^2 c_{oI}^4 \bar{A}^2}{c_\omega V^2} \cdot \sum_n \epsilon_n \sum_r \frac{\left[j_r^{2 \, rev}(\omega)\right]_{ext} A^2 \bar{f}'^2(n,r)}{M_r^2 D_{nr}}$$

$$\times \left\{ \left(\frac{c_r - c_n}{4}\right) \ln_n + \left(\frac{2c_n(b_r - b_n) - b_n(c_r - c_n)}{4\eta_n \omega_n^2}\right) \arctan_n \right.$$

$$\left. + \left(\frac{c_n - c_r}{4}\right) \ln_r + \left(\frac{2c_r(b_n - b_r) - b_r(c_n - c_r)}{4(\eta_r' + \eta_r'')\omega_r^2}\right) \arctan_r \right\} , \tag{10}$$

where $\bar{A}$ is the fuselage surface area and A is the interior
(cylinder + floor) coupling area.

For n or r = j,

$$\ln_j = \ln \left\{ \frac{\left|(1+c_\omega/2)^4 \omega^4 + b_j(1+c_\omega/2)^2 \omega^2 + c_j\right|}{\left|(1-c_\omega/2)^4 \omega^4 + b_j(1-c_\omega/2)^2 \omega^2 + c_j\right|} \right\} ,$$

$$\arctan_j = \tan^{-1}\left[\frac{(2+c_\omega)^2 \omega^2 - 4\omega_j^2}{4\eta_j \omega_j^2}\right] - \tan^{-1}\left[\frac{(2-c_\omega)^2 \omega^2 - 4\omega_j^2}{4\eta_j \omega_j^2}\right]$$

where when $j = r$, η_j above $= \eta_r' + \eta_r''$, and when $j = n$, $\eta_j = \eta_n$.

Also,

$$D_{nr} = (c_r - c_n)^2 + (b_n - b_r)(b_n c_r - b_r c_n) ,$$

$$b_n = -2\omega_n^2; \quad b_r = -2\omega_r^2 ,$$

$$c_n = \omega_n^4 (1 + \eta_n^2) ; \quad c_r = \omega_r^4 \left[1 + (\eta_r' + \eta_r'')^2\right]$$

The expression for $\bar{f}'(n,r)$, including the floor transmission loss
is given in Equation (3), and the expression for the exterior
reverberant field joint acceptance $\left[j_r^2(\omega)\right]_{ext}$ is given in
Equations 62-73, Ref.[1] using the speed of sound, c_{oE}, for
the exterior pressure field.

For high frequencies, when the acoustic modal density is high, the model was developed along the lines of [4,7,8]. The power absorbed on the interior wall of the fuselage is given by Equation 22 of Reference [1], assuming that the response is resonant acoustic. Structural modes resonant below the frequency band ($r < \Delta\omega$) and resonant in the frequency band ($r \epsilon \Delta\omega$) are included. The noise reduction at the one-third octave band frequency ω is given by

$$
\frac{\langle p_e^2 \rangle_{s,t}}{\langle p_i^2 \rangle_{s,t}} = \left\{ \frac{\alpha S}{4\rho_I c_{oI}} + \frac{\rho_I\, c_{oE}}{\rho_E\, c_{oI}} \cdot \pi n_r \left\langle \frac{A^2}{M_r} \cdot j_r^{2\,rev}(\omega) \right\rangle_{\substack{int \\ r\epsilon\Delta\omega}} \right.
$$

$$
\left. + \frac{\rho_E}{2\pi c_{oE}} \sum_{r<\Delta\omega} \left(\frac{A^2}{M_r} \cdot j_r^{2\,rev}(\omega) \right)_{int} \cdot \left(\frac{\bar{A}^2}{M_r} \cdot j_r^{2\,rev}(\omega) \right)_{ext} \right\}
$$

$$
\div \left\{ \frac{\rho_I \omega n_r}{2 c_{oI}\, \bar{n}_r} \left\langle \left(\frac{\bar{A}^2}{M_r} \cdot j_r^{2\,rev}(\omega) \right)_{\substack{ext \\ r\epsilon\Delta\omega}} \cdot \left(\frac{A^2}{M_r} \cdot j_r^{2\,rev}(\omega) \right)_{\substack{int \\ r\epsilon\Delta\omega}} \right\rangle \right.
$$

$$
\left. + \frac{\rho_I}{2\pi c_{oI}} \sum_{r<\Delta\omega} \left(\frac{A^2}{M_r} \cdot j_r^{2\,rev}(\omega) \right)_{int} \left(\frac{\bar{A}^2}{M_r} \cdot j_r^{2\,rev}(\omega) \right)_{ext} \right\}
$$

$$\tag{11}$$

where $\left(A^2 j_r^{rev}(\omega) \right)_{int}$ is given by Equation (9) and $\left(j_r^{2\,rev}(\omega) \right)_{ext}$ is given by Equations 62-73 in Reference [1] using the exterior speed of sound c_{oE}. The exterior air density is ρ_E. The band average absorption coefficient α is associated with the absorbing surface area S.

2.4 Noise Reduction due to Boundary Layer or Progressive Wave Excitation Fields

The development of the noise reduction due to an exterior field such as boundary layer or progressive wave excitation is very similar to that for the reverberant field excitation. In this

case, the blocked pressure $\langle p_{bl}^2 \rangle$ is used, rather than the exterior pressure $\langle p_e^2 \rangle$, and the exterior field joint acceptance $\left[j_r^2(\overset{ef}{\omega}) \right]_{ext}$ must be used in place of the reverberant field joint acceptance in Equation (10). This gives

$$
\frac{\langle p_i^2 \rangle_{s,t}}{\langle p_{bl}^2 \rangle_{s,t}} = \frac{\rho_I^2 c_{oI}^4 \bar{A}^2}{c_\omega V^2} \cdot \sum_n \varepsilon_n \sum_r \frac{\left[j_r^2(\overset{ef}{\omega}) \right]_{ext} A^2 \bar{F}'^2(n,r)}{M_r^2 D_{nr}}
$$

$$
x \left\{ \left(\frac{c_r - c_n}{4} \right) \ln_n + \left(\frac{2c_n(b_r - b_n) - b_n(c_r - c_n)}{4\eta_n \omega_n^2} \right) \arctan_n \quad (12) \right.
$$

$$
\left. + \left(\frac{c_n - c_r}{4} \right) \ln_r + \left(\frac{2c_r(b_n - b_r) - b_r(c_n - c_r)}{4(\eta_r' + \eta_r'')\omega_r^2} \right) \arctan_r \right\} \quad ,
$$

where the functions $b, c, D, \ln$ are defined in Equation (10). The exterior field joint acceptance is defined in Section 2.8 for boundary layer and progressive wave excitation.

Again for high frequencies, an expression similar to Equation (10) is developed, and the noise reduction is given by

$$
\frac{\langle p_{bl}^2 \rangle_{s,t}}{\langle p_i^2 \rangle_{s,t}} = \left\{ \frac{\alpha S}{4\rho_I c_{oI}} + \frac{\rho_I}{\rho_E} \frac{c_{oE}}{c_{oI}} \cdot \pi n_r \left\langle \frac{A^2}{M_r} \cdot j_r^2(\omega) \right\rangle_{\substack{int \\ r \varepsilon \Delta\omega}}^{rev} \right.
$$

$$
\left. + \frac{\rho_E}{2\pi c_{oE}} \sum_{r < \Delta\omega} \left(\frac{A^2}{M_r} \cdot j_r^2(\omega) \right)_{int}^{rev} \cdot \left(\frac{\bar{A}^2}{M_r} \cdot j_r^2(\omega) \right)_{ext}^{rev} \right\}
$$

$$
\div \left\{ \frac{\rho_I \omega n_r}{4c_{oI} \bar{n}_r} \left\langle \left(\frac{\bar{A}}{M_r} \cdot j_r^2(\overset{ef}{\omega}) \right)_{\substack{ext \\ r \varepsilon \Delta\omega}} \cdot \left(\frac{A^2}{M_r} \cdot j_r^2(\omega) \right)_{\substack{int \\ r \varepsilon \Delta\omega}}^{rev} \right\rangle \right.
$$

$$
\left. + \frac{\rho_I}{4\pi c_{oI}} \sum_{r < \Delta\omega} \left(\frac{A^2}{M_r} \cdot j_r^2(\omega) \right)_{int}^{rev} \left(\frac{\bar{A}^2}{M_r} \cdot j_r^2(\overset{ef}{\omega}) \right)_{ext} \right\} \quad (13)
$$

where $\left(A^2 j_r^{rev}(\omega)\right)_{int}$ is given by Equation (9), and $\left(j_r^{2\,ef}(\omega)\right)_{ext}$ is given in Section 2.8.

2.5 Four Element Sidewall

2.5.1 Sidewall Transfer Matrix

In Appendix A, Ref.[1], the sidewall transfer matrix is developed for a single trim element consisting of insulation and a limp mass. For present purposes the sidewall may be represented by up to 4 elements, each element being made up of a layer of insulation (or air) lined with a limp, dissipative mass.

The transfer matrix across all the elements is given by

$$\begin{Bmatrix} p_2^i \\ w_2 \end{Bmatrix} = \begin{bmatrix} a_{11} a_{12} \\ a_{21} a_{22} \end{bmatrix}_n \begin{bmatrix} a_{11} a_{12} \\ a_{21} a_{22} \end{bmatrix}_{n-1} \cdots \begin{bmatrix} a_{11} a_{12} \\ a_{21} a_{22} \end{bmatrix}_2 \begin{bmatrix} a_{11} a_{12} \\ a_{21} a_{22} \end{bmatrix}_1 \begin{Bmatrix} p_1^i \\ w_1 \end{Bmatrix}$$

$$= \begin{bmatrix} a_{11} a_{12} \\ a_{21} a_{22} \end{bmatrix} \begin{Bmatrix} p_1^i \\ w_1 \end{Bmatrix} \quad ,$$

where 1 is the element in contact with the skin, n is the finishing element in the cabin, and p and w are the pressure and displacement at the points shown in Figure 1. The coefficients a_{11} etc. are defined in Ref.[1], and are dependent on the acoustical properties of the materials used and the mass and loss factor of the limp mass lining. The complex wave impedance, W, and the propagation constant, γ, of the insulation are required for the coefficients a_{11} etc., where

$$\gamma = \alpha - i2\pi/\lambda_m \tag{15}$$

The amplitude and phase of W, the attenuation α in dB/m and the wavelength λ_m may be calculated using [9, p.258 on].

EXTERIOR

P_1^i

$\bar{x}$ $\rightarrow$ w_1

Insulation

Skin

Air

P_2^i

INTERIOR CABIN

$\rightarrow w_2$
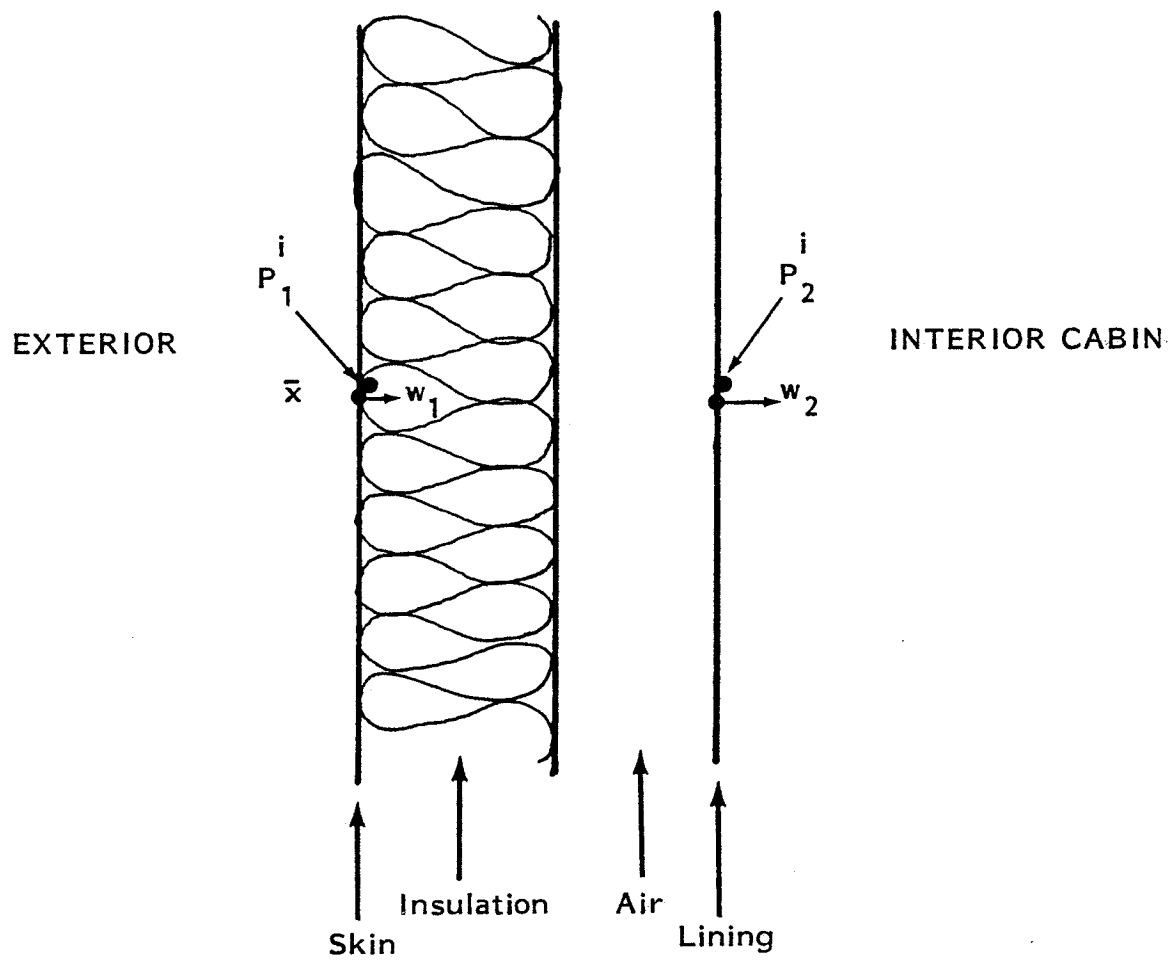
Lining

FIGURE 1.   SIDEWALL TRIM: INSULATION AND LINING

2.5.2 Sidewall Stiffness

The sidewall transfer matrix method developed in [1] assumed that the inner lining was a limp mass, and did not originally include the stiffness of an inner wall. The transfer matrix across a stiff lining may be represented by

$$
\left\{ \begin{array}{c} p_2 \\ w_2 \end{array} \right\} = \left[\begin{array}{cc} 1 & m_t(\omega^2 - \omega_t^2) + i\omega^2 n_t m_t \\ 0 & 1 \end{array} \right] \left\{ \begin{array}{c} p_1 \\ w_1 \end{array} \right\} \tag{16}
$$

where m_t = mass of lining

ω_t = fundamental resonance frequency of lining, and

n_t = loss factor associated with lining.

This approximation assumes that the lining is locally reacting as before.

The inner wall resonance frequencies are calculated for a curved panel extending from floor to floor. Because of the strong curvature, the lowest frequencies would typically have many half-wavelengths in the circumferential direction from floor to floor and one half-wavelength in the axial direction.

The inclusion of the fundamental wall resonance frequency in the transfer matrix reduces the effective mass of the inner wall and hence raises the double-wall resonance frequency slightly. However, the effect on the transmission loss of the sidewall is small. Thus inner wall stiffness is <u>not</u> included in the final analysis.

2.6 Loss Factor for Structure with Trim

The analytical model [1] introduces a total structural loss factor, n_r', when a trim is present on the sidewall. This loss

factor replaces the structural loss factor, η_r, which represents dissipation in the structure when there is no trim. According to the analysis in Ref.[1],

$$\eta_r'^2 = \frac{|C_w|^2}{m^2 \omega_r^4} - \frac{2C_w^I}{m} \frac{\eta_r}{\omega_r^2} + \eta_r^2 \qquad (17)$$

where $C_W = C_W^R + i\, C_W^I$, and m is the average surface mass of the structure.

When predictions were compared with data from scale model tests performed at NASA Langley (see Appendix E of [1]) it was found that the computed values of η_r' were much greater than measured values at low frequencies (Fig.E-17 of [1]). Consequently an upper limit of $\eta_r' = 0.15$ was introduced into the analytical model.

Further analysis by L.D. Pope [private communication] indicated that, since the trim was present only on the sidewalls, and not on the floor, the parameter m in Eq.(17) above should exclude the floor. He replaced m in Eq.(17) by

$$\bar{m} = m\, \frac{M_r}{M_r^\Xi} \qquad (18)$$

where M_r is the generalized mass for mode r of the total structure (shell plus floor) and M_r^Ξ is the corresponding generalized mass for the region of the structure covered by trim. The analytical model has been modified to incorporate Eq.(18).

2.7 Joint Acceptance for Fuselage Floor with Reverberant Excitation

The structural modes of the fuselage with floor are derived in Appendix D, Ref.[1]. The symmetric mode shape of mode r for the floor is assumed to be a finite series of the form

$$\psi^r(z,x) = \sin\frac{M\pi z}{L} \sum_{n=0}^{n^*} C_{Mn}^{pr} \cos\frac{n\pi x}{L_p} \tag{19}$$

and the antisymmetric mode is

$$\psi^r(z,x) = \sin\frac{M\pi z}{L} \sum_{n=1}^{n^*} C_{Mn}^{pr} \sin\frac{n\pi x}{L_p} \tag{20}$$

where z is the axial coordinate measured from the forward end of the fuselage and x is measured horizontally from the floor center in the lateral direction. The width of the floor L_p is given by

$$L_p = 2a \sin\theta_o$$

where θ_o is the floor angle measured from the bottom centerline. The coefficients C_{Mr}^{pr} are the generalized coordinates for mode r obtained using Appendix D, Ref.[1].

The reverberant field joint acceptance for the floor is given by

$$j_r^2(\omega) = \frac{1}{L^2 L_p^2} \iint C(\bar{x}|\bar{x}';\omega)\psi^r(\bar{x})\psi^r(\bar{x})d\bar{x}d\bar{x}' \tag{21}$$

where $C(\bar{x}|\bar{x}';\omega)$ is assumed separable in the axial and transverse directions and is given by

$$C(\bar{x}|\bar{x}';\omega) = \frac{\sin k(z-z')}{k(z-z')} \cdot \frac{\sin k(x-x')}{k(x-x')} \tag{22}$$

where

$$k = \frac{\omega}{c_{oI}}$$

The joint acceptance may be written in the form

$$j_r^{2^{\text{rev}}}(\omega) = j_M^{2^{\text{rev}}}(\omega) \sum_{n_1} \sum_{n_2} C_{Mn_1}^{pr} C_{Mn_2}^{pr} j_{n_1n_2}^{2^{\text{rev}}}(\omega) \qquad (23)$$

The axial component of the joint acceptance is given by [10] as

$$j_M^{2^{\text{rev}}}(\omega) = I_1(M) + I_2(M) + I_3(M) \qquad (24)$$

where

$$I_1(M) = \frac{1}{2\pi MkL} \{Cin(kL + M\pi) - Cin|M\pi - kL|\}$$

$$I_2(M) = \frac{1}{2kL} \{Si(kL + M\pi) - Si(M\pi - kL)\}$$

$$I_3(M) = \frac{1 - (-1)^M coskL}{(M\pi)^2 - (kL)^2}$$

Si and Cin are the sine and cosine integrals [11].

The lateral component of the joint acceptance $j_{n_1n_2}^{2^{\text{rev}}}(\omega)$ for symmetric modes is

$$\qquad (25)$$

$$j_{n_1n_2}^{2^{\text{rev}}}(\omega) = \frac{1}{L_p^2} \iint\limits_{-L_{p/2}}^{L_{p/2}} \frac{\sin k(x_1-x_2)}{k(x_1-x_2)} \cdot \cos\frac{n_1\pi x_1}{L_p} \cdot \cos\frac{n_2\pi x_2}{L_p} \cdot dx_1 dx_2$$

and for antisymmetric modes is

$$j_{n_1n_2}^{2^{\text{rev}}}(\omega) = \frac{1}{L_p^2} \iint\limits_{-L_{p/2}}^{L_{p/2}} \frac{\sin k(x_1-x_2)}{k(x_1-x_2)} \cdot \sin\frac{n_1\pi x_1}{L_p} \cdot \sin\frac{n_2\pi x_2}{L_p} \cdot dx_1 dx_2 \qquad (26)$$

It is necessary to evaluate the cross-terms of the lateral joint acceptance, when $n_1 \neq n_2$, since the individual component mode shapes for the floor are not necessarily orthogonal to one another.

Evaluating the integral in Equation (25) for symmetric modes gives

$$j_{o,o}^2(\omega) = \frac{2}{kL_p} \text{Si}(kL_p) - \frac{2}{k^2L_p^2} \ (1-\cos \ kL_p)$$

$$j_{n,n}^2(\omega) = \frac{1}{2kL_p} \left[\text{Si}(n\pi + kL_p) - \text{Si}(n\pi - kL_p) \right]$$

$$- \frac{\cos n\pi}{2kL_p n\pi} \left[\text{Cin}(n\pi + kL_p) - \text{Cin}(n\pi - kL_p) \right]$$

$$+ \frac{1-\cos n\pi \ \cos kL_p}{n^2\pi^2 - k^2L_p^2}$$

$$j_{n_1 n_2}^2(\omega) = \frac{1}{\pi kL_p(n_1^2-n_2^2)} \cdot \left\{ A\left(\text{Si}(n_1\pi+kL_p)-\text{Si}(n_1\pi-kL_p)\right) \right.$$

$$- B\left(\text{Cin}(n_1\pi+kL_p)-\text{Cin}(n_1\pi-kL_p)\right)$$

$$+ A\left(\text{Si}(n_2\pi+kL_p)-\text{Si}(n_2\pi-kL_p)\right)$$

$$\left. + C\left(\text{Cin}(n_2\pi+kL_p)-\text{Cin}(n_2\pi-kL_p)\right) \right\}$$

(27)

and Equation (26) for antisymmetric modes gives

$$j_{nn}^2(\omega) = \frac{1}{2kL_p} \left[\text{Si}(n\pi+kL_p)-\text{Si}(n\pi-kL_p) \right]$$

$$+ \frac{\cos n\pi}{2kL_p n\pi} \left[\text{Cin}(n\pi+kL_p)-\text{Cin}(n\pi-kL_p) \right]$$

$$+ \frac{1-\cos n\pi \ \cos kL_p}{n^2\pi^2-k^2L_p^2}$$

$$j_{n_1 n_2}^2(\omega) = \frac{1}{\pi k L_p (n_1^2 - n_2^2)} \left\{ -D\Big(Si(n_1\pi + kL_p) - Si(n_1\pi - kL_p)\Big) \right.$$

$$-C\Big(Cin(n_1\pi + kL_p) - Cin(n_1\pi - kL_p)\Big)$$

$$-D\Big(Si(n_2\pi + kL_p) - Si(n_2\pi - kL_p)\Big)$$

$$\left. +B\Big(Cin(n_2\pi + kL_p) - Cin(n_2\pi - kL_p)\Big) \right\}$$

(28)

where

$$A = n_1 \sin\frac{\pi n_1}{2} \cos\frac{\pi n_2}{2} - n_2 \cos\frac{\pi n_1}{2} \sin\frac{\pi n_2}{2}$$

$$B = n_1 \cos\frac{\pi n_1}{2} \cos\frac{\pi n_2}{2} + n_2 \sin\frac{\pi n_1}{2} \sin\frac{\pi n_2}{2}$$

$$C = n_1 \sin\frac{\pi n_1}{2} \sin\frac{\pi n_2}{2} + n_2 \cos\frac{\pi n_1}{2} \cos\frac{\pi n_2}{2}$$

$$D = n_1 \cos\frac{\pi n_1}{2} \sin\frac{\pi n_2}{2} - n_2 \sin\frac{\pi n_1}{2} \cos\frac{\pi n_2}{2}$$

Using Equations (24), (27) and (28) in Equation (23) gives the floor joint acceptance for reverberant field excitation.

2.8 Joint acceptance for fuselage with exterior excitation field

The joint acceptance, describing the coupling between the exterior excitation field and the fuselage structure is defined by

$$j_r^2(\omega) = \frac{1}{\bar{A}^2} \iint C(\bar{x}|\bar{x}';\omega)\psi^r)\bar{x})\psi^r(\bar{x}')d\bar{x}d\bar{x}'$$

(29)

The correlation function is assumed separable in the axial and circumferential directions and is of the form

$$C(\bar{x}|\bar{x}';\omega) = C_z(z-z',\omega) \, C_y(a(\theta-\theta'),\omega)$$

$$= C_z(z-z',\omega) \, C_y(y-y',\omega)$$

where z is the axial coordinate, θ is the angular coordinate relative to the fuselage bottom centerline and $y = a\theta$ is the distance around the circumference of the fuselage.

For a reverberant (diffuse) excitation field, the correlation functions are

$$C_z(z-z',\omega) = \frac{\sin k(z-z')}{k(z-z')} \quad \text{where } k = \frac{\omega}{c_{oE}} \qquad (30)$$

$$C_y(y-y',\omega) = \frac{\sin k(y-y')}{k(y-y')} \qquad (31)$$

For boundary layer excitation, the correlation functions for the axial and circumferential directions are given by Cockburn and Jolly [12] as

$$C_z(z-z',\omega) = \exp\left[-\left\{\left(0.1\frac{\omega}{U_c}\right)^2 + \left(\frac{0.034}{\delta^*}\right)^2\right\}^{\frac{1}{2}} |z-z'|\right]\cos\frac{\omega}{U_c}(z-z') \quad (32)$$

$$C_y(y-y',\omega) = \exp\left[-\left\{\left(0.72\frac{\omega}{U_c}\right)^2 + \left(\frac{0.244}{\delta^*}\right)^2\right\}^{\frac{1}{2}} |y-y'|\right] \qquad (33)$$

where U_c = axial trace velocity
       δ^* = boundary layer displacement thickness

The preceding analytical formulation can be readily modified to represent progressive wave excitation where the waves propagate in the axial direction. Although this excitation is not applied in the present investigation the analysis is included here for completeness. An analytical representation of this form was used to describe the pressure field over the Aft Cargo Carrier of the Space Shuttle [13], where the source is random and extends over a large volume to the rear of the vehicle.

In the axial direction, the correlation function is

$$C_z(z-z', \omega) = \exp\left[-c_z \frac{\omega}{U_z}|z-z'|\right]\cos\frac{\omega}{U_z}(z-z') \qquad (34)$$

where U_z = axial trace velocity

$\quad c_x$ = axial decay parameter

In the circumferential direction the field is assumed reverberant with a correlation function as in Eq.(31).

The structural modes of the fuselage are derived in Appendix D Ref.[1]. The symmetric mode shape of mode r for the fuselage wall is assumed to be a finite series of the form

$$\psi^r(z, \theta) = \sin\frac{M\pi z}{L}\sum_{n=0}^{n*} C_{Mn}^{sr}(-1)^n \cos n\theta \qquad (35)$$

and the antisymmetric mode is

$$\psi^r(z, \theta) = -\sin\frac{M\pi z}{L}\sum_{n=1}^{n*} C_{Mn}^{sr}(-1)^n \sin n\theta \qquad (36)$$

where M = number of longitudinal half-wavelengths for mode r

$\quad$ n = number of circumferential wavelengths in the fuselage shell

$\quad$ n* = maximum number of circumferential wavelengths used to represent mode r

$\quad C_{Mn}^{sr}$ = fuselage generalized coordinate for mode r associated with n

The joint acceptances for the axial and circumferential directions may be calculated independently for mode r using

$$j_r^2(\omega) = j_M^2(\omega) \cdot \sum_{n=0}^{n*} \left(C_{Mn}^{sr}\right)^2 j_n^2(\omega) \qquad (37)$$

where the axial joint acceptance is given by

$$j_M^2(\omega) = \frac{1}{L^2} \int\int_0^{L \quad L} C_z(z_1-z_2,\omega) \, \sin\frac{M\pi z_1}{L} \cdot \sin\frac{M\pi z_2}{L} \cdot dz_1 dz_2 \qquad (38)$$

and the circumferential joint acceptance terms are

$$j_n^2(\omega) = \frac{1}{(2\pi a)^2} \int_0^{2\pi a} \int_0^{2\pi a} C_y(y_1-y_2,\omega) \left\{ \begin{array}{cc} \cos\frac{ny_1}{a} & \cos\frac{ny_2}{a} \\ \sin\frac{ny_1}{a} & \sin\frac{ny_2}{a} \end{array} \right\} dy_1 dy_2 \qquad (39)$$

Terms in $\cos\frac{ny}{a}$ and $\sin\frac{ny}{a}$ refer to the symmetric and antisymmetric modes of the fuselage respectively. Unlike the floor joint acceptance in Section 2.7, cross terms, $j_{n_1 n_2}^2(\omega)$, are equal and opposite in sign to $j_{n_2 n_1}^2(\omega)$, since $C_y(y_1-y_2,\omega)$ is an even function, and hence do not appear in Eq.(37).

2.8.1 Axial joint acceptance for reverberant field excitation

The axial joint acceptance is given by [10] as

$$j_M^{2\,rev}(\omega) = I_1(M) + I_2(M) + I_3(M) \quad ,$$

where

$$I_1(M) = \frac{1}{2\pi MkL} \{Cin(kL + M\pi) - Cin|M\pi - kL|\}$$

$$I_2(M) = \frac{1}{2kL} \{Si(kL + M\pi) - Si(M\pi - kL)\} \qquad (40)$$

$$I_3(M) = \frac{1-(-1)^M \cos kL}{(M\pi)^2 - (kL)^2}$$

Si and Cin are the sine and cosine integrals [11] and $k = \omega/c_{oE}$ is the acoustic wavenumber.

2.8.2 Axial joint acceptance for boundary layer or progressive wave excitation

The correlation function from Eqs. (32) and (34) may be written in the general form

$$C_z(z_1 - z_2, \omega) = e^{-A|z_1 - z_2|} \cos\frac{\omega}{U} (z_1 - z_2) \tag{41}$$

where

$\quad$ U = convection or trace velocity

and for boundary layer excitation

$$A = \left\{ \left(\frac{0.1\omega}{U}\right)^2 + \left(\frac{0.034}{\delta^*}\right)^2 \right\}^{\frac{1}{2}}$$

For progressive wave excitation

$$A = c_z\frac{\omega}{U}$$

The axial joint acceptance is given by [14] as

$$j_M^2(\omega) = \frac{2}{(M\pi)^2 \Delta_M^2} \left[p_M \left\{ 1 - (-1)^M e^{-AL} \cos\frac{\omega}{U}L \right\} \right.$$
$$\left. + 4(-1)^M q_M e^{-AL} \sin\frac{\omega L}{U} + \frac{M\pi}{2} r_M \Delta_M \right] \tag{42}$$

where

$$\Delta_M = \left[1 + \left(\frac{\omega L}{UM\pi}\right)^2 + \left(\frac{AL}{M\pi}\right)^2 \right]^2 - 4\left[\frac{\omega L}{UM\pi}\right]^2$$

$$p_M = \left[1 - \left(\frac{\omega L}{UM\pi}\right)^2 + \left(\frac{AL}{M\pi}\right)^2 \right]^2 - 4\left[\frac{\omega L}{UM\pi}\right]^2 \left[\frac{AL}{M\pi}\right]^2$$

$$q_M = \left[\frac{\omega L}{UM\pi} \right] \left[\frac{AL}{M\pi} \right] \left[1 - \left(\frac{\omega L}{UM\pi} \right)^2 + \left(\frac{AL}{M\pi} \right)^2 \right]$$

$$r_M = \left[\frac{AL}{M\pi} \right] \left[1 + \left(\frac{\omega L}{UM\pi} \right)^2 + \left(\frac{AL}{M\pi} \right)^2 \right]$$

2.8.3 Circumferential joint acceptance for reverberant field joint acceptance

The circumferential joint acceptance is given by [10]. For symmetric modes

$$j_0^2(\omega) = \frac{Si(2\pi ka)}{\pi ka} - \frac{(1-\cos 2\pi ka)}{2(\pi ka)^2} \quad \text{for } n = 0$$

$$j_n^2(\omega) = I_2(n) + I_3(n) + I_1(n) \quad \text{for } n \neq 0 \tag{43}$$

And for antisymmetric modes

$$j_n^2(\omega) = I_2(n) + I_3(n) + I_1(n) \tag{44}$$

where

$$I_1(n) = \frac{1}{4\pi n \cdot 2\pi ka} \left\{ Cin \left[2\pi(n+ka) \right] - Cin \left[2\pi(n-ka) \right] \right\}$$

$$I_2(n) = \frac{1}{4\pi ka} \left\{ Si \left[2\pi(n+ka) \right] - Si \left[2\pi(n-ka) \right] \right\}$$

$$I_3(n) = \frac{1-\cos 2\pi ka}{(2\pi n)^2 - (2\pi ka)^2}$$

2.8.4 Circumferential joint acceptance for boundary layer excitation

The correlation function from Eq.(33) may be written as

$$C_y(y_1-y_2,\omega) = e^{-B|y_1-y_2|} \tag{45}$$

where

$$B = \left\{ \left(0.072 \frac{\omega}{U_C} \right)^2 + \left(\frac{0.244}{\delta^*} \right)^2 \right\}^{\frac{1}{2}}$$

Let

$$\delta = 2\pi aB$$

Expanding the techniques used in [10], the circumferential joint acceptances, for symmetric modes, are given by

$$j_0^2(\omega) = \frac{2}{\delta} - \frac{2\delta^2(1-e^{-\delta})}{\delta^2}$$

$$j_n^2(\omega) = \frac{\delta}{(2\pi n)^2 + \delta^2} - \frac{2\delta^2(1-e^{-\delta})}{\left[(2\pi n)^2 + \delta^2\right]^2} \qquad (46)$$

and for antisymmetric modes

$$j_n^2(\omega) = \frac{\delta}{(2\pi n)^2 + \delta^2} + \frac{2(2\pi n)^2(1-e^{-\delta})}{\left[(2\pi n)^2 + \delta^2\right]^2} \qquad (47)$$

3.0 SUMMARY OF METRO II TEST

The noise transmission test conducted by Prydz et al [5] on a
Fairchild Metro II fuselage was performed in an anechoic chamber
using an electropneumatic acoustic source. Aspects of the test
relevant to the present study are given here for ready refer-
ence.

3.1 Test Fuselage Structure

The test structure consisted of a section of a Fairchild
Metro II fuselage with a special floor installed about one foot
above the structural floor level of a Metro II in airline ser-
vice. The special floor could be rigidly attached by brackets
to the frames along the full length of the fuselage structure or
mounted on air mounts which were located on the structural floor
of the fuselage. Cross-sections through the test fuselage are
shown in Figure 2 for the attached and isolated floor configura-
tions.

The fuselage shell is of conventional aluminum skin-stringer-
frame construction. Basic structural properties of the shell
are listed in Table 1. Structural loss factors were measured
by Prydz et al [5] for the baseline (bare) fuselage; empirical
values are given in Table 2. As part of the test program, the
surface density of the structure was increased by the addition
of a sheet of iron-oxide vinyl with a surface density of
4.88 kg/m^2. Measured loss factors for the structure with
added vinyl are given in Table 3.

83.8 cm Rad mold line
78.7 cm Rad inside of frame
77.5 cm Rad trim

13 cm | 32 cm | 32 cm

28 cm Top of floor

36° typ

Isolators

Microphones

WL 100

WL 89
Trim structure
Isolator
Floor structure
Firestone number 16 airmount eight places
Fuselage structure Swearingen Metro II

BL 0

(a) Rigid Attachment;
Fixed Floor Configuration

(b) No Attachment;
Floating Floor Configuration
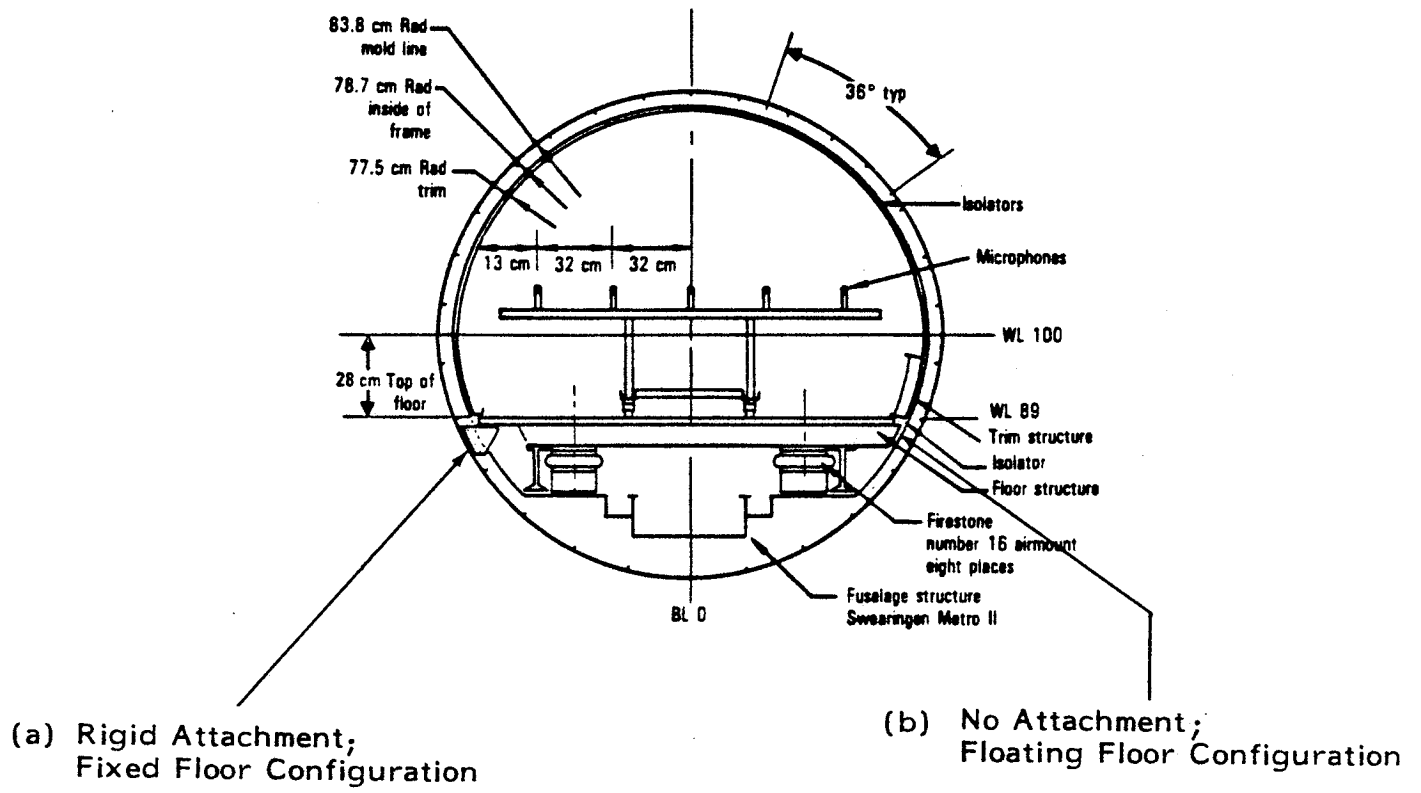
FIGURE 2. CROSS-SECTION THROUGH METRO II FUSELAGE SHOWING
FLOOR INSTALLATION FOR TEST [5]

TABLE 1 – OUTER WALL STRUCTURAL PROPERTIES OF
METRO II TEST FUSELAGE

Item	Units		Values	
	SI	English	SI	English
Cylindrical structure				
Diameter	m	(ft)	1.68	(5.5)
Length	m	(ft)	9.02	(29.6)
Skin thickness	cm	(in.)	0.102	(0.040)
Surface density of skin	kg/m^2	(psf)	2.78	(0.57)
Surface density skin plus stiffeners	kg/m^2	(psf)	4.59	(0.94)
Frames				
Spacing	cm	(in.)	38.1	(15)
Depth	cm	(in.)	5.08	(2)
Cross sectional area	cm^2	(in^2)	0.884	(0.137)
Area centroid (re: skin $\mathcal{C}_L$)	cm	(in.)	2.835	(1.116)
2nd area moment (re: skin $\mathcal{C}_L$)	cm^4	(in^4)	9.303	(0.2235)
Torsion constant	cm^4	(in^4)	0.0030	(0.73×10^{-4})
Stringers				
Spacing	cm	(in.)	18.3	(7.2)
Depth	cm	(in.)	2.223	(0.875)
Cross sectional area	cm^2	(in^2)	0.716	(0.111)
Area centroid (re: skin $\mathcal{C}_L$)	cm	(in.)	0.772	(0.304)
2nd area moment (re: skin $\mathcal{C}_L$)	cm^4	(in^4)	0.11904	(0.00286)
Torsion constant	cm^4	(in^4)	0.00450	(0.108×10^{-3})

TABLE 2 – DAMPING VALUES FOR BASELINE (BARE) FUSELAGE OUTER WALL

Dual Panel Grid		Circumferential Grid	
Frequency (Hz)	Loss Factor (%)	Frequency (Hz)	Loss Factor (%)
129.39	2.18	40.00	8.11
158.69	1.37	83.01	6.79
258.79	1.97	146.48	4.74
285.64	0.58	222.17	2.45
307.62	1.39	266.11	2.27
341.80	1.66	297.85	1.99
356.45	1.31	405.27	3.79
383.30	1.28	424.80	2.91
446.78	2.19	446.78	1.94
493.16	2.25	493.16	2.31
561.52	0.97	556.64	1.74
686.04	0.93	607.91	1.36
778.81	1.72	671.39	0.50
800.78	2.45	708.01	1.32
808.10	0.78	756.84	0.83
849.61	1.08	781.25	0.91
891.11	0.80	908.20	1.32
910.64	1.87	1037.60	1.00
1037.60	1.23	1137.70	0.91
1069.34	1.84		
1110.84	1.63		
1164.55	0.87		

TABLE 3 – DAMPING VALUES FOR FUSELAGE STRUCTURE WITH VINYL SHEET ON EXTERIOR

Single Panel Grid			
Frequency (Hz)	Loss Factor (%)	Frequency (Hz)	Loss Factor (%)
65.92	8.33	825.20	4.80
97.66	11.85	834.96	1.91
275.88	3.79	852.05	1.70
305.18	5.15	866.70	1.52
429.69	3.47	888.67	0.63
456.54	7.20	947.27	4.96
571.29	2.60	957.03	5.41
676.27	2.71	1101.07	0.82
773.93	3.73	1164.55	2.00
810.55	0.62	1191.41	9.29

TABLE 4 – INTERIOR ABSORPTION COEFFICIENTS

Frequency (Hz)	Decay Method		Reference Sound Source Method
	Bare Interior	Added Interior Absorption	Added Absorption
200	0.14	0.22	0.35
250	0.13	0.39	0.32
315	0.14	0.43	0.44
400	0.10	0.32	0.29
500	0.10	0.32	0.51
630	0.14	0.34	0.34
800	0.10	0.33	0.27
1000	0.10	0.31	0.28
1250	0.09	0.34	0.28
1600	0.10	0.38	0.26
2000	0.08	0.39	0.26
AVG	0.11	0.34	0.33

Based on a transmitting area of 28.9 m^2 (311 ft^2), $S_{TR} = 0.6\pi D_t L$.

3.2 Test Floor Structure

The cabin floor used in the Metro II tests consisted of plywood panels (1.9 cm, 0.75 inch thick) on steel I-beams. Cross-sections through parts of the floor are shown in Fig.3. The 7.6 cm (3 x .17 inch, 1.98 lb/ft) deep beams supported the floor panels in the transverse direction on a typical spacing of 1.2m (48 inches). The two 15.2 cm (6 x .23 inch, 4.3 lb/ft) deep beams were placed in the longitudinal direction, near to the edge of the floor panels and the air mounts (see Fig.2(b)).

Rigid connection between the floor and fuselage shell was achieved by bolting the plywood floor panels to brackets on the frames along the fuselage. For the "floating" floor configuration the transverse I-beams rested on air mounts with low resonance frequencies.

3.3 Excitation

Two excitation acoustic fields were used during the Metro II tests [5] -- (a) random, broadband and (b) deterministic, discrete frequency. The latter excitation is of interest here. The sound levels were generated using an electropneumatic source coupled to a horn which was pointed towards the fuselage (Fig.4). The deterministic field had strong spatial characteristics which were intended to simulate those of a propeller noise field. Longitudinal and circumferential spatial distributions of sound pressure level are shown in Fig.5. In the case of the longitudinal distribution, the sound levels are free-field values, whereas for the circumferential direction the sound levels were measured on the test cylinder and include reflection effects.

The test section of the fuselage exposed to high intensity acoustic excitation is 3.66 m (144 in) long, with the noise source at the center of the test section (Sta. 377.3).
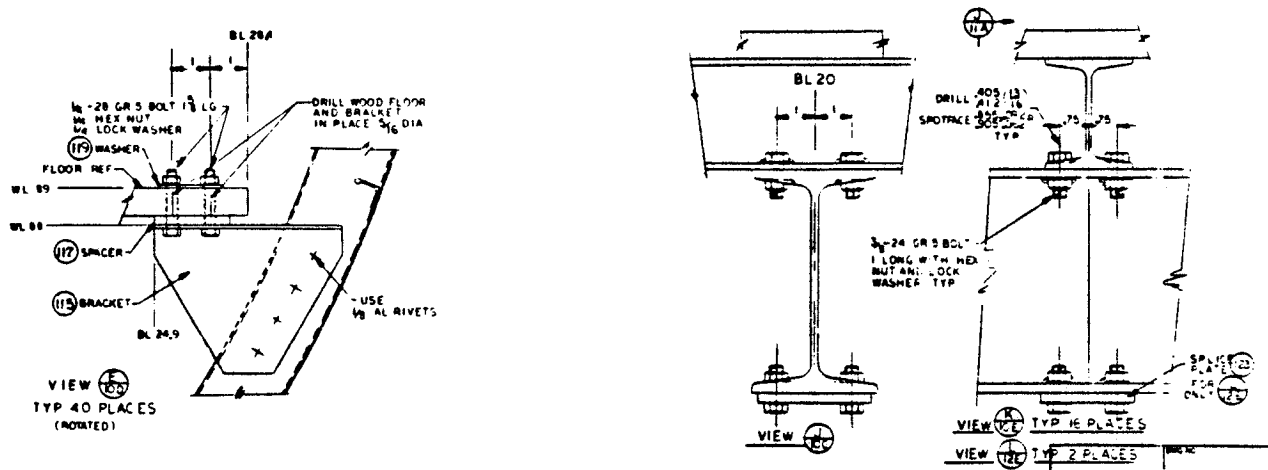
FIGURE 3.   DETAILS OF FLOOR IN METRO II TEST FUSELAGE [5]
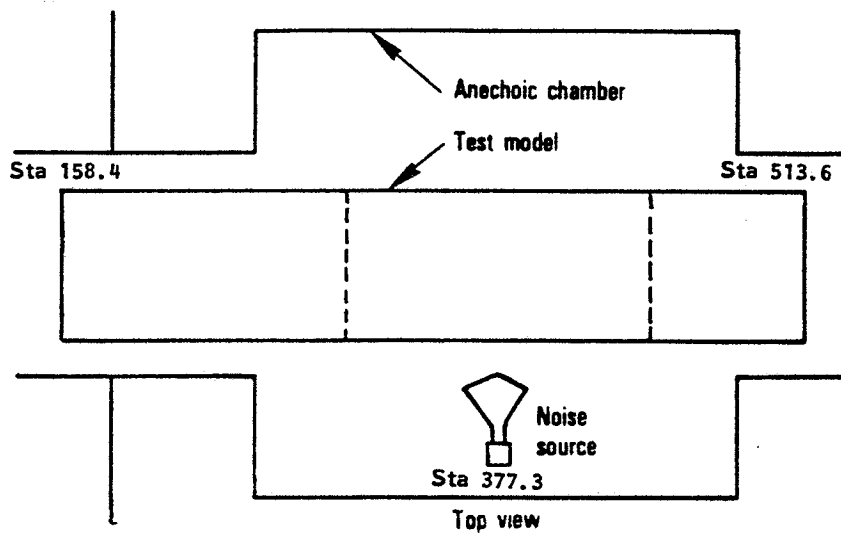
FIGURE 4.   TEST SET-UP FOR ACOUSTIC TESTS ON METRO II [5]

(a) Longitudinal Distribution of Free Field Sound Levels
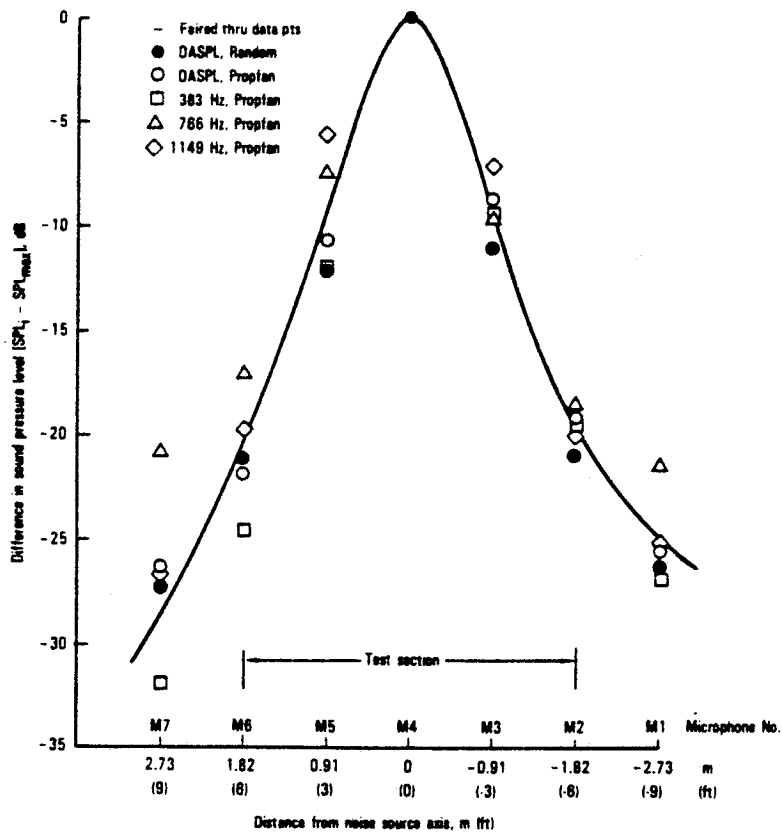
(b) Circumferential Distribution of Sound Levels on Fuselage
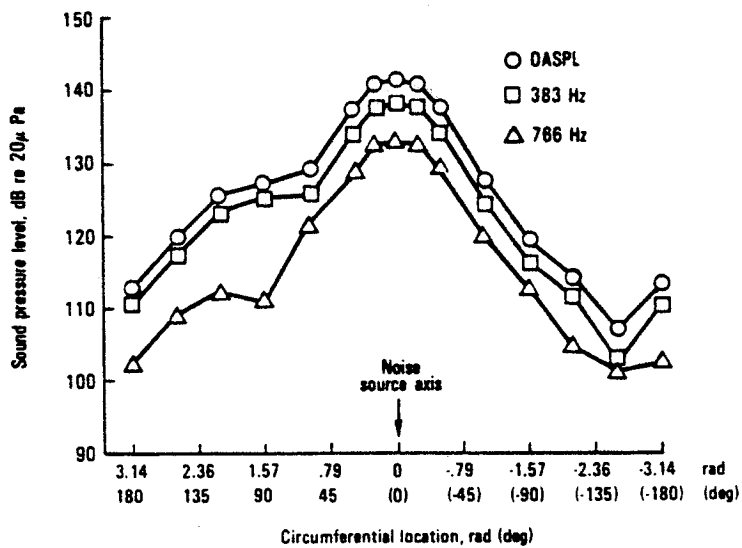
FIGURE 5. SPATIAL DISTRIBUTION OF SOUND LEVELS FOR TESTS ON
METRO II [5]

3.4 Interior Treatment

The interior treatment of the test fuselage consisted of a double-panel sidewall with a fiberglass blanket and airspace in between. Sections through the sidewall are shown in Figure 6. The fiberglass had a fiber diameter of about 2 microns and a flow resistance of approximately 257 mks rayls/cm.

The baseline interior trim panel consisted of an aluminum panel with a thickness of 0.089 cm. Additional material, in the form of one or two sheets of vinyl impregnated with iron oxide, was added to the trim panel for noise reduction parametric studies.

The acoustic absorption within the fuselage was increased by the installation of open-pore Scott foam placed on the floor near the sidewall, along the full length of the cabin. Interior absorption coefficients measured in the test fuselage with and without the foam material installed, are given in Fig. 7 and Table 4. These are normalized to the curved surface transmitting area of 28.9 m^2 (311 ft^2).

3.5 Test Configurations

Nine test configurations were investigated by Prydz et al [5]. These configurations are listed in Table 5. The first six configurations are associated with a floating floor (suspended on air mounts) and a floating trim (supported by the floor). Since the analytical model assumes that there is no structureborne path between the fuselage structure and the trim panel, it forms a reasonably good representation of the floating trim.
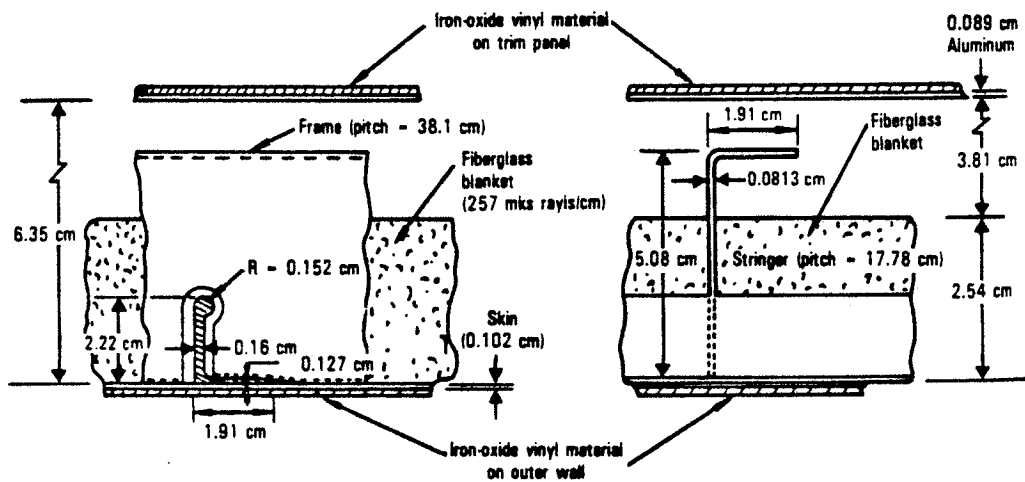
FIGURE 6. SECTIONS THROUGH SIDEWALL TREATMENT FOR TESTS ON METRO II [5]
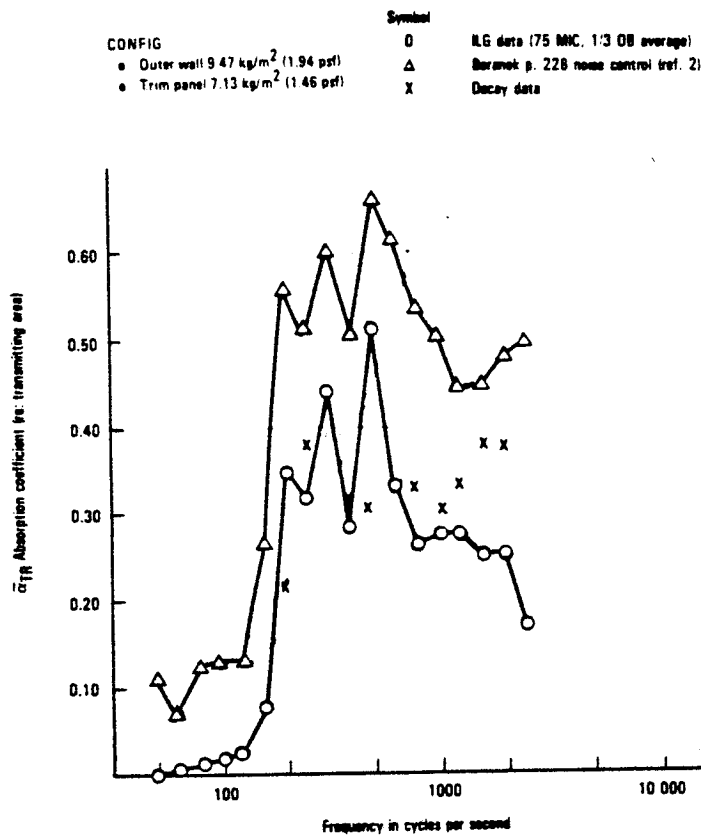
FIGURE 7. ABSORPTION COEFFICIENTS MEASURED IN TREATED METRO II FUSELAGE [5]

TABLE 5.   TEST CONFIGURATIONS

| Configura-tion No. | Surface Density, kg/m²(psf) | | Floor Configuration | Trim Configuration |
	Outer Wall σ1	Inner Wall σ2		
1	4.590* (0.94)	2.25** (0.46)	Floating	Floating
2	4.59 (0.94)	7.13 (1.46)	Floating	Floating
3	4.59 (0.94)	12.01 (2.46)	Floating	Floating
4	9.47 (1.94)	2.25 (0.46)	Floating	Floating
5	9.47 (1.94)	7.13 (1.46)	Floating	Floating
6	9.47 (1.94)	12.01 (2.46)	Floating	Floating
7	9.47 (1.94)	7.13 (1.46)	Attached	Disconn.
8	9.47 (1.94)	7.13 (1.46)	Disconn.	Attached
9	9.47 (1.94)	7.13 (1.46)	Attached	Attached

  * Baseline (bare) outer wall surface density.
 ** Baseline (bare) inner wall surface density.

4.0 ANALYTICAL REPRESENTATION OF METRO II TEST STRUCTURE

4.1 Fuselage Shell

The fuselage shell was modeled as a cylinder of uniform thickness, representing the skin and 'smeared-out' frame and stringer areas. Additional bending stiffnesses representing 'smeared-out' frame and stringer bending stiffnesses were included.

Using the structural data in Table 1, the baseline configuration was:

Surface density of skin and stiffeners = 4.59 kg/m^2 (0.94 psf)

Actual skin thickness = 0.1016 cm (0.04 in)

Equivalent (skin & stiffener) thickness = 0.1640 cm (0.064 in)

Additional stiffener bending rigidity =

$$\left[\frac{EI}{Spacing} \right]_{\substack{stiffener}} + D_{\substack{actual \\ skin}} - D_{\substack{equivalent \\ skin}}$$

Additional frame bending rigidity = 1.7655 x 10^4 N.m

Additional stringer bending rigidity = 4.4822 x 10^2 N.m

For configurations where vinyl was added to the outer wall, the only change made to the analytical model was to the mass, the total surface density becoming 9.47 kg/m^2 (1.94 psf). The skin thickness and stiffnesses were assumed to be unchanged.

4.2 Floor Structure

4.2.1 Attached Floor

The attached, or fixed, floor was modeled as a uniform plate connected to the fuselage along its longitudinal sides. The floor could either be hinged along the attachment line or

rigidly connected so that there was no relative rotation between fuselage and floor along the attachment line. Since the brackets connecting the floor to the frames (see Figures 2(a)) occur at approximately 38.1 cm (15 in) intervals, the floor was assumed to be hinged along the attachment line.

The plywood floor, 1.905 cm thick (0.75 in), was assumed to have the following characteristics:

Density = 544.6 kg/m3 (34 lb/ft3)

Young's Modulus E = 1.103 x 10^{10} N/m2 (1.6 x 10^6 lb/in)

Poisson's ratio = 0

Typical moment of inertia for 0.30m (12-inch) wide plywood panel = 8.782 x 10^{-8}m4 (0.211 in^4)

The transverse floor support beams had an average spacing of 1.224 m (48.2 in) and were 7.6-cm I-beams (3 x .17 in, 1.98 lb/ft). Two 15.2-cm I beams (6 x .23 in, 4.3 lb/ft) supported the floor longitudinally along the edges, 0.508 m (20 in.) from the floor centerline. The floor had a width of 158 cm (62.2 in) and was 28 cm (11 in.) below the fuselage centerline; the radius from the center of the fuselage to the floor/fuselage junction made an angle of 70.5° to the vertical.

The stiffeners were again assumed 'smeared-out' over the floor giving, for the fixed floor,

Surface density of floor + stiffeners = 20.879 kg/m2

Actual floor thickness = 1.905 cm (0.75 in)

Equivalent (floor + stiffener) thickness = 4.012 cm (1.58 in)

Additional transverse bending rigidity = 1.0081×10^5 N.m
Additional longitudinal bending rigidity = 1.5790×10^6 N.m

4.2.2   Floating Floor Representation

Although the plywood floor was located 28 cm (11 in) below the fuselage centerline, the floating floor was supported on air mounts attached to the structural floor (Figure 2). It was assumed therefore that the floating floor connection to the fuselage occurred 68.6 cm (27 in) below the fuselage centerline and that the floor had a width of 96.4 cm (37.95 in); the radius to the floor/fuselage junction made an angle of 35.1° to the vertical.

The same total mass was used as for the fixed floor, thus increasing the surface density of the equivalent narrower floating floor. No information was available on the structural floor of the fuselage, but it was assumed to be at least as stiff as the fixed floor. [Photographs in Figs. 4 and 6 of Ref.[5] show closely spaced circumferential frames and longitudinal stiffness in the structural floor]. The same beam stiffnesses were taken as for the attached floor, with a spacing of 38.1 cm (15 in) for the transverse beams and a spacing of 50.8 cm (20 in) for the longitudinal beams. The parameters used were

Surface density = 34.328 kg/m^2

Equivalent plywood floor thickness = 4.915 cm (1.93 in)

Additional transverse bending rigidity = 3.9536×10^5 N.m

Additional longitudinal bending rigidity = 3.1613×10^6 N.m

4.3 Structural Modes

The structural modes of the fuselage with the floating floor were calculated with and without the vinyl added to the outer skin. The modes are calculated using displacement series for both the shell and floor displacements [1], allowing 14 terms for the shell and 5 terms for the floor. The fuselage was assumed to be freely supported at its ends, allowing axial displacements.

The number of axial half-wavelengths, M, was varied from 1 to 10, and the first 20 symmetric and 20 antisymmetric modes were calculated for each value of M, giving a total of 400 modes. Tables 6, 7 and 8 list the first 16 modes for the floating floor models, without and with add-on vinyl on the outer skin and for the fixed floor with add-on vinyl. These tables list only the 5 largest coefficients associated with the circumferential shell displacement series and the 3 largest for the transverse floor displacement series, which are used in calculating the fuselage response.

Figure 8 shows the first four structural mode shapes for the floating floor configuration with add-on vinyl, for both fuselage and floor. At these frequencies, the heavy floor is acting as a rigid mass.

4.4 Measured Structural Modes

Some mode shapes were measured [5] using circumferential grids and rectangular panel grids. It was not possible to compare the mode shapes measured by the panel grid with calculations, but a comparison was made for the mode measured by the circumferential grid shown in Figure 9.

TABLE 6.   STRUCTURAL MODES FOR FLOATING FLOOR CONFIGURATION

CALAC METRO. DIAMETER 1.68M, LENGTH 9M, FLOATING FLOOR MODEL.

MODE NO	FREQ (HZ)	MODE TYPE	SHELL M	N	CMN	PLATE M	N	CMN	GENERALIZED MASS (KG) TOTAL	SHELL W	PLATE W
1	37.05	SYMM	1	1	.62286	1	0	.96513	207.28017	35.24797	144.70867
			1	2	-.49236	1	1	.03219			
			1	3	-.10472	1	2	.00383			
			1	4	.06256						
			1	5	-.02217						
2	63.31	SYMM	1	2	.55320	1	1	-.02700	34.71538	23.86738	.21441
			1	1	.31776	1	0	-.01970			
			1	3	.16779	1	3	.00091			
			1	4	-.04760						
			1	5	.01033						
3	68.26	SYMM	2	2	.68675	2	0	-.71010	142.84940	45.91989	84.23744
			2	3	.17508	2	1	-.06484			
			2	4	-.11635	2	2	-.00663			
			2	1	-.07625						
			2	5	.04187						
4	77.50	ANTI	1	2	-.56737	1	1	-.09205	40.52281	27.50887	.57172
			1	1	-.33367	1	2	.00506			
			1	3	-.26454	1	3	.00098			
			1	5	.02636						
			1	6	-.02110						
5	110.47	ANTI	2	2	-.52841	2	1	-.01106	32.80658	26.47796	.00365
			2	3	-.43466	2	2	.00514			
			2	1	-.11789	2	4	-.00063			
			2	5	.03890						
			2	4	-.03737						
6	111.10	SYMM	3	2	.83584	3	0	-.77703	160.32208	40.94124	107.73928
			3	4	-.18876	3	1	-.11255			
			3	1	-.09355	3	2	-.02188			
			3	5	.06011						
			3	3	-.01809						
7	118.19	ANTI	1	3	.52148	1	1	-.08977	54.48301	29.77090	.65431
			1	1	-.43217	1	2	-.00449			
			1	2	.23057	1	3	.00075			
			1	4	.07784						
			1	5	-.04460						
8	128.86	SYMM	2	3	.35402	2	0	.18111	29.49626	16.93045	6.79309
			2	2	.30506	2	1	.04913			
			2	1	.23350	2	2	.00878			
			2	4	.11532						
			2	5	-.04364						

TABLE 6. STRUCTURAL MODES FOR FLOATING FLOOR CONFIGURATION
(Continued)

CALAC METRO. DIAMETER 1.66M, LENGTH 9M, FLOATING FLOOR MODEL.

MODE NO	FREQ (HZ)	MODE TYPE	SHELL M	N	CMN	PLATE M	N	CMN	GENERALIZED MASS (KG) TOTAL	SHELL W	PLATE W
9	148.74	ANTI	3	3	.55293	3	1	-.10557	32.46110	26.60793	.87220
			3	2	.41645	3	2	-.00303			
			3	4	.10416	3	3	.00077			
			3	5	-.03238						
			3	1	.02200						
10	150.08	SYMM	1	3	.66104	1	1	.14830	43.01100	32.41922	5.91548
			1	4	.35581	1	0	.09829			
			1	1	-.15273	1	2	.00678			
			1	5	-.08230						
			1	8	-.01633						
11	155.91	ANTI	1	3	-.67068	1	1	.41814	263.86270	51.82781	13.07471
			1	2	.31225	1	3	-.00223			
			1	4	-.29636	1	2	.00110			
			1	1	-.07620						
			1	5	.02808						
12	158.01	SYMM	3	3	.53727	3	1	.08483	27.99393	22.04181	2.85620
			3	2	.23816	3	0	.08109			
			3	4	.23208	3	2	.00543			
			3	5	-.05570						
			3	1	.03986						
13	158.09	SYMM	4	2	-.49888	4	0	.70448	137.90877	31.43707	100.30573
			4	3	.44505	4	1	.17600			
			4	4	.32343	4	2	.03333			
			4	5	-.12543						
			4	1	.08467						
14	167.87	ANTI	2	3	.50933	2	1	-.41638	48.57781	25.81028	12.72050
			2	1	-.34493	2	2	.00339			
			2	2	-.23570	2	3	.00188			
			2	4	.19515						
			2	6	-.02677						
15	169.15	SYMM	2	3	.53493	2	1	.13796	45.46452	33.25248	.43477
			2	4	.37926	2	0	-.05060			
			2	1	-.37336	2	2	-.00437			
			2	2	-.19345						
			2	5	-.05065						
16	182.58	ANTI	1	3	-.55248	1	1	.99700	183.19356	27.31395	72.33242
			1	2	.35548	1	2	-.01273			
			1	4	-.20186	1	3	-.00266			
			1	1	-.11681						
			1	5	-.08916						

TABLE 7.   STRUCTURAL MODES FOR FLOATING FLOOR CONFIGURATION
WITH ADD-ON VINYL

CALAC METRO. DIAMETER 1.68M, LENGTH 9M, FLOATING FLOOR MODEL + ADD-ON VINYL

MODE NO	FREQ (HZ)	MODE TYPE	SHELL M	N	CMN	PLATE M	N	CMN	GENERALIZED MASS (KG) TOTAL	SHELL M	PLATE M
1	32.13	SYMM	1	1	.64654	1	0	.96994	278.29085	74.03199	145.35486
			1	2	-.47337	1	1	.02818			
			1	3	-.11099	1	2	.00287			
			1	4	.05622						
			1	5	-.01876						
2	44.16	SYMM	1	2	.56427	1	0	-.04084	71.41508	49.79321	.50673
			1	1	.30361	1	1	-.02637			
			1	3	.17175	1	3	.00094			
			1	4	-.04852						
			1	5	.01044						
3	54.18	ANTI	1	2	.56622	1	1	.08586	82.29264	56.55245	.49373
			1	1	.32882	1	2	-.00507			
			1	3	.26959	1	3	-.00099			
			1	5	-.02649						
			1	6	.02125						
4	55.75	SYMM	2	2	.87515	2	0	-.61247	179.81035	93.29758	61.82873
			2	3	.22858	2	1	-.04934			
			2	4	-.09274	2	2	-.00461			
			2	1	-.03944						
			2	5	.02793						
5	76.93	ANTI	2	2	.52744	2	1	.00938	67.61390	54.61740	.00225
			2	3	.43582	2	2	-.00510			
			2	1	.11754	2	4	.00063			
			2	5	-.03893						
			2	4	.03737						
6	84.40	ANTI	1	3	.53673	1	1	-.08989	103.49498	60.79194	.65393
			1	1	-.42439	1	2	-.00433			
			1	2	.24797	1	3	.00093			
			1	4	.08991						
			1	5	-.04624						
7	92.62	SYMM	3	2	-.88854	3	0	.65631	193.25515	94.40269	72.73724
			3	3	-.17947	3	1	.06557			
			3	4	.11794	3	2	.01107			
			3	5	-.04007						
			3	1	.03901						
8	97.22	SYMM	2	3	.42761	2	0	.32422	68.22456	35.98336	19.62781
			2	1	.26654	2	1	.05933			
			2	4	.17779	2	2	.00862			
			2	2	.17645						
			2	5	-.05306						

CALAC METRO. DIAMETER 1.68M, LENGTH 9M, FLOATING FLOOR MODEL + ADD-ON VINYL

MODE NO	FREQ (HZ)	MODE TYPE	SHELL M	N	CMN	PLATE M	N	CMN	GENERALIZED MASS (KG) TOTAL	SHELL W	PLATE W
9	104.13	ANTI	3	3	.54147	3	1	-.08738	64.99790	54.51492	.59896
			3	2	.42153	3	2	-.00263			
			3	4	.10854	3	3	.00092			
			3	5	-.03203						
			3	1	.02847						
10	106.96	SYMM	1	3	.67031	1	0	.15933	86.72721	69.77585	8.24122
			1	4	.38591	1	1	.11365			
			1	1	-.11950	1	2	.00548			
			1	5	-.07790						
			1	2	-.02692						
11	113.13	SYMM	3	3	.60286	3	0	.21069	70.82922	53.95066	10.59583
			3	4	.31593	3	1	.08481			
			3	2	.09800	3	2	.00622			
			3	5	-.06578						
			3	1	.04207						
12	118.98	SYMM	2	3	-.50907	2	0	.10587	95.55769	67.98480	.46419
			2	1	.40924	2	1	-.08537			
			2	4	-.37481	2	2	.00434			
			2	2	.18629						
			2	5	.04216						
13	124.05	ANTI	2	3	-.46676	2	1	.30973	75.85460	50.06625	6.90991
			2	1	.32713	2	2	-.00573			
			2	4	-.25978	2	3	-.00256			
			2	2	.22371						
			2	6	.03674						
14	130.09	SYMM	4	3	.67465	4	0	.32579	102.31225	71.81968	22.52389
			4	4	.41778	4	1	.09602			
			4	5	-.06966	4	2	.00749			
			4	2	-.04954						
			4	1	.02212						
15	133.98	ANTI	4	3	.56383	4	1	-.11020	59.57925	51.03835	.89649
			4	2	.29939	4	3	.00118			
			4	4	.21383	4	2	.00051			
			4	6	-.01329						
			4	7	.01160						
16	134.72	ANTI	1	3	-.59529	1	1	.34732	199.24715	96.71058	8.53262
			1	4	-.50007	1	2	-.00997			
			1	2	.43139	1	3	-.00248			
			1	1	-.23126						
			1	5	-.08406						

TABLE 8.   STRUCTURAL MODES FOR FIXED FLOOR CONFIGURATION WITH ADD-ON VINYL

CALAC METRO. DIAMETER 1.68M, LENGTH 9M, FIXED FLOOR. TREATED OUTER WALL

MODE NO	FREQ (HZ)	MODE TYPE	SHELL M	N	CMN	PLATE M	N	CMN	GENERALIZED MASS (KG) TOTAL	SHELL W	PLATE W
1	29.61	SYMM	1	1	.87018	1	0	.96780	320.41060	86.55836	139.54155
			1	3	-.07318	1	2	.03421			
			1	2	-.07747	1	4	-.00211			
			1	5	.00757						
			1	4	.00601						
2	41.95	ANTI	1	2	.82319	1	1	.45835	131.69440	86.22150	15.63568
			1	1	.29069	1	3	-.00257			
			1	3	-.05640	1	5	.00033			
			1	4	.03335						
			1	6	-.00580						
3	55.96	SYMM	1	1	-.00010	1	1	1.00009	74.43335	.00000	74.43335
			1	2	-.00007	1	0	-.00008			
			1	3	-.00007	1	2	-.00001			
			1	5	.00000						
			1	6	-.00000						
4	61.46	SYMM	2	3	-.00024	2	1	.99970	74.44376	.00001	74.44374
			2	2	-.00024	2	0	.00026			
			2	1	.00009	2	2	.00004			
			2	5	.00001						
			2	4	.00001						
5	62.25	SYMM	1	2	.44434	1	0	-.11673	57.49203	45.28598	2.05478
			1	3	.43349	1	2	-.01997			
			1	1	.12589	1	4	.00116			
			1	5	-.03115						
			1	4	.01793						
6	64.92	ANTI	2	2	-.79836	2	1	-.46852	121.00588	82.14910	16.33745
			2	3	.27349	2	3	-.00084			
			2	1	-.11395	2	5	.00011			
			2	4	-.07023						
			2	6	.01107						
7	66.14	SYMM	2	3	.57550	2	0	-.55842	138.75995	74.75489	46.98641
			2	2	.55667	2	2	-.09542			
			2	1	-.14905	2	4	.00562			
			2	5	-.03127						
			2	4	-.01075						
8	76.51	ANTI	1	3	.61991	1	1	-.15105	89.35244	63.65314	1.69812
			1	1	.39755	1	3	-.00171			
			1	2	-.14336	1	5	.00022			
			1	4	-.05400						
			1	6	.00737						

TABLE 8. STRUCTURAL MODES FOR FIXED FLOOR CONFIGURATION WITH ADD-ON VINYL (Continued)

CALAC METRO. DIAMETER 1.68M, LENGTH 9M, FIXED FLOOR. TREATED OUTER WALL

MODE NO	FREQ (HZ)	MODE TYPE	SHELL M	N	CPN	PLATE M	N	CPN	GENERALIZED MASS (KG) TOTAL	SHELL W	PLATE W
9	77.60	SYMM	3	3	-.00007	3	1	.99993	74.43382	.00000	74.43382
			3	2	-.00006	3	0	.C0006			
			3	4	.00001	3	2	.C0001			
			3	1	.00001						
			3	6	-.00000						
10	91.15	SYMM	3	3	.60873	3	0	-.51053	125.19129	71.26489	40.11496
			3	2	.50554	3	2	-.13459			
			3	4	-.06586	3	4	.00777			
			3	1	-.05469						
			3	6	.06498						
11	93.44	SYMM	2	1	.34023	2	0	.38171	76.52660	33.74691	23.40918
			2	2	.30020	2	2	.15249			
			2	3	.29719	2	4	-.C0817			
			2	4	.07544						
			2	5	-.00689						
12	98.52	ANTI	3	2	-.55749	3	1	-.42017	95.70690	68.58229	13.14369
			3	3	.54305	3	3	-.00635			
			3	4	.06168	3	5	.C0081			
			3	6	-.00806						
			3	1	-.00604						
13	99.61	ANTI	2	3	.61803	2	1	-.05609	64.33322	53.75372	.23428
			2	4	.19610	2	3	-.00144			
			2	1	.19165	2	5	.C0018			
			2	2	.14126						
			2	6	-.02395						
14	107.51	ANTI	1	3	-.61621	1	1	-.81054	342.56263	59.14559	48.96392
			1	1	.32895	1	3	-.02909			
			1	4	-.19174	1	5	.C0362			
			1	6	.02445						
			1	5	-.01653						
15	107.79	SYMM	4	3	-.00005	4	1	.99995	74.43382	.00000	74.43382
			4	2	-.00003	4	0	.C0004			
			4	4	.00002	4	2	.C0001			
			4	1	.00001						
			4	5	-.00000						
16	115.48	ANTI	1	4	.55136	1	1	-.35164	120.37357	74.54285	9.22010
			1	3	.42235	1	3	-.01540			
			1	1	-.31304	1	5	.C0190			
			1	2	.28169						
			1	6	-.04568						

CALAC METRO. DIAMETER 1.68M, LENGTH 9M, FLOATING FLOOR MODEL + ADD-ON VINYL

MODE NUMBER 1

  FREQUENCY =   32.1283   SYMMETRIC MODES   M = 1

SHELL w   FLOOR w
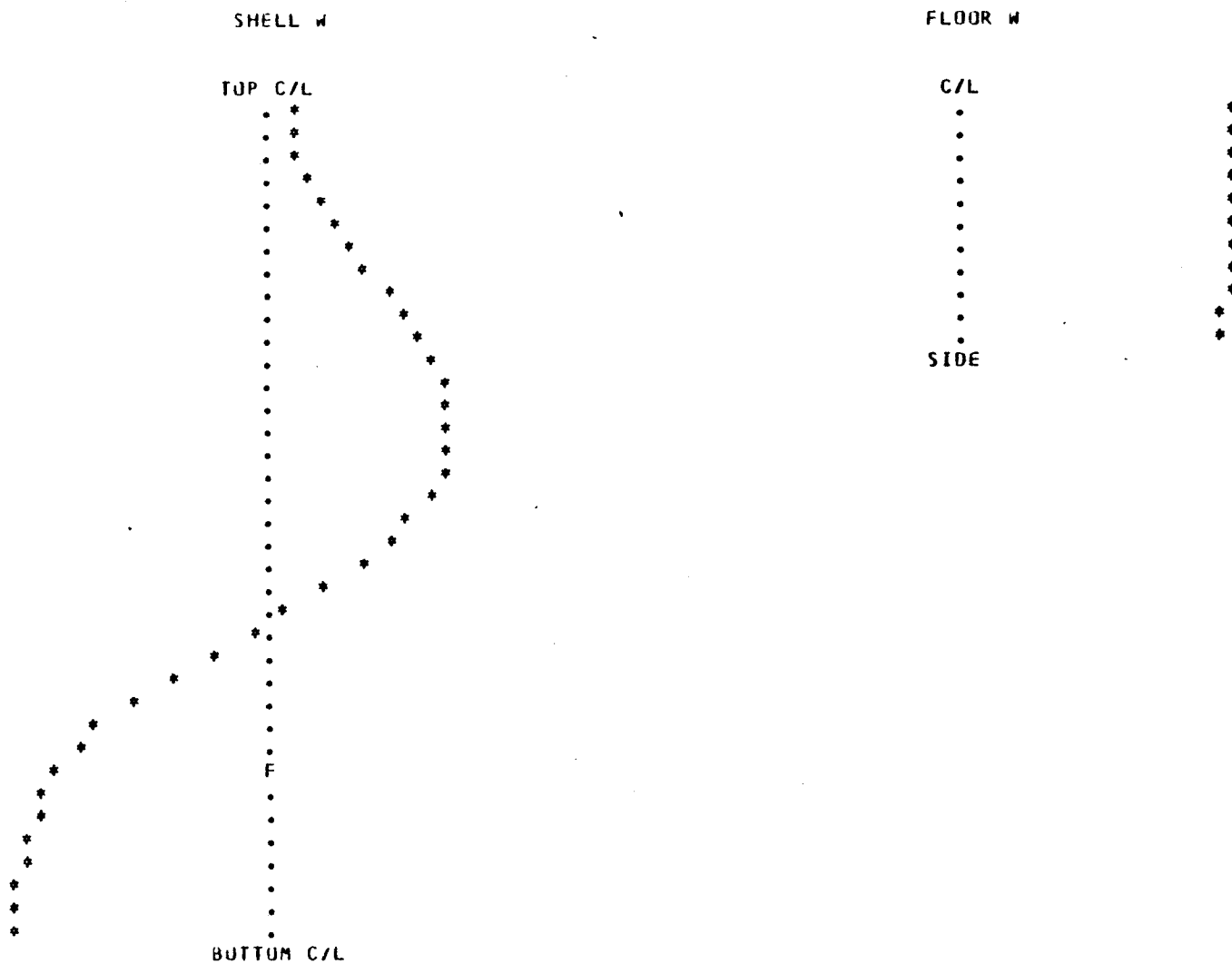
FIGURE 8. STRUCTURAL MODE SHAPES: FLOATING FLOOR CONFIGURATION
           WITH ADD-ON VINYL

CALAC METRU. DIAMETER 1.68M, LENGTH 9M, FLOATING FLOOR MODEL + ADD-ON VINYL

MODE NUMBER 2

FREQUENCY =   44.1579   SYMMETRIC MODES   M = 1
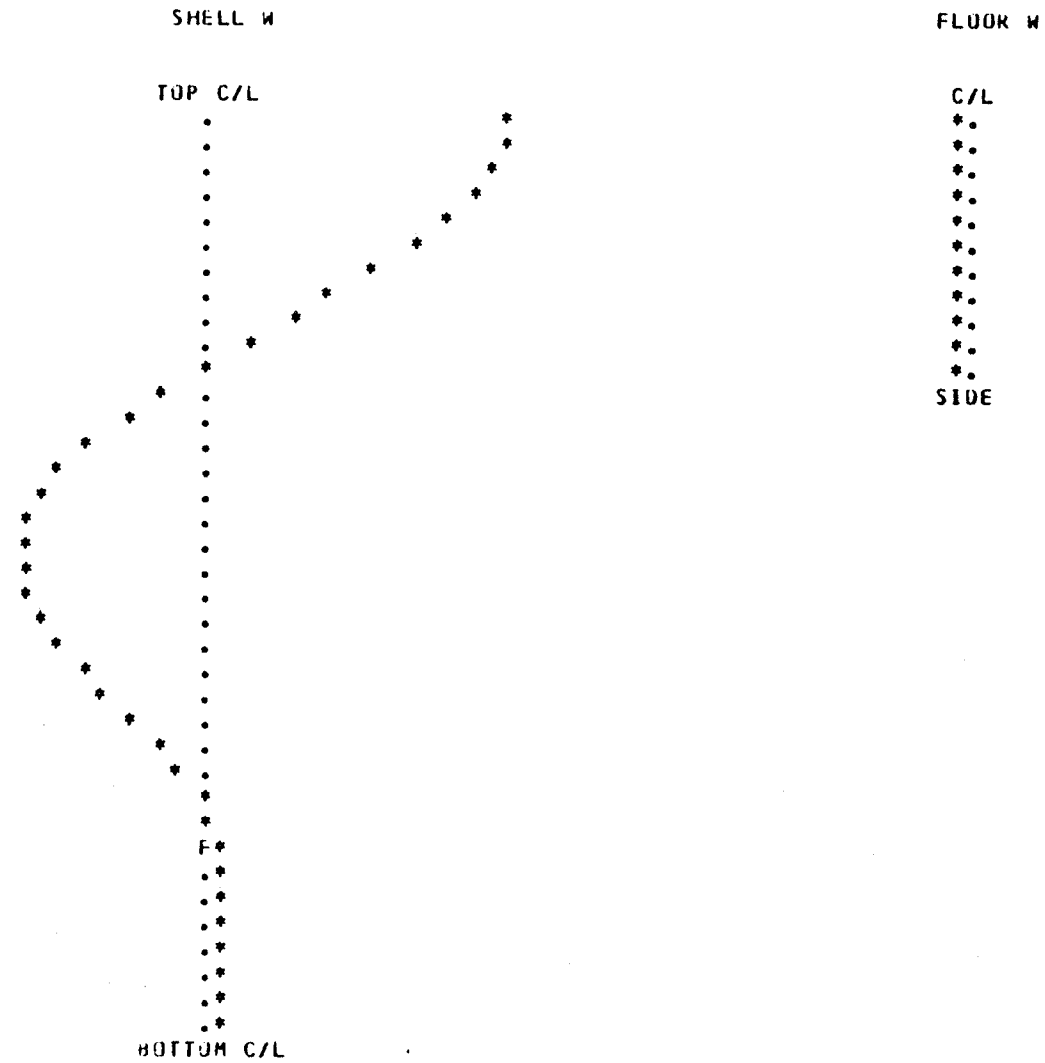
SHELL W   FLOOR W

FIGURE 8. CONTINUED

CALAC METRO. DIAMETER 1.68M, LENGTH 9M, FLOATING FLOOR MODEL + ADD-ON VINYL

MODE NUMBER 4

FREQUENCY = 55.7509   SYMMETRIC MODES   M = 2

SHELL W   FLOOR W

TOP C/L   C/L

SIDE

-48-

F

BOTTOM C/L
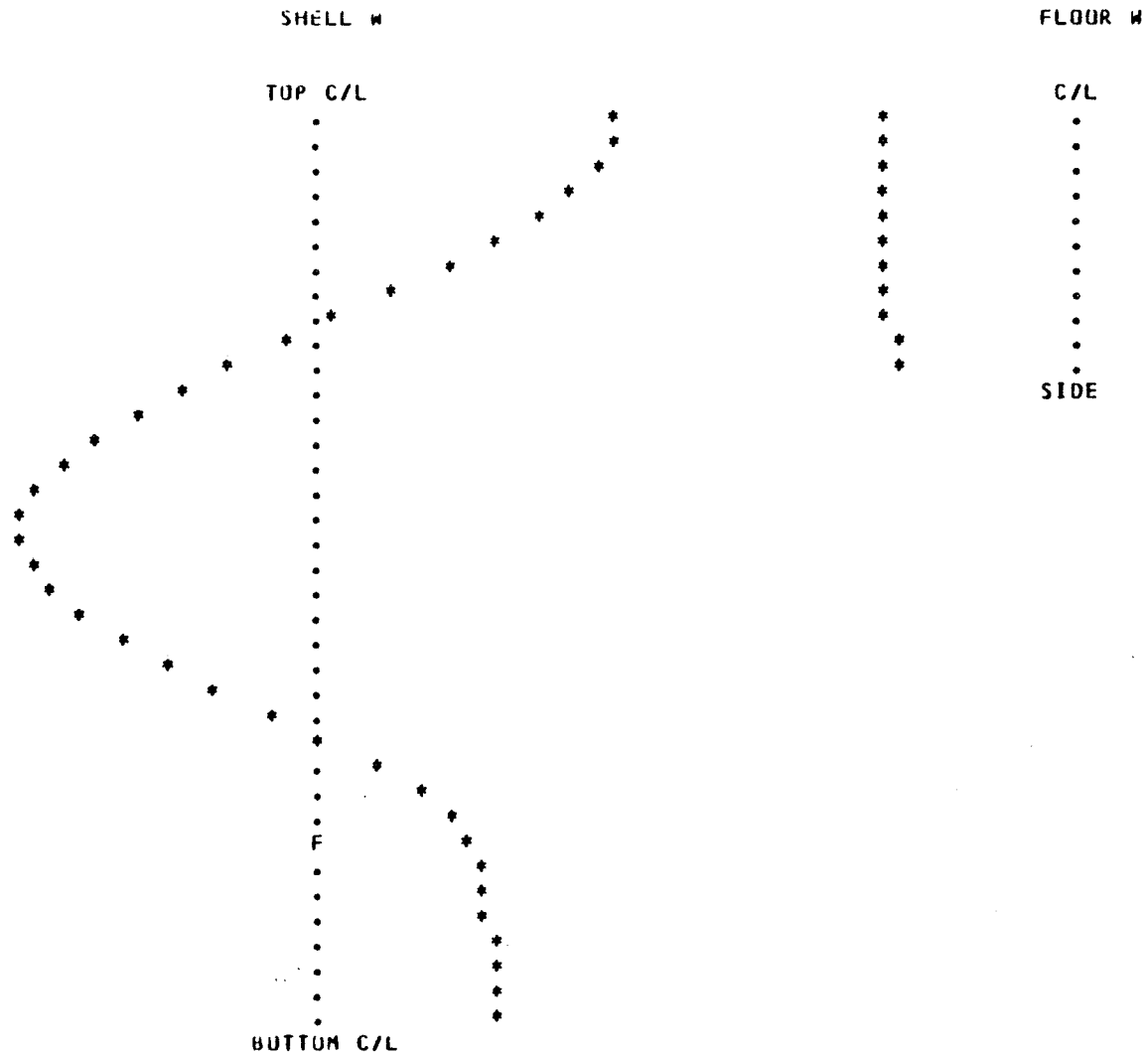
FIGURE 8. CONTINUED
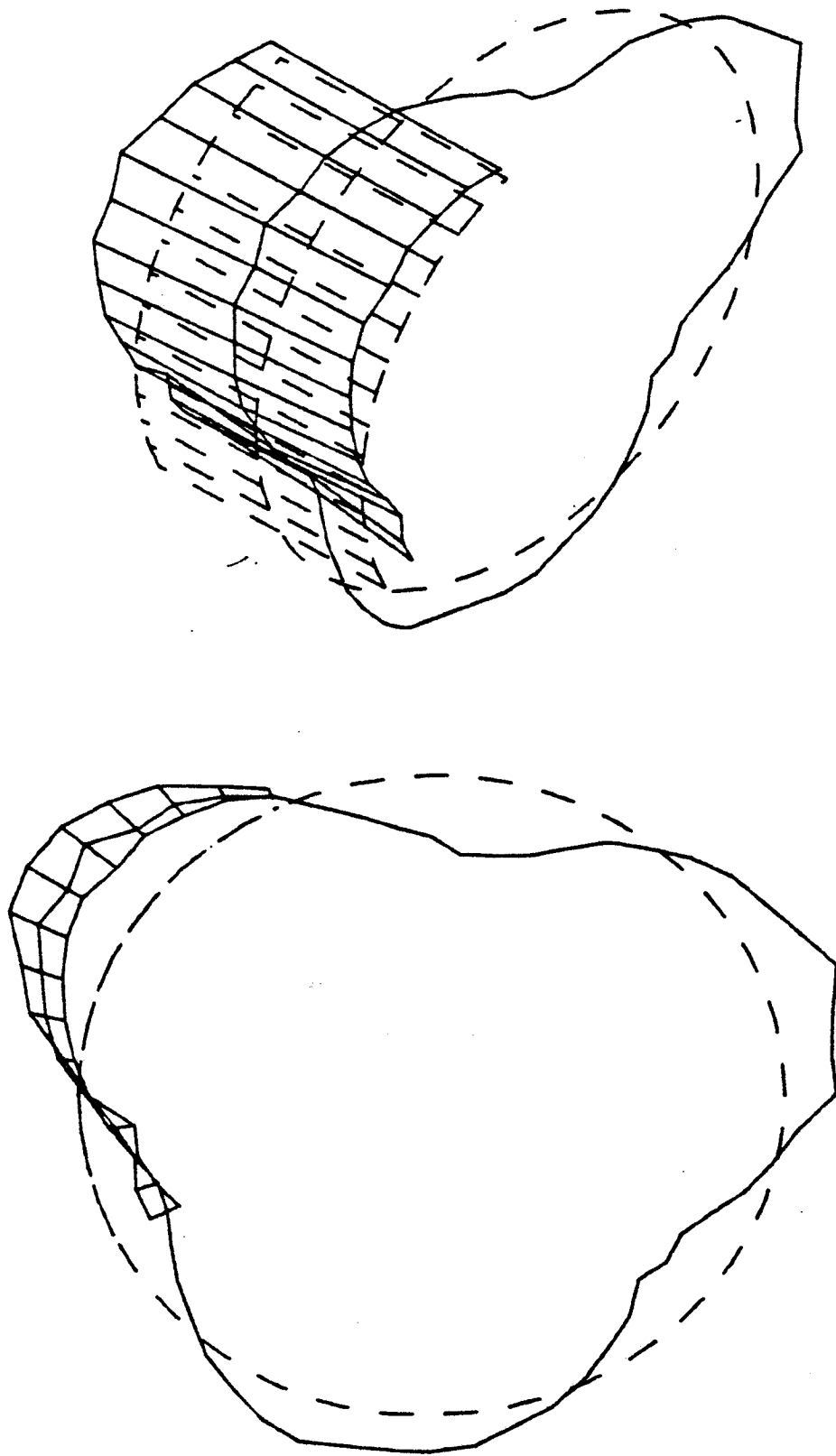
FIGURE 9. MEASURED CIRCUMFERENTIAL MODE SHAPE AT 83 Hz FOR
BARE FUSELAGE STRUCTURE [5]

This mode was assumed to be symmetric so that the displacements normal to the fuselage could be averaged for the 2 sides and then normalized to a maximum value of 1.0. Figure 10 compares the measured mode shape with that calculated for the fuselage shell only (no floor), for M = 1 and n = 3. Figures 11, 12 and 13 compare the measured mode shape and frequency with corresponding calculated values for the floating floor, rigid joint model, and the attached floor, rigid and hinged joint models. The comparison suggests that the floating floor model puts too large a constraint on the fuselage below the floor line. However, because of the uncertainty regarding the identification of the order of the measured mode, it is difficult to make any definitive conclusions. The uncertainty in measured mode order is one factor influencing the agreement between predicted and measured resonance frequencies. It is interesting to note that the measured frequency (40 Hz) of the lowest order mode of the structure is close to the predicted values of 35 Hz for the fixed floor and 37 Hz for the floating floor.

4.5 Structural Loss Factors

Measured structural loss factors for the baseline (bare) test structure are listed in Table 2. The data show large variations from frequency to frequency, and different values were obtained using different test methods. Thus, some averaging, smoothing and interpolation was performed in one-third octave frequency bands in order to obtain input data for the model. The resulting average loss factors are given in Table 9. Also, the average loss factor curve is shown superimposed on the test data in Fig. 14. The average loss factors for the increased density test structure are also shown in Table 9.
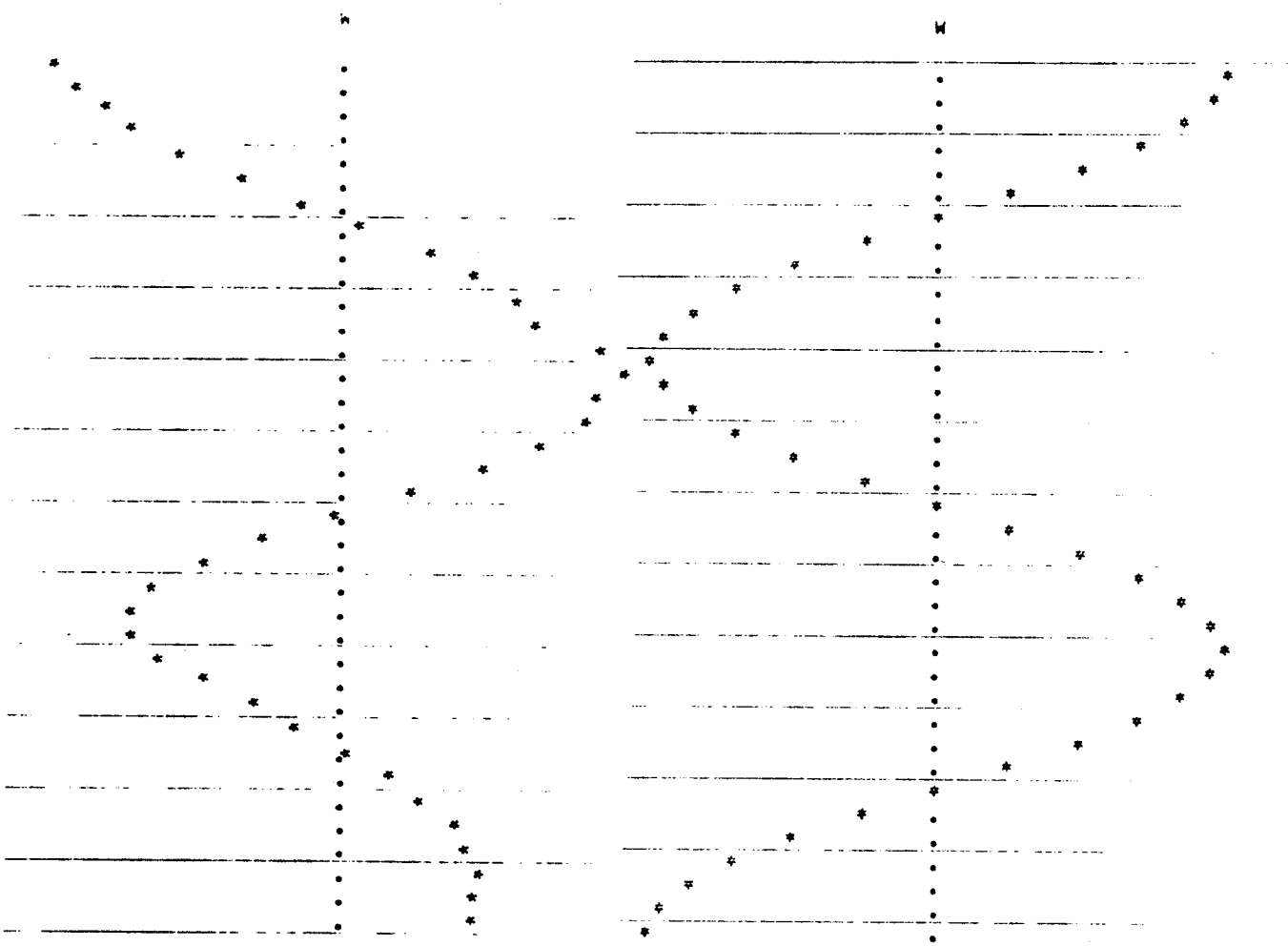
a) Measured 83 Hz   b) Calculated 120 Hz

FIGURE 10. COMPARISON OF MEASURED MODE SHAPE WITH FUSELAGE
SHELL MODEL (NO FLOOR)

-51-
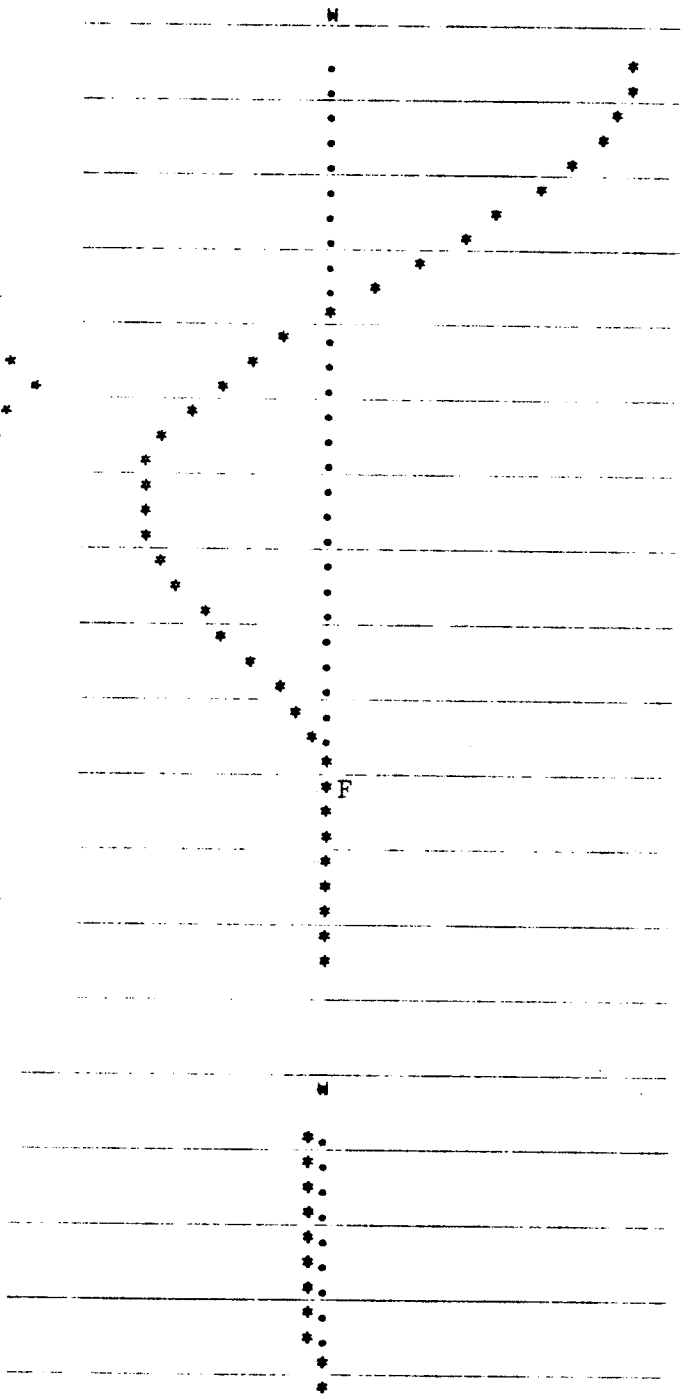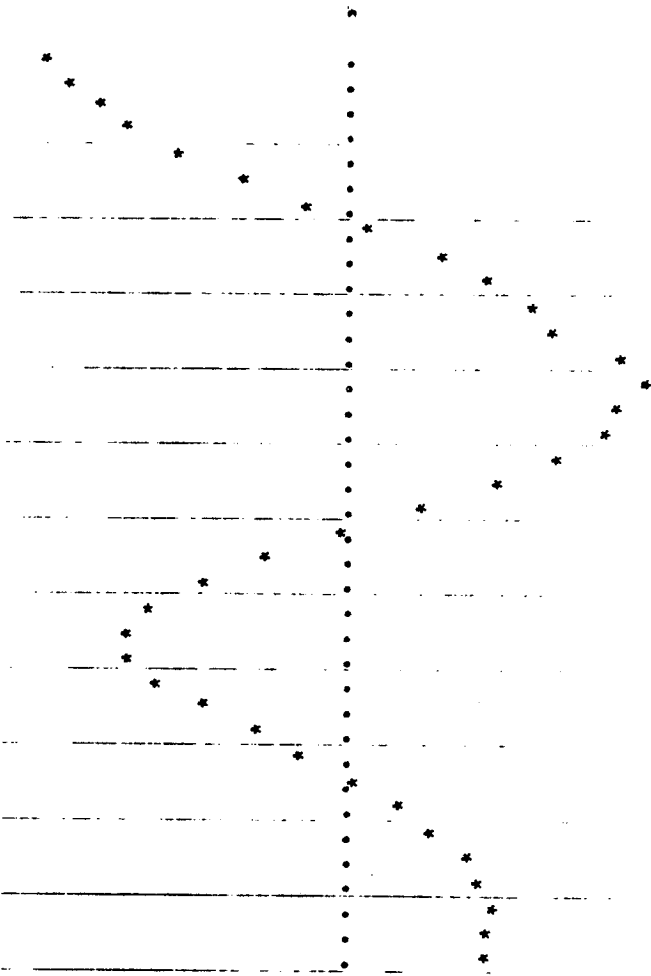
a) Measured 83 Hz   b) Calculated 63 Hz

FIGURE 11. COMPARISON OF MEASURED MODE SHAPE WITH FLOATING
FLOOR MODEL (RIGID JOINT)
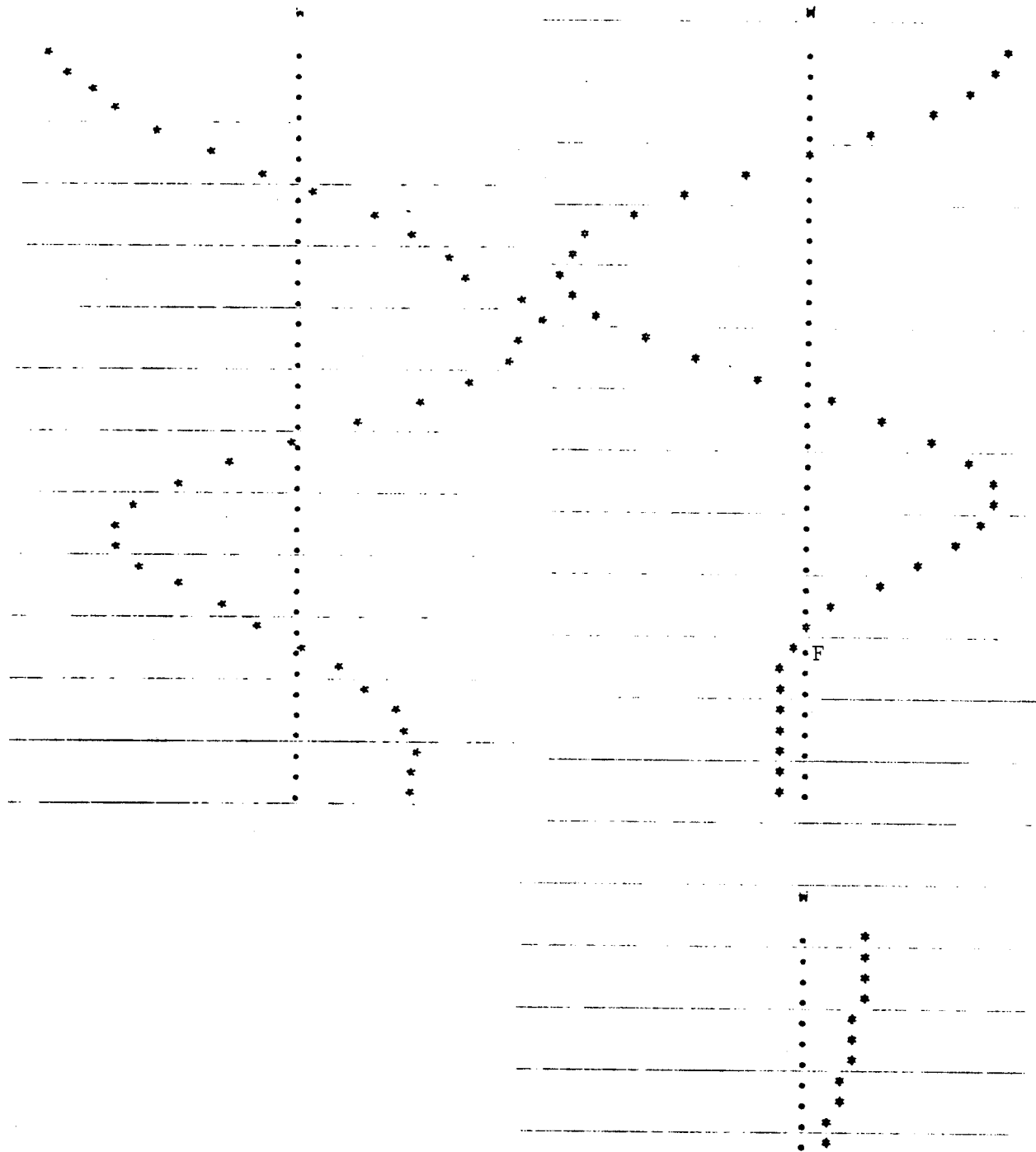
a) Measured 83 Hz   b) Calculated 150 Hz

FIGURE 11. CONTINUED

a) Measured 83 Hz   b) Calculated 88 Hz
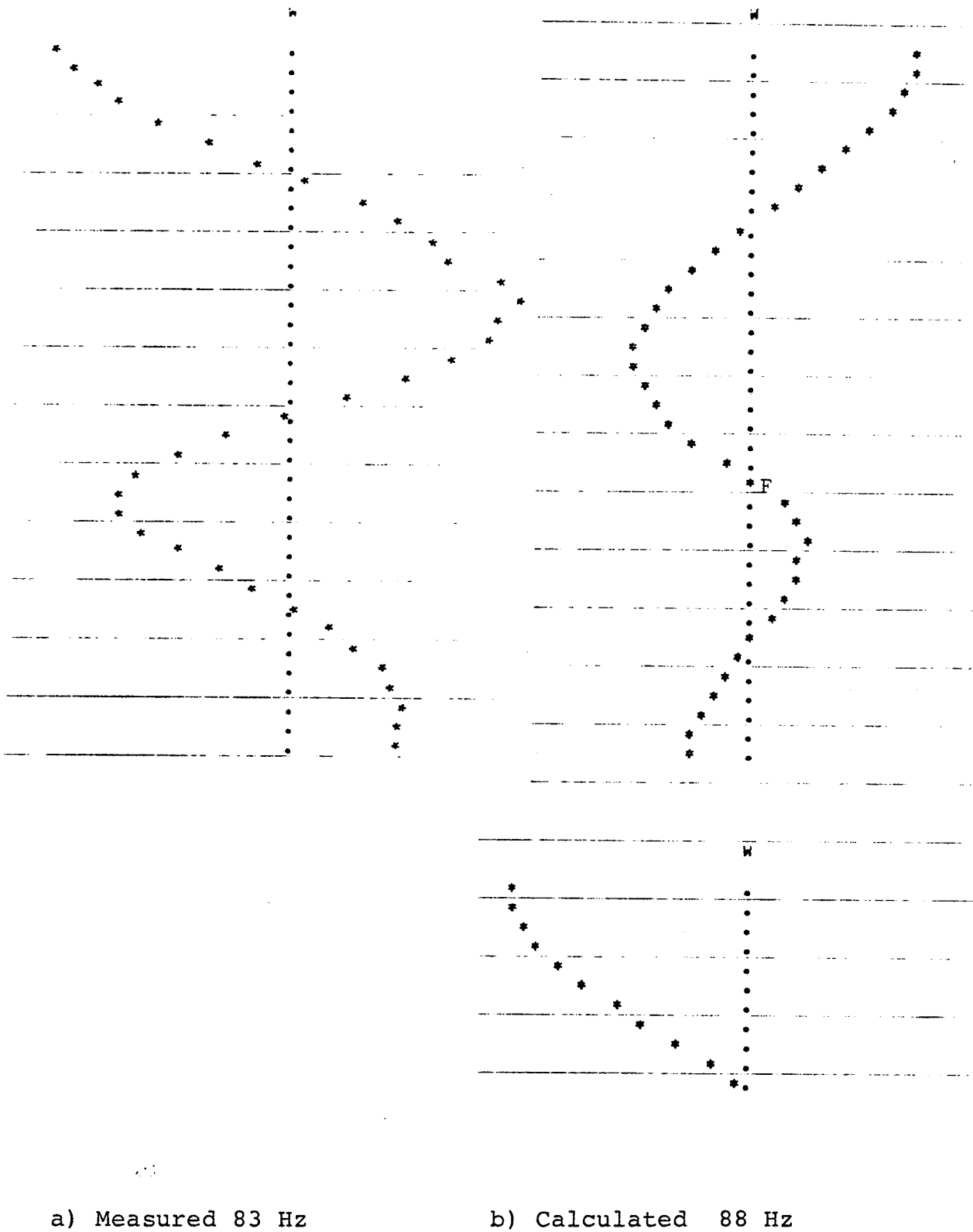
FIGURE 12. COMPARISON OF MEASURED MODE SHAPE WITH ATTACHED
FLOOR MODEL (RIGID JOINT)
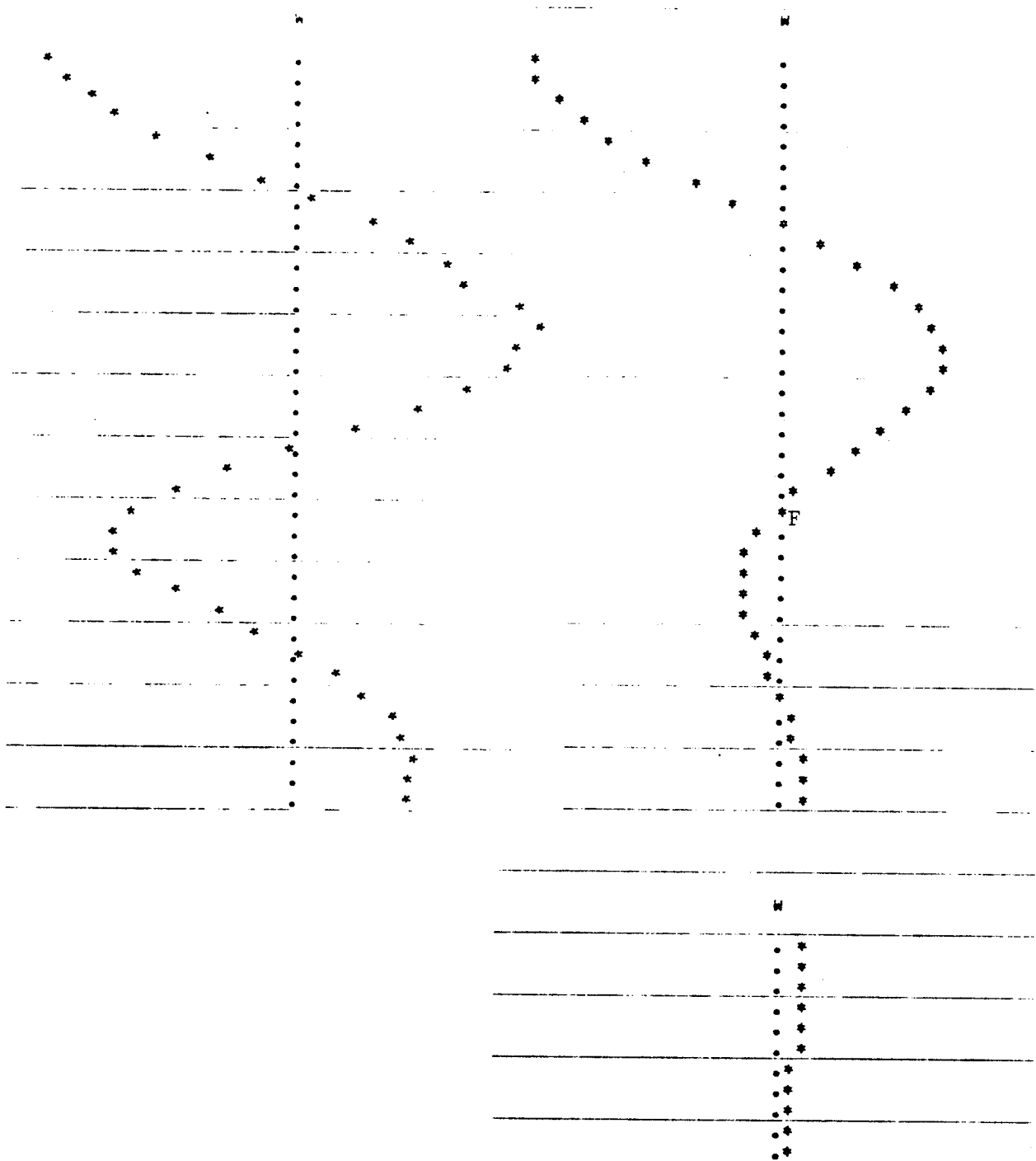
a) Measured 83 Hz   B) Calculated, 88 Hz

FIGURE 13.   COMPARISON OF MEASURED MODE SHAPE WITH ATTACHED
             FLOOR MODEL (HINGED JOINT)

TABLE 9

AVERAGE STRUCTURAL LOSS FACTORS FOR FUSELAGE

Frequency (Hz)	Average Loss Factor	
	Baseline	Increased Density
50	0.0771	0.0833
63	0.0725	0.0833
80	0.0679	0.1000
100	0.0390	0.1185
125	0.0218	0.0920
160	0.0306	0.0670
200	0.0245	0.0510
250	0.0212	0.0379
315	0.0141	0.0515
400	0.0224	0.0347
500	0.0210	0.0720
630	0.0102	0.0266
800	0.0122	0.0213
1000	0.0148	0.0373
1250	0.0089	0.0565
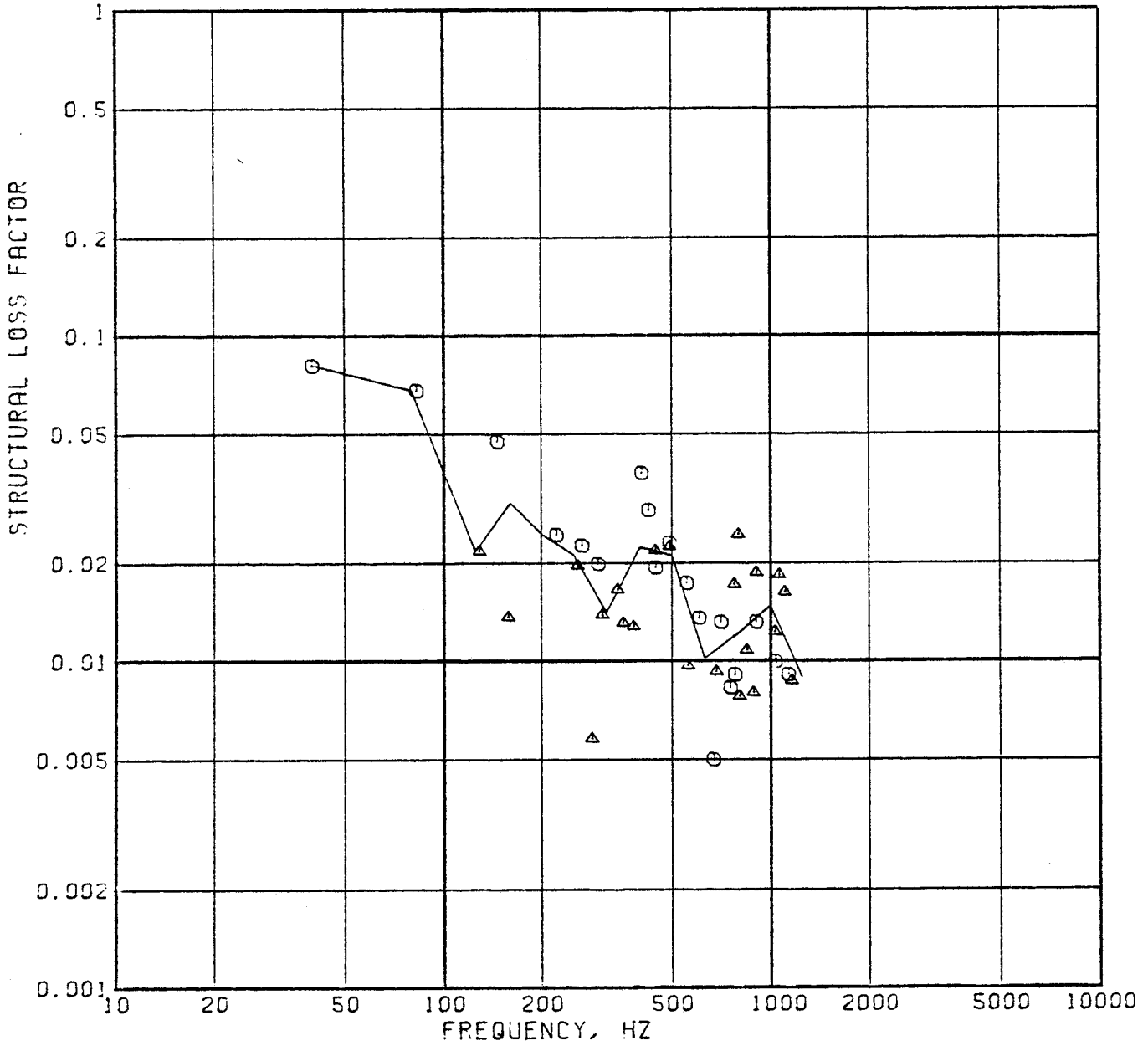
FIGURE 14. STRUCTURAL LOSS FACTORS FOR BASELINE STRUCTURE

4.6 Floor Structural Modes used in the Analytical Model

The floating floor configuration introduces an inconsistency in
the analytical representation of the coupling between floor and
cavity modes. The acoustic modes in the cavity are determined
by the physical presence of the plywood floor, which is located
28 cm (11 inches) below the fuselage centerline. In contrast
the weight of the plywood floor is supported on fuselage struc-
ture which is below the test floor line. Thus, for structural
modeling purposes, the floor line has been taken at a distance
of 68.6 cm (27 inches) below the fuselage centerline. The
inconsistency arises because the model calculates the coupling
factor between the structural and acoustic modes and, therefore,
the physical dimensions for the two sets of modes must corre-
spond.

To overcome this inconsistency, it was assumed that the floor
mode shape, calculated for the floating floor at a lower
position on the fuselage structure, could be applied to the
actual plywood floor. The transferred mode shapes were assumed
to have the same frequencies and maximum deflections, but the
corresponding modal wavelengths were increased in direct propor-
tion to the increases in the effective width of the floor. The
structural/acoustic coupling factor was then calculated for the
assumed mode shapes for the plywood floor and for the fuselage
shell above the plywood floor only. The actual generalized mass
for the floating floor was used in calculating the response.

4.7 Sidewall Treatment

The analytical representation for the sidewall treatment is dis-
cussed in Section 2.5, and the required parameters required for
the insulation are identified in Eq.(15). Values for these
parameters used in the analysis of the Metro II test fuselage
are given in Table 10 for the fiberglass material and the air-
gap. ·

TABLE 10.   ACOUSTICAL PROPERTIES OF SIDEWALL ELEMENTS

TRIM INSULATION TYPE-
   FIBERGLAS. FIBER DIAMETER 2 MICRONS.
   FLOW RESISTANCE 25700 MKS RAYLS/M

FREQUENCY HZ	ALPHA DB/M	LAMBDA M	MOD(W) MKS RAYLS	PHASE(W) DEG
50.0	1.0	2.0620	1000.0	2.20
63.0	1.3	1.6500	1001.0	2.90
80.0	2.0	1.3300	1002.0	3.80
100.0	4.0	1.0610	1005.0	4.90
125.0	7.0	.8500	1011.0	6.30
160.0	11.0	.6700	1017.0	8.20
200.0	17.4	.5339	1018.0	10.50
250.0	28.0	.4500	1010.0	13.00
315.5	43.0	.3700	988.0	16.00
400.0	60.5	.3048	977.8	19.00
500.0	85.0	.2650	955.0	22.30
630.0	111.0	.2250	925.0	25.10
800.0	138.0	.1948	880.9	27.50
1000.0	166.0	.1650	821.0	28.20
1250.0	190.0	.1480	756.0	28.30
1600.0	216.2	.1267	702.8	28.00

TRIM INSULATION TYPE-
   AIR GAP

FREQUENCY HZ	ALPHA DB/M	LAMBDA M	MOD(W) MKS RAYLS	PHASE(W) DEG
50.0	0.0	6.8600	413.0	0.00
63.0	0.0	5.4440	413.0	0.00
80.0	0.0	4.2880	413.0	0.00
100.0	0.0	3.4300	413.0	0.00
125.0	0.0	2.7440	413.0	0.00
160.0	0.0	2.1430	413.0	0.00
200.0	0.0	1.7150	413.0	0.00
250.0	0.0	1.3720	413.0	0.00
315.5	0.0	1.0889	413.0	0.00
400.0	0.0	.8575	413.0	0.00
500.0	0.0	.6860	413.0	0.00
630.0	0.0	.5444	413.0	0.00
800.0	0.0	.4288	413.0	0.00
1000.0	0.0	.3430	413.0	0.00
1250.0	0.0	.2744	413.0	0.00
1600.0	0.0	.2144	413.0	0.00

The sidewall model was not used to calculate the acoustic loss factors of the modes in the cavity, but it was used to calculate the transmission loss through the sidewall and the effective damping of the sidewall on the structure [1, Appendix A].

The mass of the interior trim lining was changed for the different sidewall configurations, as shown in Table 11. These masses can be used, in a simplified analysis, to estimate sidewall resonance frequencies based on a mass-spring-mass model,

$$f_{dw} = \frac{1}{2\pi} \sqrt{\frac{\rho c^2 (m_1 + m_2)}{d m_1 m_2}}$$

where d is the distance between the panels of surface density m_1 and m_2. The resulting frequencies are listed in Table 11. The mechanics of the analytical model for sidewall transmission are, however, somewhat different in that the model utilizes the trim mass in the trim transfer matrix (Eq.(16)) and, thence, in the trim transmission coefficient (Eq.(A.6)[1]) and the damping of the outer panel (Eq.(17)).

The loss factor associated with the lining was taken as 0.50 in all cases. This value might be high for the sidewall configuration without add-on vinyl but, as the mass-spring-mass double wall resonances lie below 200 Hz, the effect of lining loss factor will not be too important.

The lowest resonance frequencies of the inner trim panel were calculated for the test section, as a 3.66 m long (144 in) curved panel extending from floor to floor. Because of the strong curvature, the lowest frequencies were found to be about 50 Hz for the modes with one half-wavelength in the axial direction and 10 to 15 half-wavelengths from floor to floor. When the effect of the fundamental resonance frequency of the wall

was included in the transfer matrix, the effective mass of the
inner wall was reduced and the double-wall resonance frequency
was raised slightly. However, above 200 Hz, the effect on the
transmission loss of the sidewall was small; thus the inner wall
stiffness was *not* included in the final computations.

TABLE 11.   SIDEWALL RESONANCE FREQUENCIES

Configuration No.	Surface density, kg/m^2		Double-Wall Resonance, Hz
	Outer Wall	Inner Wall	
1	4.59	2.25	193.5
2	4.59	7.13	142.3
3	4.59	12.01	130.4
4	9.47	2.25	176.3
5	9.47	7.13	117.9
6	9.47	12.01	103.3

4.8 Cavity Model

4.8.1 Cavity Modes

Resonance frequencies and mode shapes for the acoustic modes
inside the fuselage were computed using the finite difference
method developed for the analytical model. Examples of the
predicted modes are shown in Figure 15 for modes with zero axial
half-wavelengths (q = 0) in the cavity for the first 12 circum-
ferential modes (i = 0 to 11).

A total of 400 acoustic modes were included in the analysis, for
q = 0 to 19 axially, and i = 0 to 19 circumferentially, where

    q = no of axial half-wavelengths
    i = assigned order of 2-dimensional modal pattern
        in cylinder cross section.

Because of the length of the cavity, 9.02 m (29.6 ft), the 400
acoustic modes cover only the frequency range 19 Hz to 670 Hz.
Calculations made using the low frequency modal model (indivi-
dual acoustic modes) will therefore not be valid above the
500 Hz one-third octave band.

4.8.2 Acoustic Loss Factors

Acoustic absorption coefficients were measured by Prydz et al
[5] for the bare and treated interiors of the test fuselage.
Two methods were tried, one being the use of a standard sound
source of known acoustic output power and the other being the
sound level decay method. The decay method was used for the
bare interior, and both methods were applied to the treated
cabin. Resulting data are presented in Table 4 and Fig.7 where
it is seen that the two methods can, at some frequencies, give
quite different values.

Data from Table 4 and Fig.7 were combined to provide a mean absorption coefficient spectrum over the frequency range of interest. The absorption coefficient α was then converted to the associated acoustic loss factor η_n by means of the relationship

$$\eta_n = \frac{\alpha c_o S}{4\omega V}$$

where V is the volume of the cavity (14.08 m3) and S the transmitting surface area (28.9 m2). Values for the mean absorption coefficient and acoustic loss factor are given in Table 12. These empirical loss factor data were used as input to the computation process instead of using the analytical model itself to calculate acoustic loss factors on the basis of the dynamic characteristics of the trim panels. This approach of inserting empirical acoustic loss factor data as data input was used because much of the acoustic dissipation within the test fuselage was provided by the foam placed along the edges of the floor, rather than by a uniform distribution over the sidewall treatment. The analytical model was not designed to cater for the test situation.

It should be noted that the value of area S used to compute α was not the total surface area in the cavity. The value was associated with the curved, transmitting area since this was the area used by Prydz et al [5] to calculate average values for the absorption coefficient α.

TABLE 12.

ACOUSTIC ABSORPTION COEFFICIENTS AND LOSS FACTORS FOR THE INTERIOR OF THE TREATED TEST FUSELAGE

Frequency (Hz)	Absorption Coefficient	Loss Factor
50	0.005	0.00280
63	0.01	0.00445
80	0.015	0.00525
100	0.02	0.00560
125	0.03	0.00672
160	0.08	0.01401
200	0.285	0.03992
250	0.355	0.03978
315	0.435	0.03868
400	0.305	0.02136
500	0.415	0.02325
630	0.34	0.01512
800	0.30	0.01050
1000	0.295	0.00826
1250	0.31	0.00695
1600	0.32	0.00560
2000	0.325	0.00455

5.0 ANALYTICAL REPRESENTATION OF METRO II TEST EXCITATION

The analytical model requires that the exterior acoustic
pressure field be described at a series of points on a grid
covering the sidewall of the cylinder. The description of the
field is given in terms of the free field pressure amplitude and
phase for a particular frequency of interest, the model having
been developed for harmonics of a propeller blade passage
frequency. The grid points (k,ℓ) used for defining the pressure
field are shown in Figure 16, the grid spacing being 0.1463 m
(5.76 in). In the case of the Metro II tests, the point (8,1)
was 1.3 m from the electropneumatic noise source; for applica-
tion in this model, the pressure field was described over a
region of the fuselage approximately 1 meter forward and aft of
the noise source.

Free field test data were provided for the Metro II along the
longitudinal axis of the grid point array and "blocked" pres-
sures along the circumferential direction. These data are shown
in Figure 5. Since the model requires that the acoustic
pressures be free field, the circumferential pressure
distribution was converted to an equivalent free-field pattern
using the inverse of the equation contained in the computer
program (see Eq.(43) of [1]).

$$p_{blk} = \left\{ 10^{[0.3 -0.000224 \ e^{0.08\gamma}]} \right\} p_{free} \tag{48}$$

where γ is the "incidence angle" in degrees, which in this case
is the angle between a line connecting the center of the horn to
the grid point on the fuselage and the normal to the surface at
that point, (see Figure 17). The calculated reflection effects
in the vertical plane containing the noise source axis are given
in Table 13. Furthermore, the three distribution patterns shown
in Fig. 5(b) for three frequencies were normalized relative to
peak values, and an average spatial distribution was calculated.
This was then combined with the reflection effect to give an
estimated circumferential free field distribution in Table 13.

FIGURE 16. GRID USED FOR PROPELLER NOISE PREDICTIONS
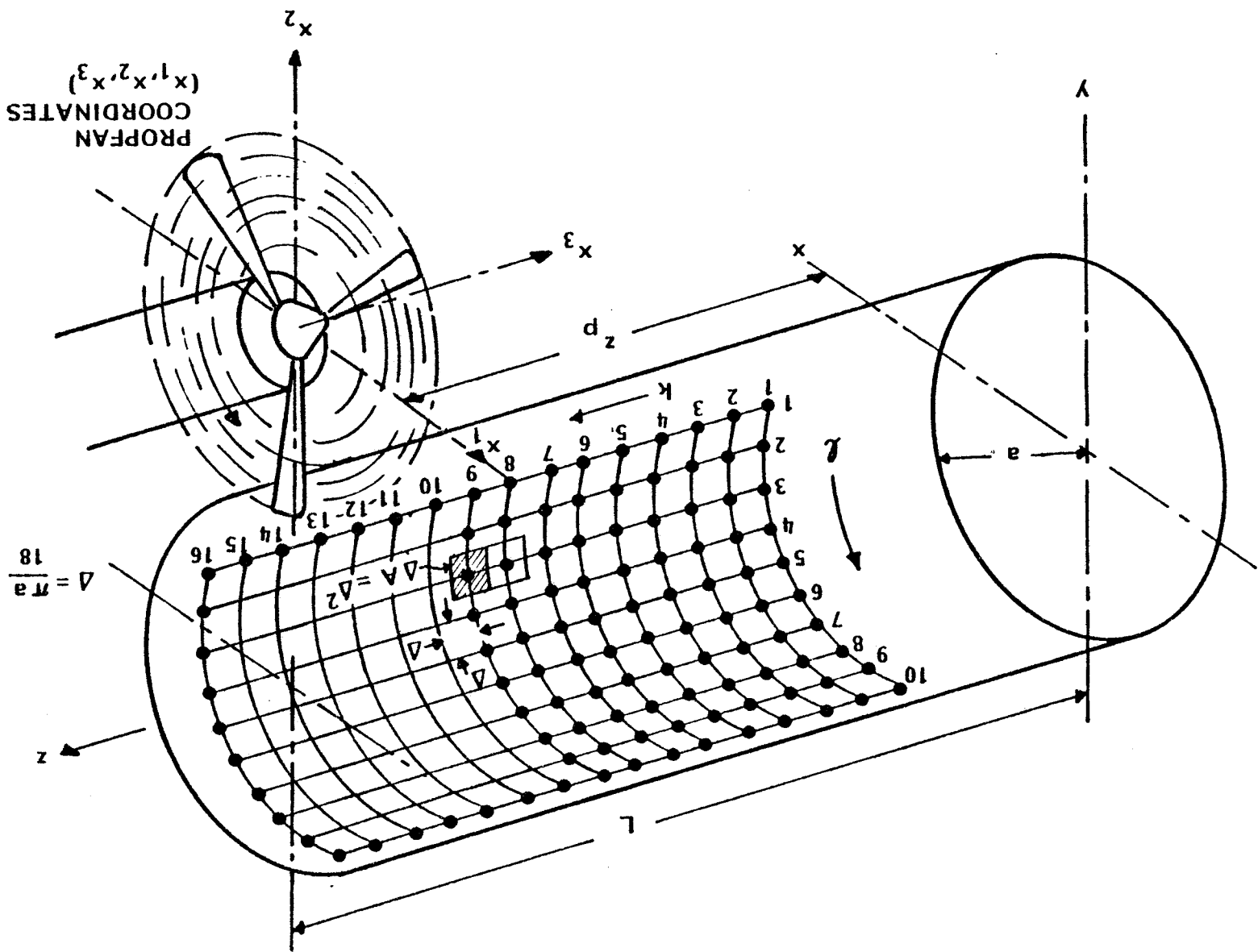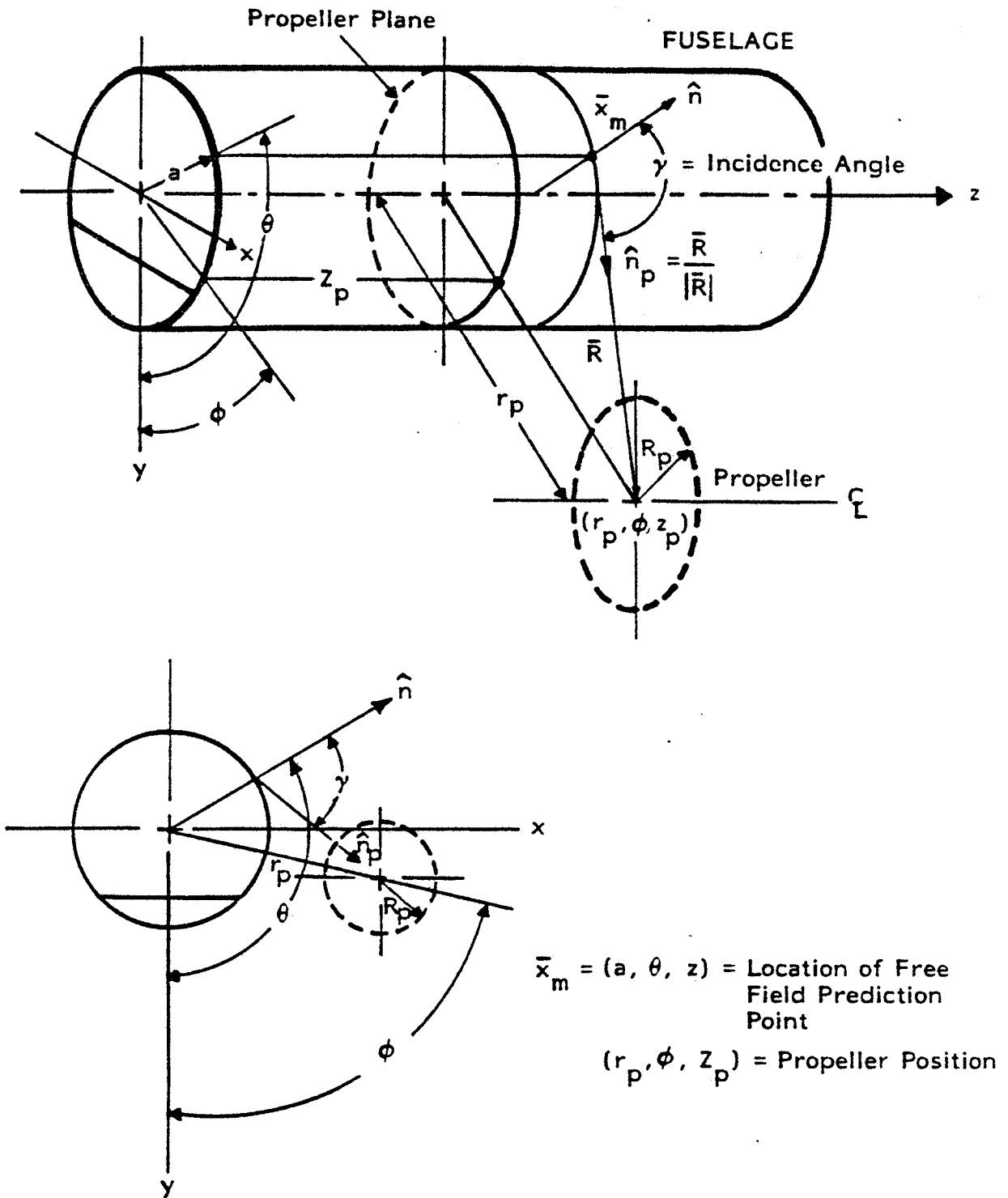
FIGURE 17. PROPELLER AND FUSELAGE SURFACE POINT GEOMETRY

-69-

TABLE 13
CIRCUMFERENTIAL VARIATION OF FREE FIELD PRESSURE

Grid Point		Reflection effect (dB)	Average Measured spatial variation (dB re max)	Estimated free field variation (dB re max)
k	ℓ			
8	10	0	-18.9	-12.9
8	9	0	-17.1	-11.1
8	8	0	-14.8	-10.0*
8	7	2.6	-12.9	-9.5
8	6	4.6	-9.9	-8.5
8	5	5.5	-6.8	-6.3
8	4	5.8	-4.0	-3.8
8	3	5.9	-1.3	-1.2
8	2	6.0	-0.2	-0.2
8	1	6.0	-0.0	0

* Interpolated value

TABLE 14
AXIAL VARIATION OF FREE FIELD PRESSURE

Grid Point		Axial Distance From Source Plane (m)	Free Field Variation (dB re max)
k	ℓ		
8	1	0	0
9	1	.146	-.45
10	1	.293	-1.30
11	1	.439	-2.65
12	1	.585	-4.30
13	1	.731	-6.40
14	1	.878	-8.35
15	1	1.024	-10.70
16	1	1.170	-12.30

The longitudinal free field distribution from Fig. 5(a) is given
in Table 14. It was assumed that the maximum pressure at any
longitudinal station was defined by Fig. 5(a), along the grid
line (ℓ=1). It was also assumed that the circumferential free
field distribution could be applied at any longitudinal station,
so that the pressure amplitude at all grid points could be
calculated. A maximum sound pressure level of 134 dB was
assumed for the array as a whole. The actual value of the
maximum level was not critical to the analysis because only
noise reduction was being calculated. The 134 dB level was
chosen as a typical value used in the test program.

Phase angle data were not available from the Metro II test.
Consequently, an analytical model had to be constructed for
relative phase angle at each frequency of interest. This was
accomplished by assuming that the sound field consisted of
spherical waves originating in the horn. The distance from horn
to the grid fuselage structure was calculated for each grid
point and converted to relative phase using the appropriate
values for the speed of sound and frequency. In this case the
relative phase angle is the same for similar grid points above
and below the grid longitudinal centerline; the two phase angles
would have different values for propeller noise because of pro-
peller rotation.

The "blocked" pressure amplitude and phase calculated for the
frequencies 383, 766 and 1149 Hz are shown in Table 15. It can
be seen that the amplitude falls off 11 - 12 dB over the axial
distance covered by the grid points.

PROPELLER HARMONIC 1 AT 343.0 HZ

CIRCUM. LOCATION L	THETA	AXIAL LOCATION K= 1 Z=2.439	2 2.586	3 2.732	4 2.878	5 3.025	6 3.171	7 3.317	8 3.464	9 3.610	10 3.756	11 3.902	12 4.049	13 4.195	14 4.341	15 4.488	16 4.634
						PRESSURE AMPLITUDE, DB RE 20 MICRO PA											
19	180.00	110.4	112.8	114.7	116.8	118.5	119.8	120.6	121.1	120.6	119.8	118.5	116.8	114.7	112.8	110.4	108.8
18	170.00	112.2	114.5	116.5	118.6	120.3	121.6	122.4	122.9	122.4	121.6	120.3	118.6	116.5	114.5	112.2	110.6
17	160.00	113.3	115.7	117.6	119.7	121.4	122.7	123.5	124.0	123.5	122.7	121.4	119.7	117.6	115.7	113.3	111.7
16	150.00	116.2	118.6	120.6	122.7	124.4	125.8	126.6	127.1	126.6	125.8	124.4	122.7	120.6	118.6	116.2	114.5
15	140.00	119.1	121.5	123.5	125.7	127.4	128.8	129.6	130.1	129.6	128.8	127.4	125.7	123.5	121.5	119.1	117.4
14	130.00	122.2	124.6	126.6	128.8	130.5	131.8	132.7	133.2	132.7	131.8	130.5	128.8	126.6	124.6	122.2	120.5
13	120.00	125.1	127.5	129.5	131.7	133.3	134.7	135.6	136.0	135.6	134.7	133.3	131.7	129.5	127.5	125.1	123.5
12	110.00	127.9	130.3	132.3	134.4	136.1	137.4	138.3	138.7	138.3	137.4	136.1	134.4	132.3	130.3	127.9	126.3
11	100.00	129.0	131.4	133.3	135.5	137.1	138.5	139.3	139.8	139.3	138.5	137.1	135.5	133.3	131.4	129.0	127.3
10	90.00	129.2	131.6	133.6	135.7	137.3	138.7	139.5	140.0	139.5	138.7	137.3	135.7	133.6	131.6	129.2	127.6
9	80.00	129.0	131.4	133.3	135.5	137.1	138.5	139.3	139.8	139.3	138.5	137.1	135.5	133.3	131.4	129.0	127.3
8	70.00	127.9	130.3	132.3	134.4	136.1	137.4	138.3	138.7	138.3	137.4	136.1	134.4	132.3	130.3	127.9	126.3
7	60.00	125.1	127.5	129.5	131.7	133.3	134.7	135.6	136.0	135.6	134.7	133.3	131.7	129.5	127.5	125.1	123.5
6	50.00	122.2	124.6	126.6	128.8	130.5	131.8	132.7	133.2	132.7	131.8	130.5	128.8	126.6	124.6	122.2	120.5
5	40.00	119.1	121.5	123.5	125.7	127.4	128.8	129.6	130.1	129.6	128.8	127.4	125.7	123.5	121.5	119.1	117.4
4	30.00	116.2	118.6	120.6	122.7	124.4	125.8	126.6	127.1	126.6	125.8	124.4	122.7	120.6	118.6	116.2	114.5
3	20.00	113.3	115.7	117.6	119.7	121.4	122.7	123.5	124.0	123.5	122.7	121.4	119.7	117.6	115.7	113.3	111.7
2	10.00	112.2	114.5	116.5	118.6	120.3	121.6	122.4	122.9	122.4	121.6	120.3	118.6	116.5	114.5	112.2	110.6
1	0.00	110.4	112.8	114.7	116.8	118.5	119.8	120.6	121.1	120.6	119.8	118.5	116.8	114.7	112.8	110.4	108.8
						PHASE (DEGREES)											
19	180.00	128.2	105.8	86.3	70.1	57.3	48.1	42.5	40.6	42.5	48.1	57.3	70.1	86.3	105.8	128.2	153.6
18	170.00	77.2	53.5	32.9	15.8	2.2	352.4	346.4	344.4	346.4	352.4	2.2	15.8	32.9	53.5	77.2	103.9
17	160.00	25.0	359.9	338.0	319.8	305.3	294.8	288.4	286.2	288.4	294.8	305.3	319.8	338.0	359.9	25.0	53.1
16	150.00	333.1	306.4	283.1	263.6	248.0	236.7	229.9	227.6	229.9	236.7	248.0	263.6	283.1	306.4	333.1	2.9
15	140.00	283.3	254.9	230.1	209.1	192.3	180.1	172.7	170.2	172.7	180.1	192.3	209.1	230.1	254.9	283.3	314.9
14	130.00	237.7	207.6	181.0	158.5	140.5	127.4	119.3	116.5	119.3	127.4	140.5	158.5	181.0	207.6	237.7	271.1
13	120.00	198.6	166.8	138.6	114.6	95.3	81.2	72.5	69.6	72.5	81.2	95.3	114.6	138.6	166.8	198.6	233.7
12	110.00	168.4	135.1	105.5	80.2	59.8	44.7	35.5	32.4	35.5	44.7	59.8	80.2	105.5	135.1	168.4	205.0
11	100.00	149.2	114.9	84.3	58.1	36.9	21.2	11.6	8.4	11.6	21.2	36.9	58.1	84.3	114.9	149.2	186.8
10	90.00	142.7	108.0	77.0	50.5	29.0	13.1	3.3	0.0	3.3	13.1	29.0	50.5	77.0	108.0	142.7	-179.4
9	80.00	149.2	114.9	84.3	58.1	36.9	21.2	11.6	8.4	11.6	21.2	36.9	58.1	84.3	114.9	149.2	-173.2
8	70.00	168.4	135.1	105.5	80.2	59.8	44.7	35.5	32.4	35.5	44.7	59.8	80.2	105.5	135.1	168.4	-155.0
7	60.00	-161.4	166.8	138.6	114.6	95.3	81.2	72.5	69.6	72.5	81.2	95.3	114.6	138.6	166.8	-161.4	-126.3
6	50.00	-122.3	-152.4	-179.0	158.5	140.5	127.4	119.3	116.5	119.3	127.4	140.5	158.5	-179.0	-152.4	-122.3	-88.9
5	40.00	-76.7	-105.1	-130.0	-150.9	-167.7	-179.9	172.7	170.2	172.7	-179.9	-167.7	-150.9	-130.0	-105.1	-76.7	-45.1
4	30.00	-26.9	-53.6	-76.9	-96.4	-112.0	-123.3	-130.1	-132.4	-130.1	-123.3	-112.0	-96.4	-76.9	-53.6	-26.9	2.9
3	20.00	25.0	-.1	-22.0	-40.2	-54.7	-65.2	-71.6	-73.8	-71.6	-65.2	-54.7	-40.2	-22.0	-.1	25.0	53.1
2	10.00	77.2	53.5	32.9	15.8	2.2	-7.6	-13.6	-15.6	-13.6	-7.6	2.2	15.8	32.9	53.5	77.2	103.9
1	0.00	128.2	105.8	86.3	70.1	57.3	48.1	42.5	40.6	42.5	48.1	57.3	70.1	86.3	105.8	128.2	153.6

TABLE 15.   SIMULATED PROPELLER BLOCKED PRESSURE AMPLITUDE AND PHASE

PROPELLER HARMONIC 2 AT 766.0 HZ

CIRCUM. LOCATION	K= 1	2	3	4	5	6	AXIAL LOCATION 7	8	9	10	11	12	13	14	15	16
L THETA	Z=2.439	2.586	2.732	2.878	3.025	3.171	3.317	3.464	3.610	3.756	3.902	4.049	4.195	4.341	4.488	4.634

PRESSURE AMPLITUDE, DB RE 20 MICRO PA

L	THETA	1	2	3	4	5	6	7	8	9	10	11	12	13	14	15	16
19	180.00	110.4	112.8	114.7	116.8	118.5	119.8	120.6	121.1	120.6	119.8	118.5	116.8	114.7	112.8	110.4	108.8
18	170.00	112.2	114.5	116.5	118.6	120.3	121.6	122.4	122.9	122.4	121.6	120.3	118.6	116.5	114.5	112.2	110.6
17	160.00	113.3	115.7	117.6	119.7	121.4	122.7	123.5	124.0	123.5	122.7	121.4	119.7	117.6	115.7	113.3	111.7
16	150.00	116.2	118.6	120.6	122.7	124.4	125.8	126.6	127.1	126.6	125.8	124.4	122.7	120.6	118.6	116.2	114.5
15	140.00	119.1	121.5	123.5	125.7	127.4	128.8	129.6	130.1	129.6	128.8	127.4	125.7	123.5	121.5	119.1	117.4
14	130.00	122.2	124.6	126.6	128.8	130.5	131.8	132.7	133.2	132.7	131.8	130.5	128.8	126.6	124.6	122.2	120.5
13	120.00	125.1	127.5	129.5	131.7	133.3	134.7	135.6	136.0	135.6	134.7	133.3	131.7	129.5	127.5	125.1	123.5
12	110.00	127.9	130.3	132.3	134.4	136.1	137.4	138.3	138.7	138.3	137.4	136.1	134.4	132.3	130.3	127.9	126.3
11	100.00	129.0	131.4	133.3	135.5	137.1	138.5	139.3	139.8	139.3	138.5	137.1	135.5	133.3	131.4	129.0	127.3
10	90.00	129.2	131.6	133.6	135.7	137.3	138.7	139.5	140.0	139.5	138.7	137.3	135.7	133.6	131.6	129.2	127.6
9	80.00	129.0	131.4	133.3	135.5	137.1	138.5	139.3	139.8	139.3	138.5	137.1	135.5	133.3	131.4	129.0	127.3
8	70.00	127.9	130.3	132.3	134.4	136.1	137.4	138.3	138.7	138.3	137.4	136.1	134.4	132.3	130.3	127.9	126.3
7	60.00	125.1	127.5	129.5	131.7	133.3	134.7	135.6	136.0	135.6	134.7	133.3	131.7	129.5	127.5	125.1	123.5
6	50.00	122.2	124.6	126.6	128.8	130.5	131.8	132.7	133.2	132.7	131.8	130.5	128.8	126.6	124.6	122.2	120.5
5	40.00	119.1	121.5	123.5	125.7	127.4	128.8	129.6	130.1	129.6	128.8	127.4	125.7	123.5	121.5	119.1	117.4
4	30.00	116.2	118.6	120.6	122.7	124.4	125.8	126.6	127.1	126.6	125.8	124.4	122.7	120.6	118.6	116.2	114.5
3	20.00	113.3	115.7	117.6	119.7	121.4	122.7	123.5	124.0	123.5	122.7	121.4	119.7	117.6	115.7	113.3	111.7
2	10.00	112.2	114.5	116.5	118.6	120.3	121.6	122.4	122.9	122.4	121.6	120.3	118.6	116.5	114.5	112.2	110.6
1	0.00	110.4	112.8	114.7	116.8	118.5	119.8	120.6	121.1	120.6	119.8	118.5	116.8	114.7	112.8	110.4	108.8

PHASE (DEGREES)

L	THETA	1	2	3	4	5	6	7	8	9	10	11	12	13	14	15	16
19	180.00	256.5	211.5	172.6	140.2	114.7	96.2	85.0	81.3	85.0	96.2	114.7	140.2	172.6	211.5	256.5	307.2
18	170.00	154.4	107.0	65.9	31.6	4.4	344.8	332.9	328.9	332.9	344.8	4.4	31.6	65.9	107.0	154.4	207.7
17	160.00	50.0	359.7	316.1	279.5	250.5	229.5	216.8	212.5	216.8	229.5	250.5	279.5	316.1	359.7	50.0	106.2
16	150.00	306.2	252.8	206.2	167.1	136.0	113.4	99.7	95.1	99.7	113.4	136.0	167.1	206.2	252.8	306.2	5.8
15	140.00	206.6	149.8	100.1	58.2	24.7	.3	345.5	340.5	345.5	.3	24.7	58.2	100.1	149.8	206.6	269.7
14	130.00	115.4	55.1	2.0	317.1	281.1	254.7	238.7	233.3	238.7	254.7	281.1	317.1	2.0	55.1	115.4	182.2
13	120.00	37.3	333.5	277.2	229.2	190.7	162.4	145.0	139.2	145.0	162.4	190.7	229.2	277.2	333.5	37.3	107.5
12	110.00	336.8	270.2	211.0	160.4	119.6	89.5	71.0	64.8	71.0	89.5	119.6	160.4	211.0	270.2	336.8	50.0
11	100.00	298.5	229.8	168.7	116.3	73.8	42.4	23.2	16.7	23.2	42.4	73.8	116.3	168.7	229.8	298.5	13.6
10	90.00	-74.7	-144.1	154.1	101.0	58.0	26.1	6.6	0.0	6.6	26.1	58.0	101.0	154.1	-144.1	-74.7	1.1
9	80.00	-61.5	-130.2	168.7	116.3	73.8	42.4	23.2	16.7	23.2	42.4	73.8	116.3	168.7	-130.2	-61.5	13.6
8	70.00	-23.2	-89.8	-149.0	160.4	119.6	89.5	71.0	64.8	71.0	89.5	119.6	160.4	-149.0	-89.8	-23.2	50.0
7	60.00	37.3	-26.5	-82.8	-130.8	-169.3	162.4	145.0	139.2	145.0	162.4	-169.3	-130.8	-82.8	-26.5	37.3	107.5
6	50.00	115.4	55.1	2.0	-42.9	-78.9	-105.3	-121.3	-126.7	-121.3	-105.3	-78.9	-42.9	2.0	55.1	115.4	-177.8
5	40.00	-153.4	149.8	100.1	58.2	24.7	.3	-14.5	-19.5	-14.5	.3	24.7	58.2	100.1	149.8	-153.4	-90.3
4	30.00	-53.8	-107.2	-153.8	167.1	136.0	113.4	99.7	95.1	99.7	113.4	136.0	167.1	-153.8	-107.2	-53.8	5.8
3	20.00	50.0	-.3	-43.9	-80.5	-109.5	-130.5	-143.2	-147.5	-143.2	-130.5	-109.5	-80.5	-43.9	-.3	50.0	106.2
2	10.00	154.4	107.0	65.9	31.6	4.4	-15.2	-27.1	-31.1	-27.1	-15.2	4.4	31.6	65.9	107.0	154.4	-152.3
1	0.00	-103.5	-148.5	172.6	140.2	114.7	96.2	85.0	81.3	85.0	96.2	114.7	140.2	172.6	-148.5	-103.5	-52.8

TABLE 15. CONTINUED

PROPELLER HARMONIC 3 AT 1149.0 HZ

CIRCUM. LOCATION		AXIAL LOCATION														
LOCATION	K= 1	2	3	4	5	6	7	8	9	10	11	12	13	14	15	16
L THETA	Z=2.439	2.586	2.732	2.878	3.025	3.171	3.317	3.464	3.610	3.756	3.902	4.049	4.195	4.341	4.488	4.634

PRESSURE AMPLITUDE, DB RE 20 MICRO PA

L THETA	1	2	3	4	5	6	7	8	9	10	11	12	13	14	15	16
19 180.00	110.4	112.8	114.7	116.8	118.5	119.8	120.6	121.1	120.6	119.8	118.5	116.8	114.7	112.8	110.4	108.8
18 170.00	112.2	114.5	116.5	118.6	120.3	121.6	122.4	122.9	122.4	121.6	120.3	118.6	116.5	114.5	112.2	110.6
17 160.00	113.3	115.7	117.6	119.7	121.4	122.7	123.5	124.0	123.5	122.7	121.4	119.7	117.6	115.7	113.3	111.7
16 150.00	116.2	118.6	120.6	122.7	124.4	125.8	126.6	127.1	126.6	125.8	124.4	122.7	120.6	118.6	116.2	114.5
15 140.00	119.1	121.5	123.5	125.7	127.4	128.8	129.6	130.1	129.6	128.8	127.4	125.7	123.5	121.5	119.1	117.4
14 130.00	122.2	124.6	126.6	128.8	130.5	131.8	132.7	133.2	132.7	131.8	130.5	128.8	126.6	124.6	122.2	120.5
13 120.00	125.1	127.5	129.5	131.7	133.3	134.7	135.6	136.0	135.6	134.7	133.3	131.7	129.5	127.5	125.1	123.5
12 110.00	127.9	130.3	132.3	134.4	136.1	137.4	138.3	138.7	138.3	137.4	136.1	134.4	132.3	130.3	127.9	126.3
11 100.00	129.0	131.1	133.3	135.5	137.1	138.5	139.3	139.8	139.3	138.5	137.1	135.5	133.3	131.1	129.0	127.3
10 90.00	129.2	131.6	133.6	135.7	137.1	138.7	139.5	140.0	139.5	138.7	137.3	135.7	133.6	131.6	129.2	127.6
9 80.00	129.0	131.4	133.3	135.5	137.1	138.5	139.3	139.8	139.3	138.5	137.1	135.5	133.3	131.4	129.0	127.3
8 70.00	127.9	130.3	132.3	134.4	136.1	137.4	138.3	138.7	138.3	137.4	136.1	134.4	132.3	130.3	127.9	126.3
7 60.00	125.1	127.5	129.5	131.7	133.3	134.7	135.6	136.0	135.6	134.7	133.3	131.7	129.5	127.5	125.1	123.5
6 50.00	122.2	124.6	126.6	128.8	130.5	131.8	132.7	133.2	132.7	131.8	130.5	128.8	126.6	124.6	122.2	120.5
5 40.00	119.1	121.5	123.5	125.7	127.4	128.8	129.6	130.1	129.6	128.8	127.4	125.7	123.5	121.5	119.1	117.4
4 30.00	116.2	118.6	120.6	122.7	124.4	125.8	126.6	127.1	126.6	125.8	124.4	122.7	120.6	118.6	116.2	114.5
3 20.00	113.3	115.7	117.6	119.7	121.4	122.7	123.5	124.0	123.5	122.7	121.4	119.7	117.6	115.7	113.3	111.7
2 10.00	112.2	114.5	116.5	118.6	120.3	121.6	122.4	122.9	122.4	121.6	120.3	118.6	116.5	114.5	112.2	110.6
1 0.00	110.4	112.8	114.7	116.8	118.5	119.8	120.6	121.1	120.6	119.8	118.5	116.8	114.7	112.8	110.4	108.8

PHASE (DEGREES)

L THETA	1	2	3	4	5	6	7	8	9	10	11	12	13	14	15	16
19 180.00	24.7	317.3	259.0	210.4	172.0	144.3	127.5	121.9	127.5	144.3	172.0	210.4	259.0	317.3	24.7	100.8
18 170.00	231.6	160.5	98.8	47.4	6.6	337.2	319.3	313.3	319.3	337.2	6.6	47.4	98.8	160.5	231.6	311.6
17 160.00	74.9	359.6	294.1	239.3	195.8	164.3	145.2	138.7	145.2	164.3	195.8	239.3	294.1	359.6	74.9	159.4
16 150.00	279.2	199.2	129.4	70.7	24.1	350.2	329.6	322.7	329.6	350.2	24.1	70.7	129.4	199.2	279.2	8.6
15 140.00	129.9	44.7	330.2	267.2	217.9	180.4	158.2	150.7	158.2	180.4	217.0	267.2	330.2	44.7	129.9	224.6
14 130.00	353.2	262.7	183.1	115.6	61.6	22.1	358.0	349.9	358.0	22.1	61.6	115.6	183.1	262.7	353.2	93.3
13 120.00	235.9	140.3	55.8	343.9	286.0	243.5	217.6	208.8	217.6	243.5	286.0	343.9	55.8	140.3	235.9	341.2
12 110.00	145.3	45.2	316.5	240.6	179.3	134.2	106.6	97.2	106.6	134.2	179.3	240.6	316.5	45.2	145.3	255.0
11 100.00	87.7	344.7	253.0	174.4	110.7	63.7	34.8	25.1	34.8	63.7	110.7	174.4	253.0	344.7	87.7	200.4
10 90.00	68.0	-36.1	-128.9	151.5	86.9	39.2	9.9	0.0	9.9	39.2	86.9	151.5	-128.9	-36.1	68.0	-178.3
9 80.00	87.7	-15.3	-107.0	174.4	110.7	63.7	34.8	25.1	34.8	63.7	110.7	174.4	-107.0	-15.3	87.7	-159.6
8 70.00	145.3	45.2	-43.5	-119.4	179.3	134.2	106.6	97.2	106.6	134.2	179.3	-119.4	-43.5	45.2	145.3	-105.0
7 60.00	-124.1	140.3	55.8	-16.1	-74.0	-116.5	-142.4	-151.2	-142.4	-116.5	-74.0	-16.1	55.8	140.3	-124.1	-18.8
6 50.00	-6.8	-77.3	-176.9	115.6	51.6	22.1	-2.0	-10.1	-2.0	22.1	61.6	115.6	-176.9	-97.3	-6.8	93.3
5 40.00	129.9	44.7	-29.9	-92.8	-143.0	-179.6	158.2	150.7	158.2	-179.6	-143.0	-92.8	-29.9	44.7	129.9	-135.4
4 30.00	-80.8	-160.8	129.4	70.7	24.1	-9.8	-30.4	-37.3	-30.4	-9.8	24.1	70.7	129.4	-160.8	-80.8	8.6
3 20.00	74.9	-.4	-65.9	-120.7	-164.2	164.3	145.2	138.7	145.2	164.3	-164.2	-120.7	-65.9	-.4	74.9	159.4
2 10.00	-128.4	160.5	98.8	47.4	6.6	-22.9	-40.7	-46.7	-40.7	-22.9	6.6	47.4	98.8	160.5	-128.4	-48.4
1 0.00	24.7	-42.7	-101.0	-149.6	172.0	144.3	127.5	121.9	127.5	144.3	172.0	-149.6	-101.0	-42.7	24.7	100.8

-74-

TABLE 15. CONTINUED

6.0 PREDICTED AND MEASURED NOISE REDUCTIONS FOR METRO II TEST

Nine test conditions were considered by Prydz et al [5] in the Metro II experimental program. These configurations are listed in Table 5. The first seven configurations are associated with either a floating or a disconnected trim panel. Since the analytical model assumes that there is no structureborne path between the fuselage structure and the trim panel, it forms a reasonably good representation of the floating trim. Thus, comparisons between measured and predicted noise reductions have been restricted to Configurations 1 through 7.

The computations were performed at six discrete frequencies. Three of these frequencies were the same as those used in the Metro II tests [5], i.e., 383, 766, and 1149 Hz. The frequencies were computed as harmonics of a fundamental frequency of 191.5 Hz. Following the criterion given in Section 2.2, the low frequency form of the analytical model was applied at frequencies below 630 Hz and the high frequency form at frequencies above 630 Hz.

The peak exterior sound pressure level was assumed to be 134 dB at each frequency. This value represents a free-field sound pressure level and is consistent with the Metro II data [5]. Space-average sound pressure levels were calculated for the interior of the test fuselage and noise reduction computed by taking the difference between the exterior free field level of 134 dB and the interior space-average level [5]. The relationship between the free-field and blocked pressures is given by Eq.(48). The relationship corresponds to empirical data of Magliozzi [15].

The analytical model described herein and in Ref.[1] considers the fuselage cylindrical shell and cabin floor as a single unit. Thus the modeling of the floor is important to the computation

of noise reduction. The floor used in the test fuselage, described in Sections 3.2 and 4.0, is of unusual construction and installation relative to normal aircraft design. Thus, the appropriate analytical modeling of the floor has been of concern in the present study.

In summary, the test floor is a heavy, stiff structure which is either mounted on vibration isolators or attached to the fuselage frames by means of brackets. Certain assumptions introduced in the modeling are discussed in Section 4.0. In addition, the floor treatment transmission coefficient, τ_F, described in Section 2.2 can be used as a means of representing vibration isolation provided by the air mounts supporting the floating floor.

The influence of the floor treatment transmission coefficient can be seen in Figures 18 through 20 which compare predicted noise reductions for Configurations 1 through 6. The noise reductions were computed for four values of the floor treatment transmission coefficient, of which transmission losses of 0, 20 and 400 dB are shown in the figures. The transmission loss of 0 dB represents the case where the untreated floor is rigidly attached to the fuselage shell, and the transmission loss of 400 dB represents, essentially, a situation where there is no acoustic transmission via the floor structure. The intermediate, 20 dB, case is a possible model for the floating floor of the test structure.

Inspection of Figures 18 through 20 shows that the influence of the floor can dominate the noise transmission into the fuselage interior if zero transmission loss is assumed for the floor treatment (or mounts). Thus, in Figure 18, increases in the sidewall treatment transmission loss have little or no effect on the noise reduction for the fuselage as a whole. As the assumed transmission loss through the floor installation is increased,

(a) Baseline Fuselage Structure

Floor TL = 0 dB

Config.
#2,3
#1

Noise Reduction, dB

Frequency, Hz

(b) Heavy Fuselage Structure

Floor TL = 0 dB

Config.
#5,6
#4

Noise Reduction, dB

Frequency, Hz
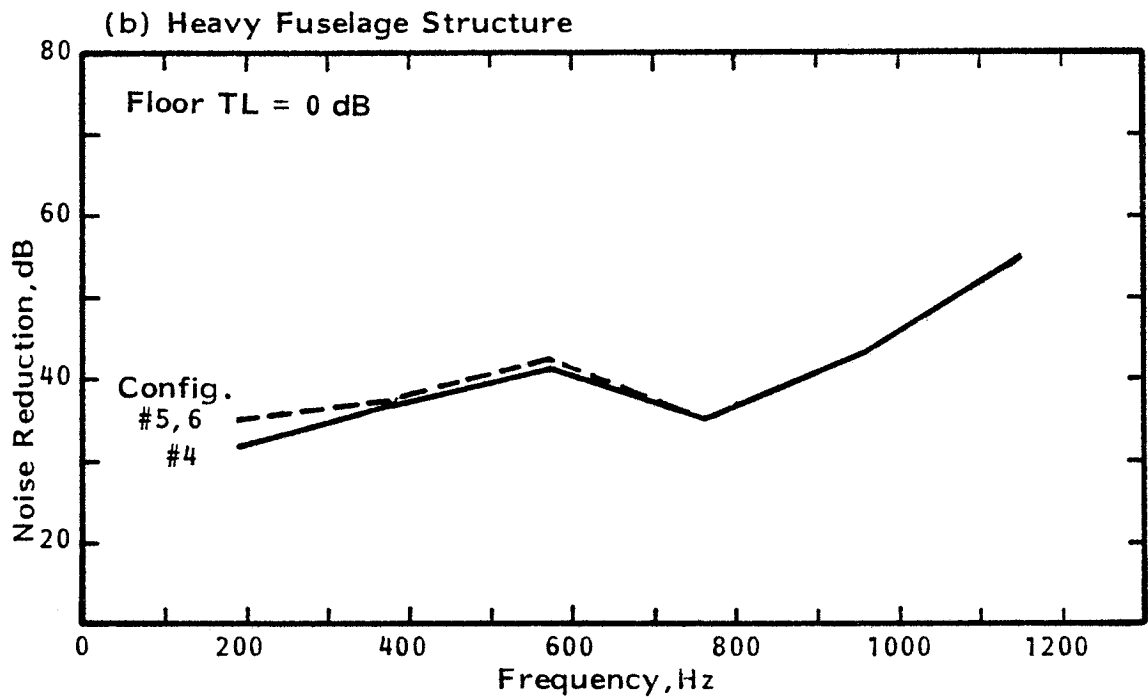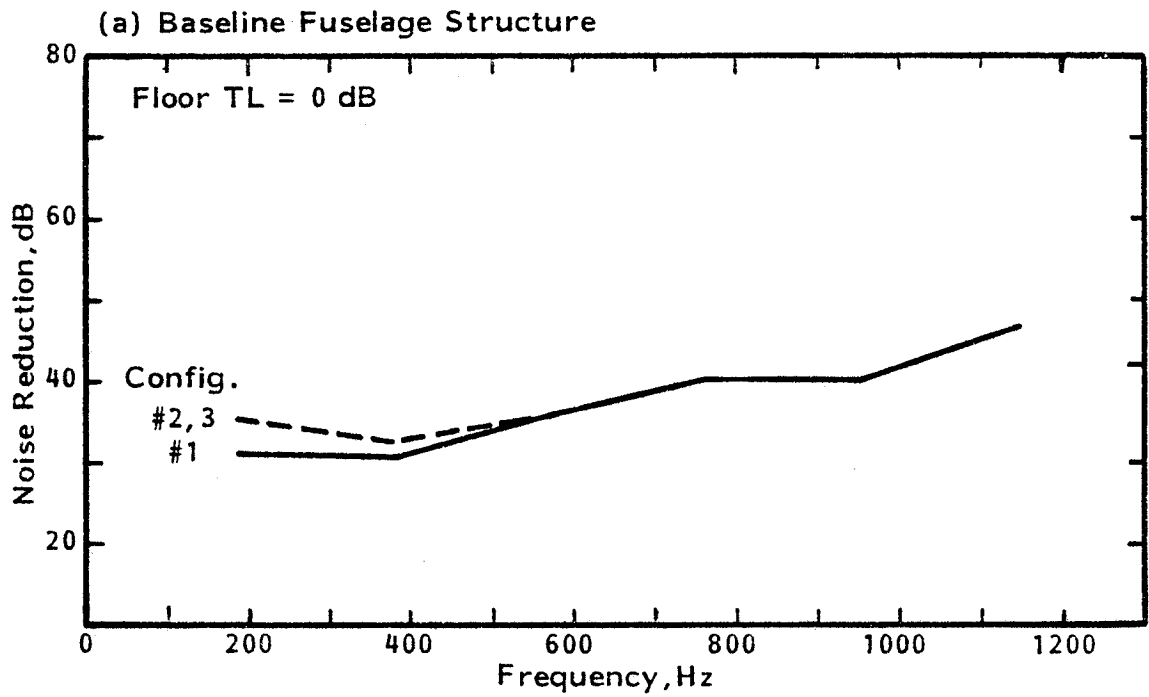
FIGURE 18.   PREDICTED NOISE REDUCTIONS FOR METRO II TEST FUSELAGE
EXPOSED TO ELECTROPNEUMATIC EXCITATION
(Floor Treatment Transmission Loss = 0 dB)

(a) Baseline Fuselage Structure

Floor TL = 20 dB

Config.
#3
#2
#1

(b) Heavy Fuselage Structure

Floor TL = 20 dB

Config.
#6
#5
#4
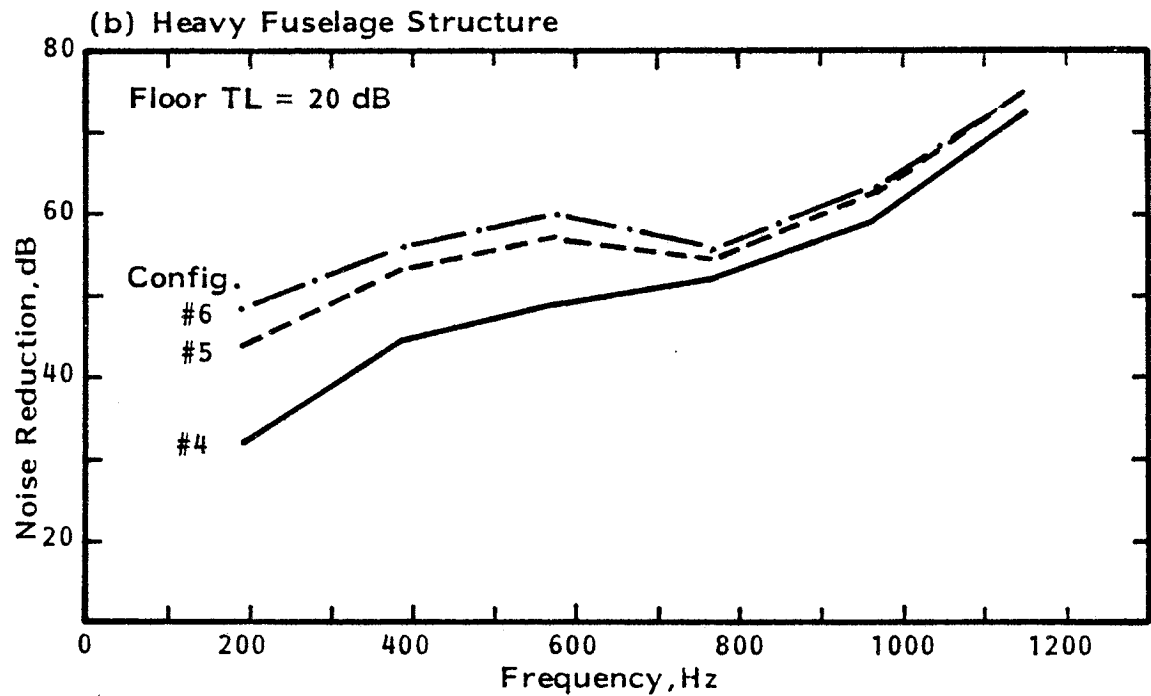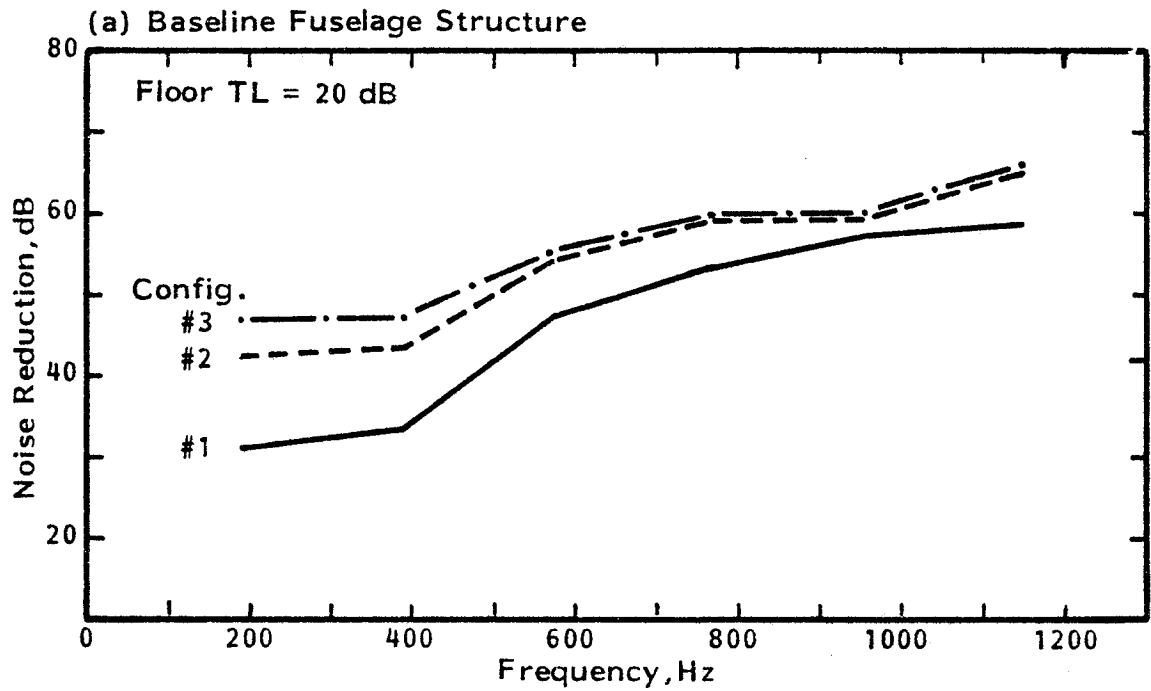
FIGURE 19. PREDICTED NOISE REDUCTIONS FOR METRO II TEST FUSELAGE EXPOSED TO ELECTROPNEUMATIC EXCITATION (Floor Treatment Transmission Loss = 20 dB)

(a) Baseline Fuselage Structure

Floor TL = 400 dB

Config.
#3
#2
#1

(b) Heavy Fuselage Structure

Floor TL = 400 dB

Config.
#6
#5
#4
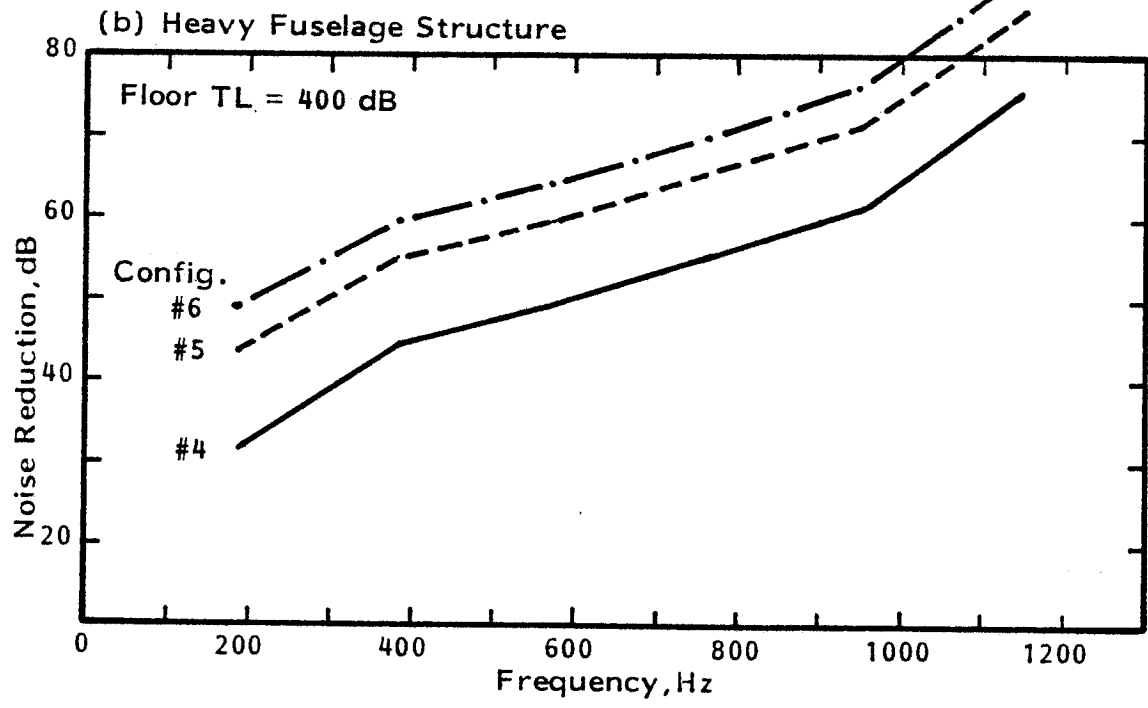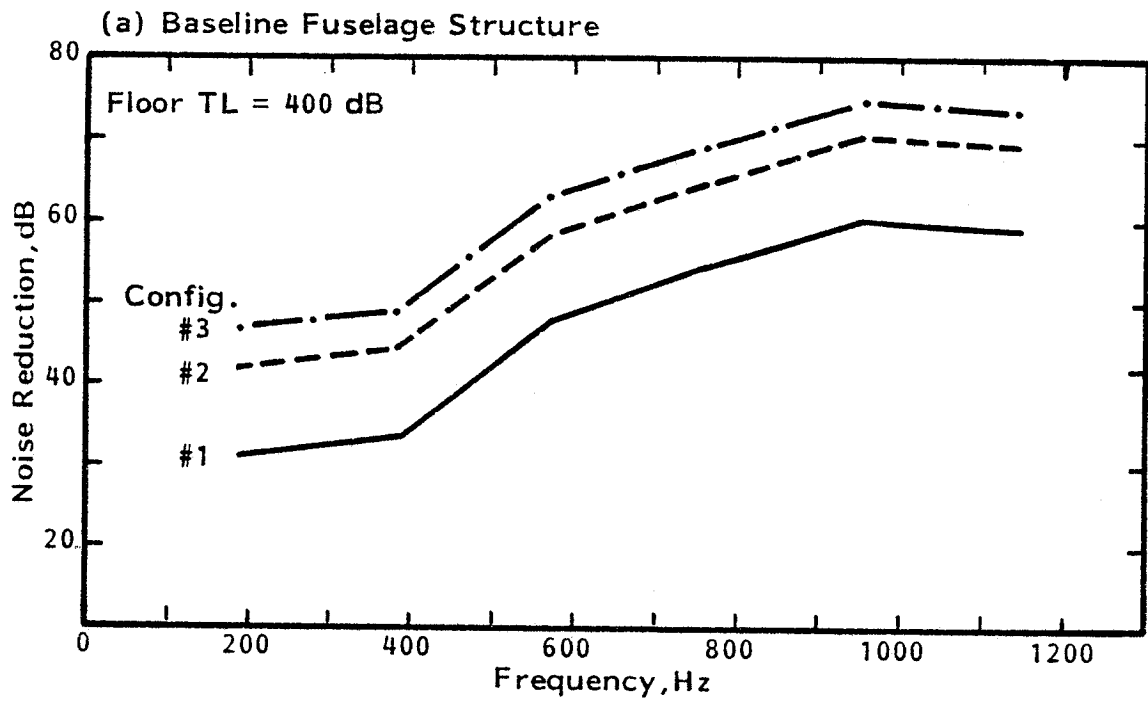
FIGURE 20. PREDICTED NOISE REDUCTIONS FOR METRO II TEST FUSELAGE
EXPOSED TO ELECTROPNEUMATIC EXCITATION
(Floor Treatment Transmission Loss = 400 dB)

-79-

the sidewall treatment has greater influence. The full benefit
of the sidewall treatment is achieved only when the floor treat-
ment transmission loss is of similar magnitude. The predicted
transmission loss provided by the sidewall treatment alone is
represented by the trim factor plotted in Figure 21. The trim
factor is defined as $10 \log (1/\tau_t)$ where τ_t is the trim trans-
mission coefficient discussed in Section 2.2 and in Appendix A
of Ref.[1]. Figure 21 contains predicted trim factor spectra
for the three sidewall treatments investigated in the Metro II
tests. A comparison of Figures 20 and 21 shows that the rela-
tive effect of the sidewall treatments can be seen when a high
value (400 dB) is assumed for the floor treatment transmission
loss. (It should be noted that the trim factor is not the only
parameter describing the effect of the sidewall treatment on
noise transmission into the cabin. The analytical model also
allows the treatment to influence the response of the outer
structure through the structural loss factor η_r', Eq.(17)).

The noise reduction spectra shown in Figures 18 through 20 can
be superimposed on the corresponding measured noise reductions
[5] for Configurations 1 through 6. The comparison is shown in
Figure 22. The immediate observation is that, by choosing
appropriate values for the floor treatment transmission loss,
the predicted noise reductions can be made to envelope the
measured values. The closest agreement between predicted and
measured noise reductions for the Configurations (1 through 3)
with the baseline outer wall is achieved when the floor
treatment transmission loss is about 20 dB. A somewhat higher
value is appropriate for Configurations 4 through 6 for the
heavy outer wall. This difference is reasonable since the
addition of iron-oxide vinyl to the fuselage shell changes the
predicted structural modes and fuselage response.
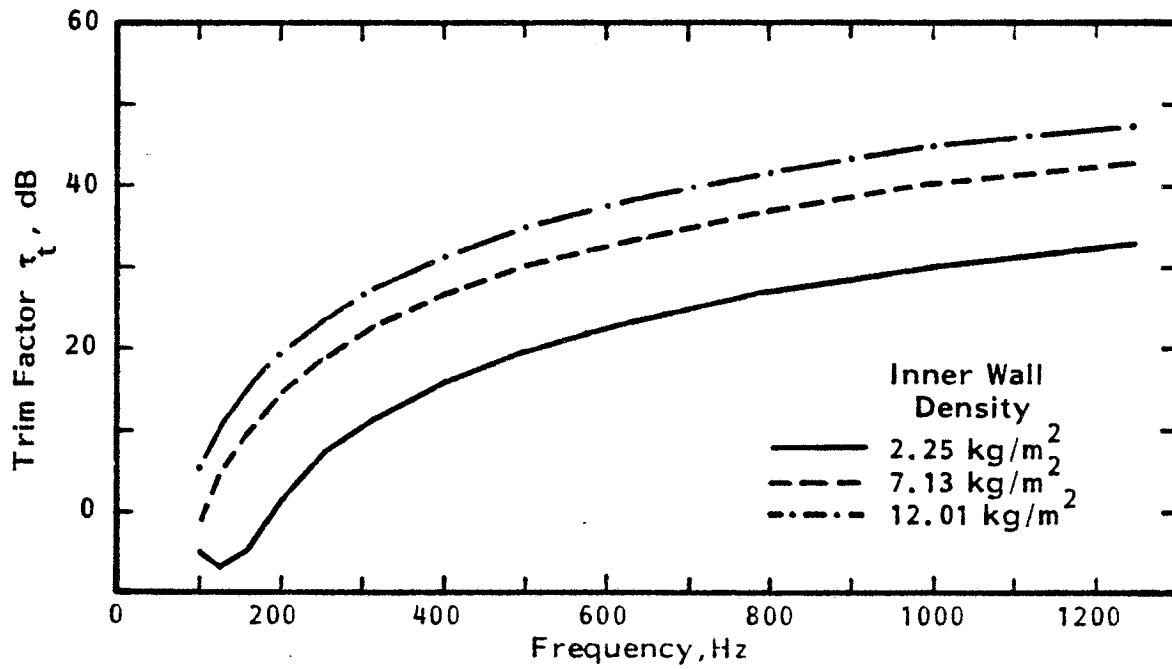
FIGURE 21. PREDICTED TRIM FACTOR (Sidewall Treatment Transmission Loss) FOR METRO II TEST TREATMENTS
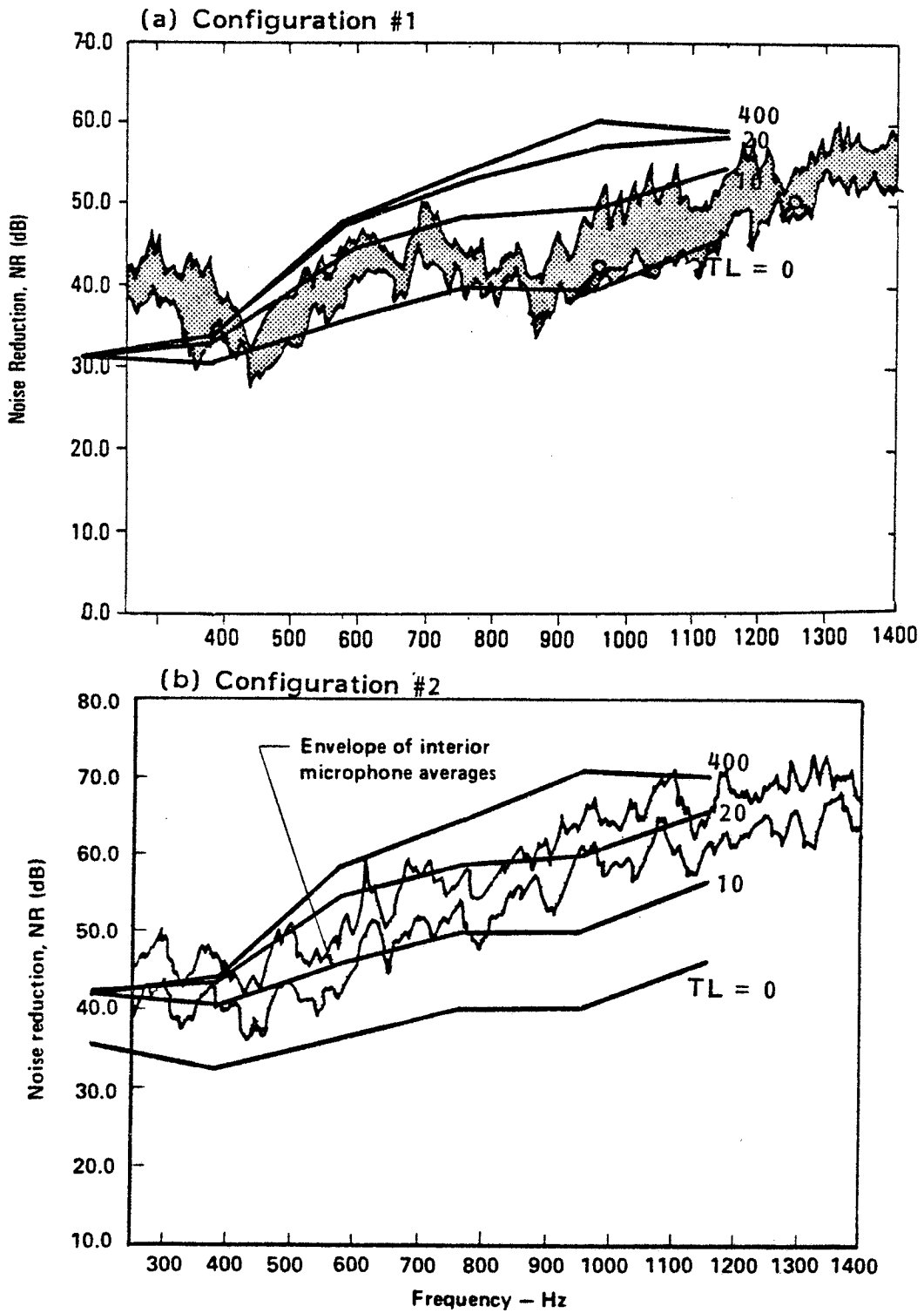
FIGURE 22. COMPARISON OF MEASURED AND PREDICTED NOISE REDUCTIONS
FOR METRO II TEST FUSELAGE AND ELECTROPNEUMATIC
EXCITATION (Different Assumed Floor Treatment Transmission Losses)

(c) Configuration #3

(d) Configuration #4

FIGURE 22.   CONTINUED

(e) Configuration #5

(f) Configuration #6
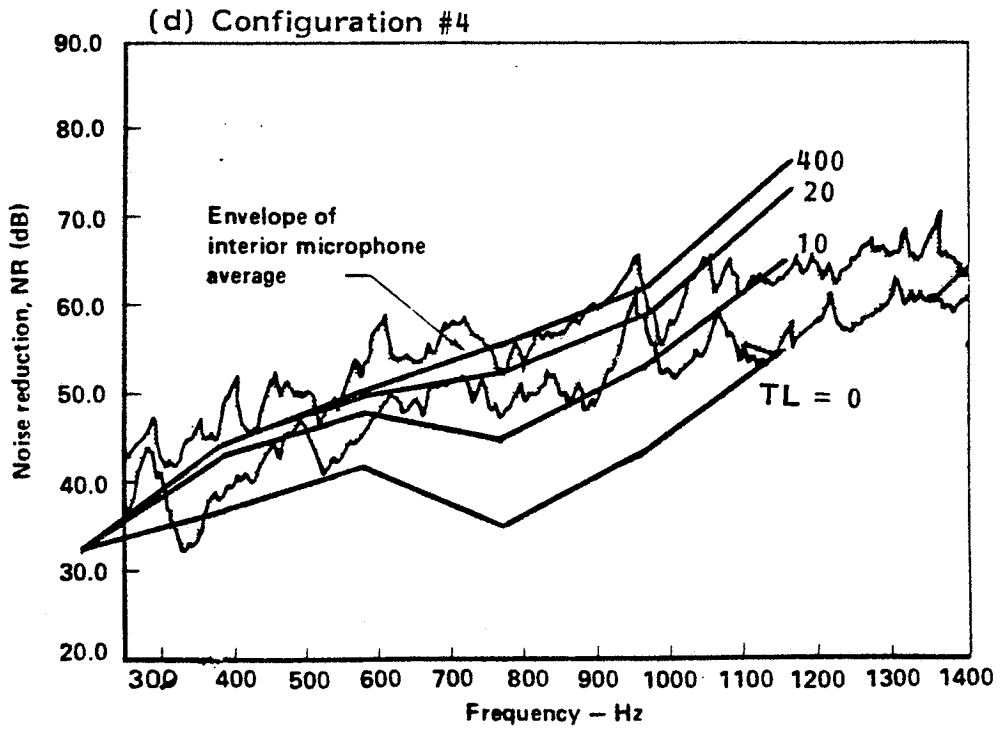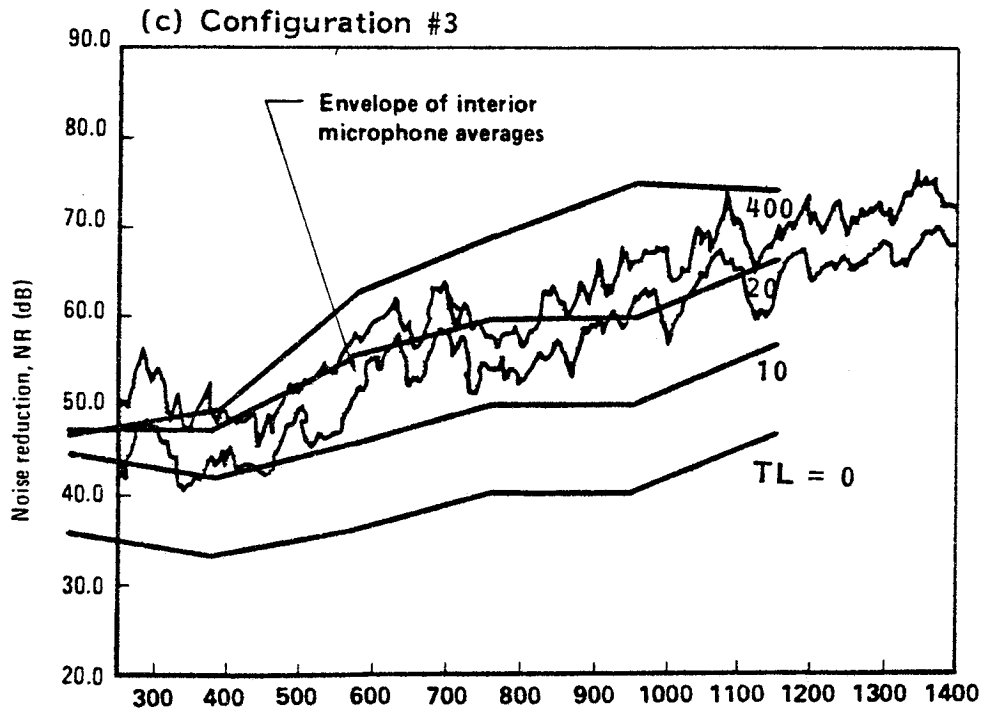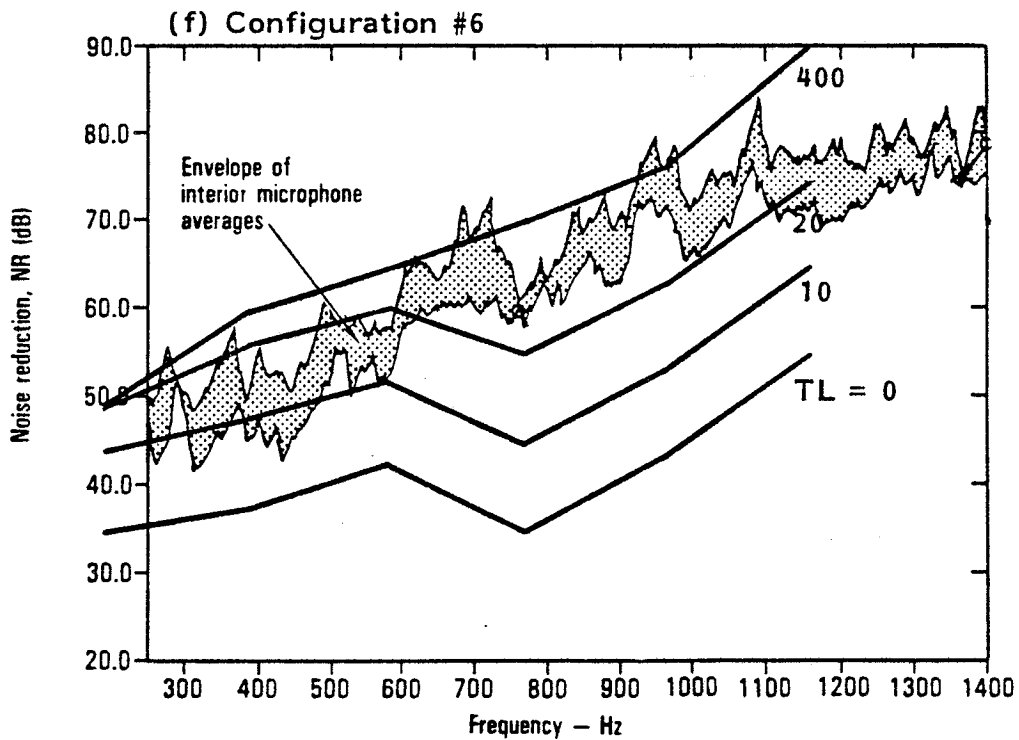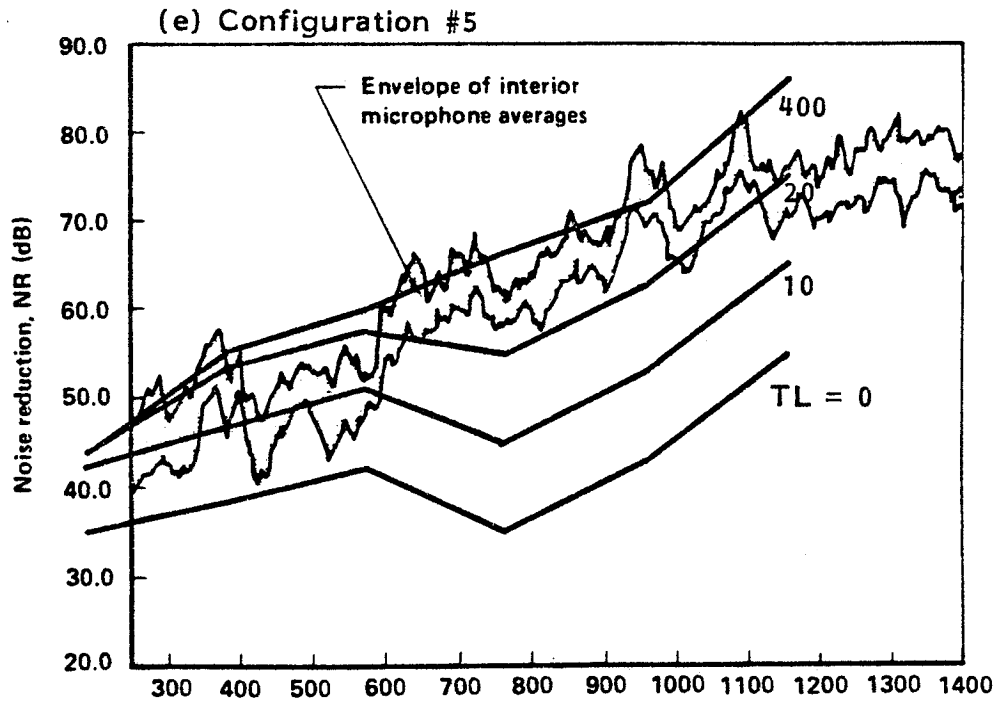
FIGURE 22.   CONTINUED

The predicted noise reduction spectra assume that the floor treatment transmission loss is independent of frequency. This is a simplification; a better fit between measured and predicted results could be achieved by making the transmission loss frequency dependent. However, such a detailed fit, although physically reasonable is considered to be outside the objective of the present comparison.

The data in Figure 22 generally show better agreement between measured and predicted noise reductions for Configurations 1 through 3, with the baseline outer wall, than for Configurations 4 through 6 for the heavy outer wall. One possible reason for this difference lies in the analytical representation for the fuselage shell. In practice, the heavy wall was achieved by bonding a sheet of iron-oxide vinyl to the fuselage skin; the analytical model assumed simply that the skin panel had an increased skin density.

Fuselage test Configuration 7 is similar to Configuration 5 with respect to the fuselage structure and sidewall treatment, except that the floor is attached directly to the fuselage shell rather than being supported on air mounts. Thus the structural modeling is different for the two configurations. Predicted noise reduction spectra, associated with Configuration 7, are shown in Figure 23 for different assumed values for the floor treatment transmission loss. The predicted results are compared with a single measured spectrum [5]. (Ref.5 does not present a range of measured noise reductions). In this case it appears that closest agreement between measured and predicted noise reductions occurs for a floor treatment transmission loss of 10 dB rather than the 20 dB or higher value appropriate to the floating floor configurations. This reduction in effective floor treatment transmission loss is consistent with test data (Figure 76 of [5]), reproduced in Figure 24, which show that the vibration levels measured on the attached floor are higher than

Legend:
— Configuration No. 5 (floor/trim floating)
- - - Configuration No. 8 (trim attached)
— - — Configuration No. 7 (floor attached)
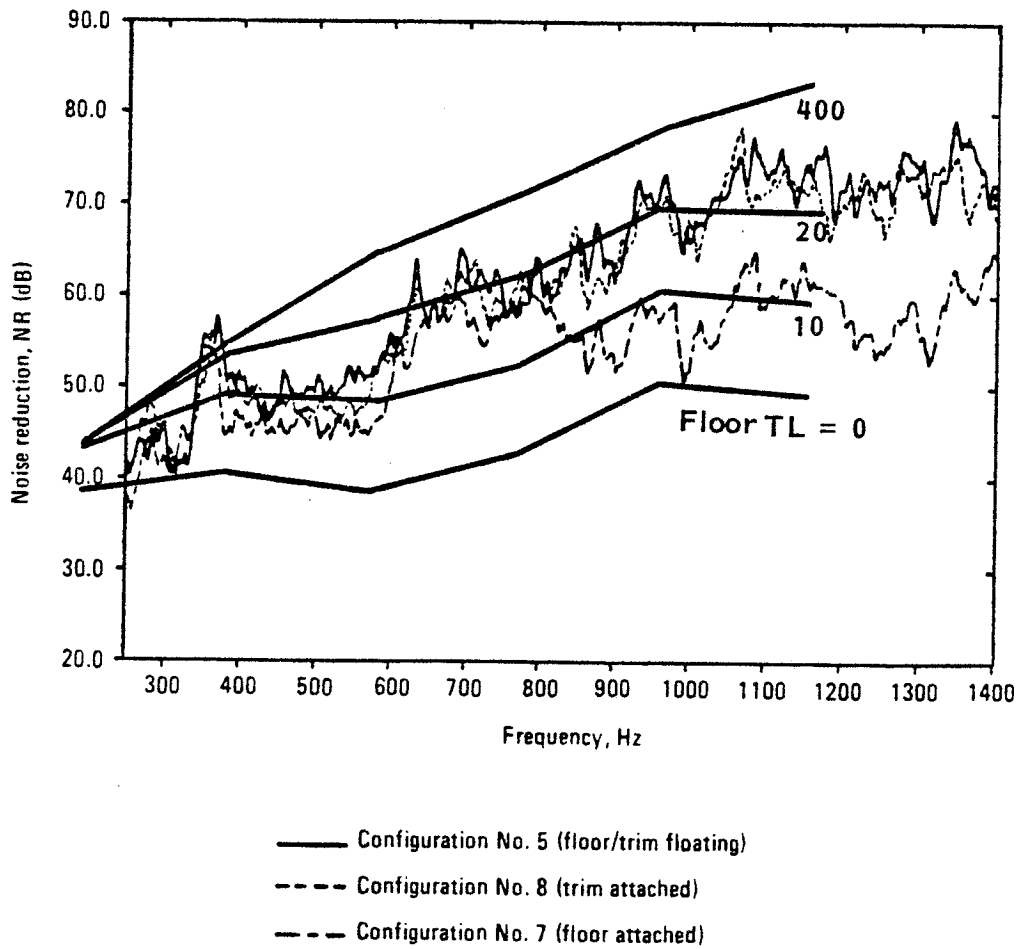
FIGURE 23. MEASURED AND PREDICTED NOISE REDUCTIONS FOR METRO II TEST CONFIGURATION WITH ATTACHED FLOOR (Configuration #7)
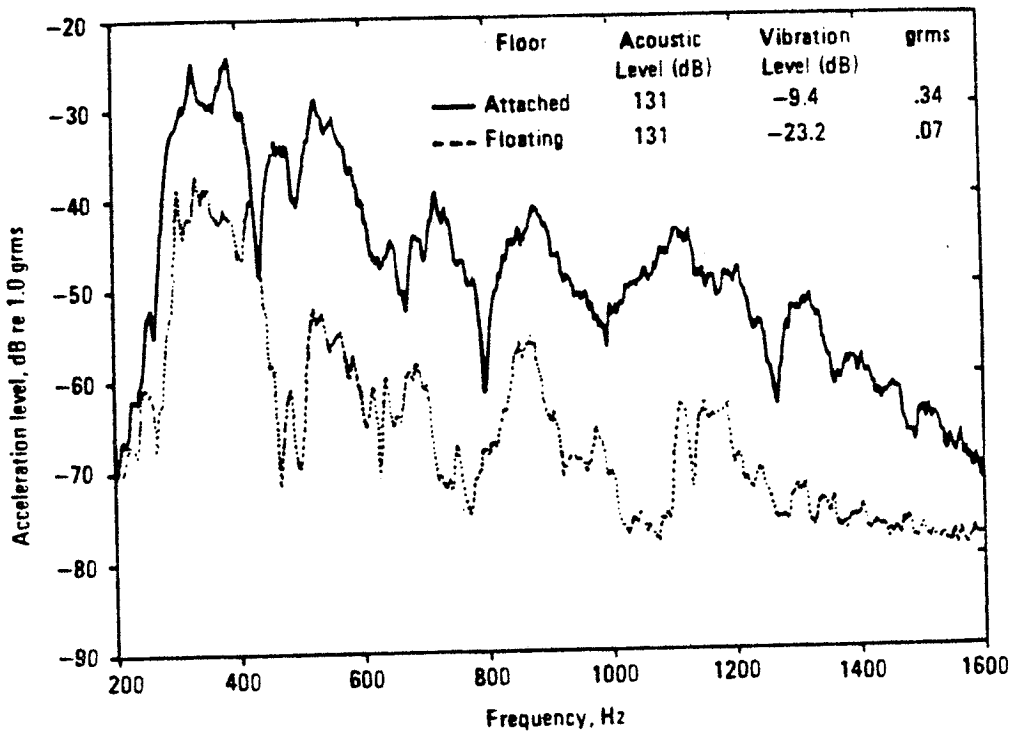
FIGURE 24. COMPARISON OF FLOOR VIBRATION LEVELS WITH AND WITHOUT
THE FLOOR ATTACHED TO THE FUSELAGE FRAMES [5]
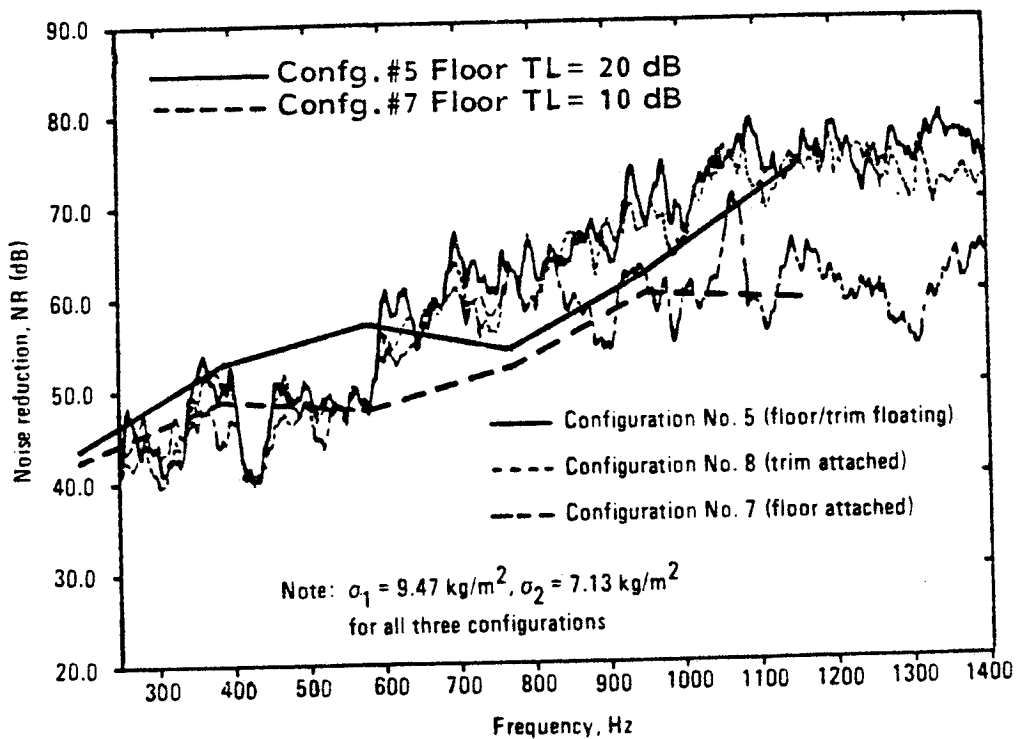
FIGURE 25. MEASURED [5] AND PREDICTED INTERIOR SOUND LEVELS
FOR DIFFERENT FLOOR MOUNTINGS

-87-

those on the floating floor. Thus, if the floor treatment transmission loss is interpreted as a representation of the isolation provided by the attachment method, it can take into account the attenuation provided by the air mounts.

Figure 25 compares predicted noise reductions for Configuration 5, assuming a floor treatment transmission loss of 20 dB, and Configuration 7, with a transmission loss of 10 dB. The figure also shows measured noise reduction spectra for the two configurations. The agreement is generally good, but it could be improved by selection of frequency-dependent transmission losses for the floor treatment parameter.

The uncertainty regarding the participation of the test floor arises because of problems encountered in the analytical modeling of the floor structure. These problems have been discussed earlier in this report but are worth repeating. First, the test floor structure did not form an integral part of the fuselage structure as it would in a production airplane and as it is modeled in the analysis. Secondly, when the floor is mounted on the air mounts, the structural mode shapes of the fuselage and floor have to be determined by modeling the test floor. However, the coupling between the modes of the floor and the cabin volume has to be modeled with the test floor represented as a vibrating partition in its actual location. Finally the air mounts will influence the vibration levels of the test floor, but such an effect is not included in the analytical model except through the floor treatment transmission coefficient. For these reasons, the test configuration does not provide a very good basis for evaluating the analytical model.

7.0 EFFECT OF EXCITATION CHARACTERISTICS

The original analytical model [1-4] utilized in this study was
constructed to represent propeller noise (deterministic) and
reverberant field (random) excitations. Then, as described in
Section 1, the model has been extended to include other excita-
tions. The discussion in Section 6 is concerned with only one
type of excitation, that associated with an electropneumatic
source with directivity designed to represent a high-speed
propeller. In the present section four other exterior pressure
fields will be considered for the Metro II fuselage, with empha-
sis being placed on test Configuration 1. These pressure fields
are:

(a) General aviation airplane propeller
(b) Turbulent boundary layer on a general aviation airplane
    fuselage
(c) Turbulent boundary layer on an ATP airplane fuselage
(d) Reverberant pressure field.

7.1 General Aviation Propeller

The propeller noise field has to be described for the analytical
model in terms of amplitude and phase over the fuselage grid-
point array shown in Figure 16. Since the prediction of such a
pressure field distribution can be time-consuming, use was made
of an existing distribution computed for a general aviation type
propeller [1]. The pressure field was then modified to fit the
dimensions of the Metro II fuselage.

Scaling of the propeller noise field was performed on the basis of cylinder or fuselage radius, while maintaining the same propeller tip speed. The reference cylinder [1] had a diameter of 1.12m (3.67 ft) and the propeller had a diameter of 0.76m (2.49 ft). Thus, scaling to Metro II dimensions, with a fuselage diameter of 1.67m (5.5 ft), the propeller diameter becomes 1.26m (4.1 ft). The clearance between the fuselage and propeller tip is 0.13m (0.41 ft) or ten percent of the propeller diameter. In order to maintain the same tip speed, the propeller rpm was taken to be 2424; the blade passage frequency is then 121.2 Hz for a three-bladed propeller.

The amplitude and phase components of the propeller pressure field are listed in Table 16 for the three-lowest-order harmonics. The presentation follows the same format as that given in Table 15 for the electropneumatic excitation. Now, however, the phase angle in the lower quadrant of the fuselage differs from that in the upper quadrant to take into account the rotation of the propeller pressure field. In the case of the electropneumatic source the phase angle distribution is symmetric about the grid axes.

Noise reductions predicted for the propeller excitation are shown in Figure 26 for fuselage test Configuration 1 and four assumed values of the floor treatment transmission loss. The noise reduction spectra show a broad peak centered at the fifth harmonic (606 Hz). This peak seems to be associated with reduced excitation efficiency of the fuselage structure.

7.2 Turbulent Boundary Layer

Turbulent boundary layer pressure fields were predicted for two flight conditions typical of general aviation (GA) and advanced turboprop (ATP) airplane cruise conditions. These conditions are listed in Table 17. The conditions were selected mainly to explore the effect of airspeed on the noise transmission.

PROPELLER HARMONIC 1 AT 121.2 HZ

PRESSURE AMPLITUDE, DB RE 20 MICRO PA

CIRCUM. LOCATION		AXIAL LOCATION															
L	THETA	K= 1	2	3	4	5	6	7	8	9	10	11	12	13	14	15	16
		Z=2.439	2.586	2.732	2.878	3.025	3.171	3.317	3.464	3.610	3.756	3.902	4.049	4.195	4.341	4.488	4.634
19	180.00	94.6	95.9	97.0	98.0	98.9	99.6	100.3	100.9	101.4	101.7	101.7	101.4	100.9	100.2	99.3	98.3
18	170.00	95.4	96.8	98.0	99.1	100.0	100.8	101.4	101.7	102.4	102.6	102.6	102.2	101.5	100.7	99.6	78.4
17	160.00	96.3	98.1	99.5	100.8	101.7	102.4	102.9	103.4	103.8	104.0	103.8	103.2	102.3	101.3	99.9	78.4
16	150.00	97.2	99.4	101.1	102.7	103.9	104.6	104.8	105.1	105.5	105.7	105.3	104.5	103.2	101.8	100.1	98.3
15	140.00	100.5	103.2	105.5	107.7	109.4	110.2	110.3	110.2	110.6	110.8	110.1	108.7	106.8	104.9	102.7	100.4
14	130.00	102.7	106.0	108.9	111.8	114.2	115.4	115.2	114.6	115.3	115.4	114.2	112.1	109.5	107.0	104.2	101.5
13	120.00	103.7	107.7	111.2	115.0	118.4	120.5	120.4	118.7	120.0	119.9	117.8	114.7	111.2	108.0	104.6	101.4
12	110.00	103.8	108.3	112.5	117.1	121.6	125.0	125.7	122.5	125.2	124.1	120.6	116.4	112.0	108.2	104.3	100.6
11	100.00	103.4	108.3	112.9	118.3	123.7	128.4	130.7	125.9	130.0	127.3	122.5	117.3	112.2	108.0	103.6	99.6
10	90.00	103.3	108.3	113.0	118.5	124.0	129.0	131.7	126.6	130.9	127.8	122.8	117.4	112.2	107.9	103.4	99.4
9	80.00	103.4	108.3	112.9	118.3	123.7	128.4	130.7	125.9	130.0	127.3	122.5	117.3	112.2	108.0	103.6	99.6
8	70.00	103.8	108.3	112.5	117.1	121.6	125.0	125.7	122.5	125.2	124.1	120.6	116.4	112.0	108.2	104.3	100.6
7	60.00	103.7	107.7	111.2	115.0	118.4	120.5	120.4	118.7	120.0	119.9	117.8	114.7	111.2	108.0	104.6	101.4
6	50.00	102.7	106.0	108.9	111.8	114.2	115.4	115.2	114.6	115.3	115.4	114.2	112.1	109.5	107.0	104.2	101.5
5	40.00	100.5	103.2	105.5	107.7	109.4	110.2	110.3	110.2	110.6	110.8	110.1	108.7	106.8	104.9	102.7	100.4
4	30.00	97.2	99.4	101.1	102.7	103.9	104.6	104.8	105.1	105.5	105.7	105.3	104.5	103.2	101.8	100.1	98.3
3	20.00	96.3	98.1	99.5	100.8	101.7	102.4	102.9	103.4	103.8	104.0	103.8	103.2	102.3	101.3	99.9	98.4
2	10.00	95.4	96.8	98.0	99.1	100.0	100.8	101.4	101.7	102.4	102.6	102.6	102.2	101.5	100.7	99.6	98.4
1	0.00	94.6	95.9	97.0	98.0	98.9	99.6	100.3	100.9	101.4	101.7	101.7	101.4	100.9	100.2	99.3	98.3

PHASE (DEGREES)

L	THETA	K= 1	2	3	4	5	6	7	8	9	10	11	12	13	14	15	16
19	180.00	-153.5	-156.2	-157.2	-156.3	-153.3	-148.3	-141.8	-134.5	-127.3	-120.5	-114.3	-108.5	-102.8	-97.7	-91.6	-85.1
18	170.00	-170.6	-173.8	-175.0	-174.4	-171.3	-165.6	-157.7	-148.8	-140.1	-132.3	-125.6	-119.7	-114.1	-109.1	-103.2	-96.9
17	160.00	171.2	167.5	165.7	165.8	168.8	175.1	-175.3	-163.7	-152.6	-143.3	-136.1	-130.2	-124.9	-120.3	-114.8	-108.9
16	150.00	157.8	153.4	151.0	150.4	152.8	159.4	171.0	-173.6	-158.9	-147.8	-140.2	-134.7	-130.2	-126.2	-121.5	-116.2
15	140.00	149.1	144.2	141.3	139.8	141.2	147.2	160.6	-178.7	-158.6	-145.6	-138.3	-133.8	-130.4	-127.5	-123.7	-119.2
14	130.00	146.0	140.9	137.5	135.2	135.4	140.0	154.0	-177.7	-149.8	-135.7	-129.7	-126.9	-125.0	-123.2	-120.6	-117.0
13	120.00	152.5	147.2	143.4	140.4	139.3	141.8	154.3	-166.4	-127.5	-114.8	-111.3	-110.5	-110.3	-109.8	-108.4	-105.8
12	110.00	166.3	160.9	157.0	153.6	151.6	152.0	160.7	-147.4	-97.6	-89.2	-88.2	-87.0	-90.1	-90.6	-90.2	-88.4
11	100.00	-172.3	-177.7	178.4	174.8	172.2	171.1	175.7	-120.3	-64.1	-60.1	-60.9	-62.7	-64.5	-65.6	-65.8	-64.7
10	90.00	-139.5	-144.9	-148.9	-152.5	-155.2	-156.4	-152.7	-86.1	-29.3	-26.1	-27.2	-29.1	-31.0	-32.2	-32.6	-31.6
9	80.00	-107.8	-113.2	-117.2	-120.8	-123.4	-124.4	-119.9	-55.8	.4	4.4	3.5	1.8	-.0	-1.1	-1.4	-.2
8	70.00	-76.1	-81.4	-85.4	-88.8	-90.8	-90.4	-81.7	-29.8	20.0	28.5	29.4	28.6	27.5	27.0	27.4	29.2
7	60.00	-52.7	-58.0	-61.8	-64.7	-65.8	-63.3	-50.9	-11.6	27.4	40.1	43.6	44.4	44.6	45.1	46.4	49.0
6	50.00	-36.7	-41.8	-45.3	-47.5	-47.4	-42.7	-28.7	-.4	27.5	41.6	47.6	50.4	52.3	54.0	56.7	60.3
5	40.00	-22.8	-27.6	-30.6	-32.1	-30.7	-24.6	-11.3	9.5	29.6	42.5	49.9	54.3	57.7	60.6	64.4	69.0
4	30.00	-11.8	-16.1	-18.5	-19.1	-16.8	-10.2	1.4	16.8	31.6	42.7	50.3	55.7	60.3	64.2	68.9	74.3
3	20.00	-2.2	-5.9	-7.7	-7.6	-4.7	1.7	11.3	22.9	34.0	43.3	50.5	56.4	61.7	66.3	71.7	77.7
2	10.00	7.6	4.5	3.2	3.8	6.9	12.6	20.5	29.4	38.1	45.9	52.6	58.5	64.1	69.1	75.0	81.3
1	0.00	13.0	10.3	9.4	10.3	13.2	18.2	24.8	32.1	39.3	46.0	52.2	58.0	63.7	68.8	74.9	81.4

TABLE 16. BLOCKED PRESSURE AMPLITUDE AND PHASE FOR GENERAL AVIATION PROPELLER

PROPELLER HARMONIC 2 AT 242.4 HZ

CIRCUM. LOCATION								AXIAL LOCATION									
L THETA	K= 1 Z=2.439	2 2.586	3 2.732	4 2.878	5 3.025	6 3.171	7 3.317	8 3.464	9 3.610	10 3.756	11 3.902	12 4.049	13 4.195	14 4.341	15 4.488	16 4.634

PRESSURE AMPLITUDE, DB RE 20 MICRO PA

L THETA	1	2	3	4	5	6	7	8	9	10	11	12	13	14	15	16
19 180.00	75.5	77.6	79.3	81.0	82.5	83.7	84.6	85.3	85.6	85.6	85.1	84.3	83.1	81.8	80.0	78.1
18 170.00	75.7	78.2	80.1	82.1	83.6	84.9	85.8	86.4	86.6	86.5	85.9	84.8	83.4	81.8	79.8	77.6
17 160.00	75.9	78.8	81.2	83.5	85.3	86.6	87.5	88.0	88.1	87.8	86.9	85.5	83.6	81.7	79.3	76.7
16 150.00	75.9	79.4	82.3	85.2	87.5	89.1	89.8	90.1	90.0	89.4	88.2	86.3	83.8	81.4	73.4	75.4
15 140.00	78.1	82.4	86.2	90.0	93.2	95.3	96.0	95.9	95.6	94.7	92.8	90.0	86.6	83.4	79.7	76.0
14 130.00	78.9	84.2	88.9	93.9	98.3	101.3	102.3	101.5	101.1	99.8	96.9	92.9	88.4	84.3	79.8	75.4
13 120.00	78.2	84.5	90.3	96.8	102.9	107.6	109.3	107.5	107.5	105.5	100.8	95.0	89.0	83.8	78.3	73.2
12 110.00	76.6	83.7	90.5	98.5	106.4	113.2	116.7	113.7	114.7	110.8	103.9	96.2	88.7	82.4	76.0	70.3
11 100.00	74.5	82.4	90.0	99.1	108.5	117.3	123.3	119.2	121.2	114.8	105.8	96.6	87.8	80.7	73.6	67.3
10 90.00	74.1	82.1	89.9	99.1	108.8	118.0	124.5	120.3	122.4	115.5	106.1	96.6	87.6	80.4	73.2	66.8
9 80.00	74.5	82.4	90.0	99.1	108.5	117.3	123.3	119.2	121.2	114.8	105.8	96.6	87.8	80.7	73.6	67.3
8 70.00	76.6	83.7	90.5	98.5	106.4	113.2	116.7	113.7	114.7	110.8	103.9	96.2	88.7	82.4	76.0	70.3
7 60.00	78.2	84.5	90.3	96.8	102.9	107.6	109.3	107.5	107.5	105.5	100.8	95.0	89.0	83.8	78.3	73.2
6 50.00	78.9	84.2	88.9	93.9	98.3	101.3	102.3	101.5	101.1	99.8	96.9	92.9	88.4	84.3	79.8	75.4
5 40.00	78.1	82.4	86.2	90.0	93.2	95.3	96.0	95.9	95.6	94.7	92.8	90.0	86.6	83.4	79.7	76.0
4 30.00	75.9	79.4	82.3	85.2	87.5	89.1	89.8	90.1	90.0	89.4	88.2	86.3	83.8	81.4	78.4	75.4
3 20.00	75.9	78.8	81.2	83.5	85.3	86.6	87.5	88.0	88.1	87.8	86.9	85.5	83.6	81.7	79.3	76.7
2 10.00	75.7	78.2	80.1	82.1	83.6	84.9	85.8	86.4	86.6	86.5	85.9	84.8	83.4	81.8	79.8	77.6
1 0.00	75.5	77.6	79.3	81.0	82.5	83.7	84.6	85.3	85.6	85.6	85.1	84.3	83.1	81.8	80.0	78.1

PHASE (DEGREES)

L THETA	1	2	3	4	5	6	7	8	9	10	11	12	13	14	15	16
19 180.00	179.0	168.6	161.6	156.6	154.7	155.7	159.4	164.9	171.6	178.9	-173.2	-164.6	-155.0	-145.5	-133.5	-120.2
18 170.00	148.1	137.2	129.9	124.6	122.8	124.4	129.2	136.2	144.2	152.5	160.9	169.6	179.1	-171.6	-159.8	-146.5
17 160.00	115.5	104.2	96.5	90.8	88.9	91.0	97.3	106.7	117.0	126.8	135.5	144.0	153.0	161.8	173.1	-174.0
16 150.00	92.3	80.7	72.8	66.8	64.6	67.0	75.0	87.9	101.9	113.5	122.3	129.9	137.6	145.3	155.6	167.7
15 140.00	78.2	66.7	58.8	52.7	50.1	52.4	61.9	79.9	99.7	113.3	121.4	127.0	132.5	138.5	147.1	158.0
14 130.00	75.4	64.2	56.6	50.5	47.5	49.1	59.3	84.5	113.5	128.4	134.2	136.9	139.5	143.2	149.7	159.0
13 120.00	91.2	80.7	73.5	67.6	64.2	64.4	73.5	109.2	151.5	164.5	166.8	166.3	165.9	167.0	171.0	178.3
12 110.00	121.1	111.3	104.5	98.9	95.1	93.8	99.9	147.4	-157.9	-150.1	-150.8	-153.3	-155.8	-156.6	-154.8	-149.2
11 100.00	165.4	156.1	149.7	144.2	140.2	137.8	140.4	-160.4	-99.1	-96.3	-98.7	-102.3	-105.8	-107.8	-107.4	-103.2
10 90.00	-128.9	-138.1	-144.4	-149.8	-153.9	-156.5	-154.5	-92.8	-31.0	-29.1	-31.7	-35.5	-39.1	-41.2	-41.0	-37.1
9 80.00	-65.7	-75.0	-81.4	-86.9	-90.9	-93.3	-90.7	-31.5	29.8	32.6	30.2	26.6	23.1	21.1	21.5	25.8
8 70.00	-3.7	-13.5	-20.2	-25.9	-29.7	-31.0	-24.9	22.7	77.3	85.1	84.5	81.9	79.4	78.6	80.5	86.0
7 60.00	40.9	30.4	23.2	17.3	13.9	14.1	23.2	58.9	101.2	114.2	116.5	116.0	115.5	116.7	120.7	128.0
6 50.00	69.9	58.8	51.1	45.1	42.1	43.7	53.9	79.1	108.0	123.0	128.7	131.4	134.1	137.8	144.3	153.5
5 40.00	94.5	83.0	75.1	68.9	66.4	68.7	78.2	96.1	115.9	129.6	137.6	143.2	148.7	154.8	163.4	174.3
4 30.00	113.2	101.6	93.6	87.7	85.5	87.9	95.9	108.8	122.8	134.4	143.2	150.8	158.5	166.2	176.5	-171.4
3 20.00	128.7	117.3	109.6	104.0	102.0	104.1	110.5	119.8	130.2	139.9	148.7	157.2	166.1	175.0	-173.8	-160.9
2 10.00	144.6	133.7	126.4	121.1	119.2	120.8	125.6	132.6	140.7	148.9	157.3	166.0	175.5	-175.1	-163.3	-150.1
1 0.00	152.1	141.6	134.7	129.7	127.7	128.8	132.5	138.0	144.7	152.0	159.9	168.5	178.1	-172.4	-160.4	-147.1

TABLE 16. CONTINUED

PROPELLER HARMONIC 3 AT   363.6 HZ

CIRCUM.   AXIAL LOCATION

L	THETA	K=1	2	3	4	5	6	7	8	9	10	11	12	13	14	15	16
		Z=2.439	2.586	2.732	2.878	3.025	3.171	3.317	3.464	3.610	3.756	3.902	4.049	4.195	4.341	4.488	4.634

PRESSURE AMPLITUDE, DB RE 20 MICRO PA

L	THETA	1	2	3	4	5	6	7	8	9	10	11	12	13	14	15	16
19	180.00	57.2	60.1	62.5	64.8	66.8	68.3	69.5	70.1	70.3	69.9	69.0	67.6	65.7	63.7	61.0	58.2
18	170.00	56.9	60.2	62.9	65.6	67.8	69.5	70.6	71.2	71.3	70.7	69.6	67.9	65.6	63.3	60.3	57.1
17	160.00	56.3	60.2	63.5	66.7	69.4	71.3	72.4	72.9	72.7	71.9	70.3	68.1	65.3	62.5	59.0	55.3
16	150.00	55.2	60.0	64.0	68.1	71.5	73.9	75.1	75.2	74.7	73.4	71.3	68.3	64.8	61.3	57.1	52.9
15	140.00	56.1	62.0	67.1	72.5	77.1	80.4	81.9	81.7	80.6	78.7	75.6	71.4	66.7	62.3	57.2	52.1
14	130.00	55.5	62.6	69.0	76.0	82.4	87.2	89.3	88.5	87.0	84.3	79.7	73.8	67.5	61.8	55.7	49.8
13	120.00	52.9	61.4	69.4	78.5	87.3	94.6	98.2	96.6	95.2	91.2	83.9	75.4	66.9	59.8	52.4	45.6
12	110.00	49.4	59.1	68.5	79.7	91.0	101.3	107.5	105.1	104.4	97.7	87.3	76.1	65.5	56.8	48.2	40.5
11	100.00	46.1	56.6	67.0	79.7	93.1	106.1	115.8	112.8	112.5	102.3	89.2	75.9	63.3	53.3	43.4	34.6
10	90.00	45.0	55.9	66.6	79.6	93.4	106.9	117.3	114.4	114.0	103.1	89.5	75.8	63.1	53.0	43.1	34.7
9	80.00	46.1	56.6	67.0	79.7	93.1	106.1	115.8	112.8	112.5	102.3	89.2	75.9	63.3	53.3	43.4	34.6
8	70.00	49.4	59.1	68.5	79.7	91.0	101.3	107.5	105.1	104.4	97.7	87.3	76.1	65.5	56.8	48.2	40.5
7	60.00	52.9	61.4	69.4	78.5	87.3	94.6	98.2	96.6	95.2	91.2	83.9	75.4	66.9	59.8	52.4	45.6
6	50.00	55.5	62.6	69.0	76.0	82.4	87.2	89.3	88.5	87.0	84.3	79.7	73.8	67.5	61.8	55.7	49.8
5	40.00	56.1	62.0	67.1	72.5	77.1	80.4	81.9	81.7	80.6	78.7	75.6	71.4	66.7	62.3	57.2	52.1
4	30.00	55.2	60.0	64.0	68.1	71.5	73.9	75.1	75.2	74.7	73.4	71.3	68.3	64.8	61.3	57.1	52.9
3	20.00	56.3	60.2	63.5	66.7	69.4	71.3	72.4	72.9	72.7	71.9	70.3	68.1	65.3	62.5	59.0	55.3
2	10.00	56.9	60.2	62.9	65.6	67.8	69.5	70.6	71.2	71.3	70.7	69.6	67.9	65.6	63.3	60.3	57.1
1	0.00	57.2	60.1	62.5	64.8	66.8	68.3	69.5	70.1	70.3	69.9	69.0	67.6	65.7	63.7	61.0	58.2

PHASE (DEGREES)

L	THETA	1	2	3	4	5	6	7	8	9	10	11	12	13	14	15	16
19	180.00	154.3	135.4	121.8	110.2	102.9	99.6	100.2	103.9	110.1	118.2	128.0	139.6	153.3	167.3	-174.7	-154.4
18	170.00	109.4	90.0	76.0	64.1	56.8	54.0	55.5	60.6	68.0	77.0	87.3	99.1	112.7	126.6	144.4	164.6
17	160.00	61.8	41.9	27.7	15.7	8.5	6.2	9.1	16.3	26.0	36.3	46.9	58.3	71.2	84.6	101.9	121.8
16	150.00	27.9	8.2	-5.8	-17.5	-24.4	-26.0	-21.5	-11.1	2.0	14.0	24.2	34.2	45.4	57.4	73.6	92.6
15	140.00	7.6	-11.3	-24.5	-35.3	-41.6	-42.7	-36.5	-21.4	-2.4	11.7	20.4	27.2	35.2	44.7	58.8	76.5
14	130.00	4.2	-13.4	-25.3	-34.9	-40.5	-41.4	-34.2	-12.1	17.1	32.7	38.0	40.3	43.8	49.8	60.7	76.3
13	120.00	29.5	13.4	2.9	-5.4	-10.6	-12.1	-5.5	26.6	71.0	84.3	85.3	83.2	81.9	83.6	90.5	102.7
12	110.00	76.8	61.6	52.0	44.4	39.2	36.5	40.5	83.7	142.0	149.2	147.0	142.4	137.9	136.1	138.6	147.0
11	100.00	143.6	130.3	121.5	114.2	108.8	105.1	106.1	160.4	-134.2	-132.4	-136.3	-141.7	-147.5	-151.3	-151.3	-144.4
10	90.00	-121.6	-133.1	-140.6	-147.1	-152.2	-155.9	-155.6	-98.9	-32.8	-31.9	-35.8	-41.0	-46.1	-48.7	-46.5	-37.3
9	80.00	-23.0	-36.4	-45.1	-52.4	-57.8	-61.5	-60.6	-6.2	59.2	61.0	57.1	51.7	45.9	42.1	42.1	49.0
8	70.00	69.7	54.5	44.9	37.3	32.0	29.3	33.3	76.6	134.8	142.0	139.9	135.3	130.8	128.9	131.5	139.9
7	60.00	134.0	117.9	107.4	99.1	94.0	92.4	99.0	131.1	175.5	-171.2	-170.2	-172.3	-173.6	-171.9	-165.0	-152.8
6	50.00	176.0	158.4	146.5	136.9	131.3	130.4	137.7	159.7	-171.0	-155.4	-150.1	-147.8	-144.4	-138.4	-127.4	-111.9
5	40.00	-148.0	-166.9	179.9	169.1	162.7	161.7	167.9	-177.0	-158.0	-143.9	-135.2	-128.4	-120.4	-110.9	-96.8	-79.1
4	30.00	-120.8	-140.5	-154.3	-166.2	-173.1	-174.7	-170.1	-159.8	-146.7	-134.7	-124.4	-114.5	-103.2	-91.3	-75.1	-56.0
3	20.00	-98.5	-118.3	-132.6	-144.5	-151.8	-154.0	-151.1	-143.9	-134.0	-124.0	-113.4	-102.0	-89.0	-75.7	-58.4	-38.5
2	10.00	-75.9	-95.4	-109.4	-121.2	-128.6	-131.4	-129.9	-124.8	-117.3	-108.3	-98.0	-86.3	-72.7	-58.9	-41.0	-20.8
1	0.00	-66.1	-84.9	-98.6	-110.1	-117.5	-120.7	-120.2	-116.4	-110.3	-102.2	-92.4	-80.7	-67.1	-53.1	-35.1	-14.8

TABLE 16.   CONTINUED
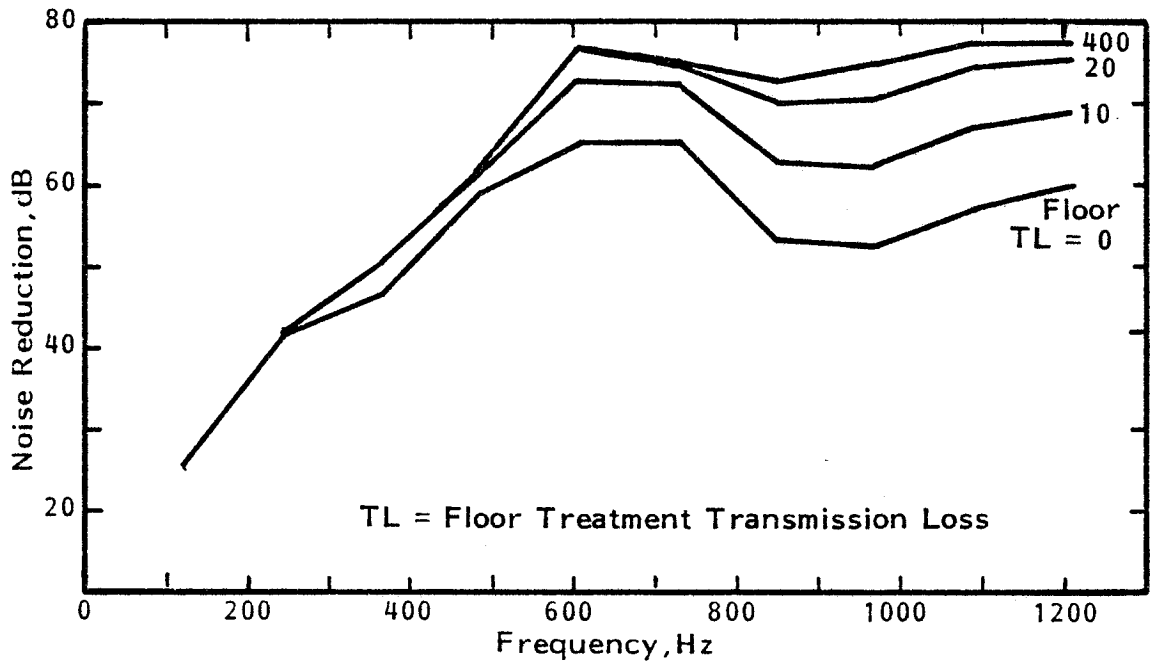
FIGURE 26. PREDICTED NOISE REDUCTIONS FOR TYPICAL G.A. PROPELLER
NOISE EXCITATION (METRO II TEST FUSELAGE CONFIGURATION #1)

TABLE 17

FLIGHT CONDITIONS ASSOCIATED WITH BOUNDARY LAYER ESTIMATES

Parameter	GA Airplane	ATP Airplane
Airspeed m/s (ft/sec)	95 (416)	182 (796)
Altitude m (ft)	3650 (12000)	9150 (30000)
Distance from airplane nose to point of interest on fuselage m (ft)	6.1 (20)	16.9 (55.5)
Boundary layer thickness mm (in)	70 (2.8)	174 (6.8)
Boundary layer displacement thickness mm (in)	8.8 (0.35)	21.7 (0.86)

Parameters required for the analytical model are the pressure field convection velocity and the boundary layer displacement thickness (see Eqs.(41) and (45)). The convection velocity was taken to be 80% of the flight airspeed.

Since the turbulent boundary layer pressure field is broadband and random in character, use is made of the analytical model feature which predicts noise reduction in one-third octave frequency bands rather than the deterministic, tonal transmission calculation used for propeller noise and the electropneumatic source. The relevant part of the analytical model is described in Section 2. Predicted noise reductions associated with the GA boundary layer pressure field are shown in Figure 27 for fuselage test Configuration 1 and four assumed values of the floor treatment transmission loss. The results show a general increase of noise reduction with frequency, except for a spectral trough at 125 Hz associated with sidewall resonance. In this case noise reduction refers to the surface or blocked pressure on the exterior of the fuselage rather than the free field sound pressure used for the propeller and electropneumatic noise sources discussed in preceding sections.

7.3 Comparison of Predicted Noise Reductions

Noise reductions predicted for boundary layer, GA propeller noise and simulated propeller (electropneumatic) excitations are compared in Figure 28. Two values of the floor treatment transmission loss (0 dB and 20 dB) are considered. Again, it should be remembered that the reference sound level for propeller and electropneumatic noise sources is the free field value, whereas the surface pressure is used as the reference for the boundary layer cases. If surface (blocked) pressure were used in all cases the noise reductions for propeller and electropneumatic noise excitation should be increased by 6 dB.
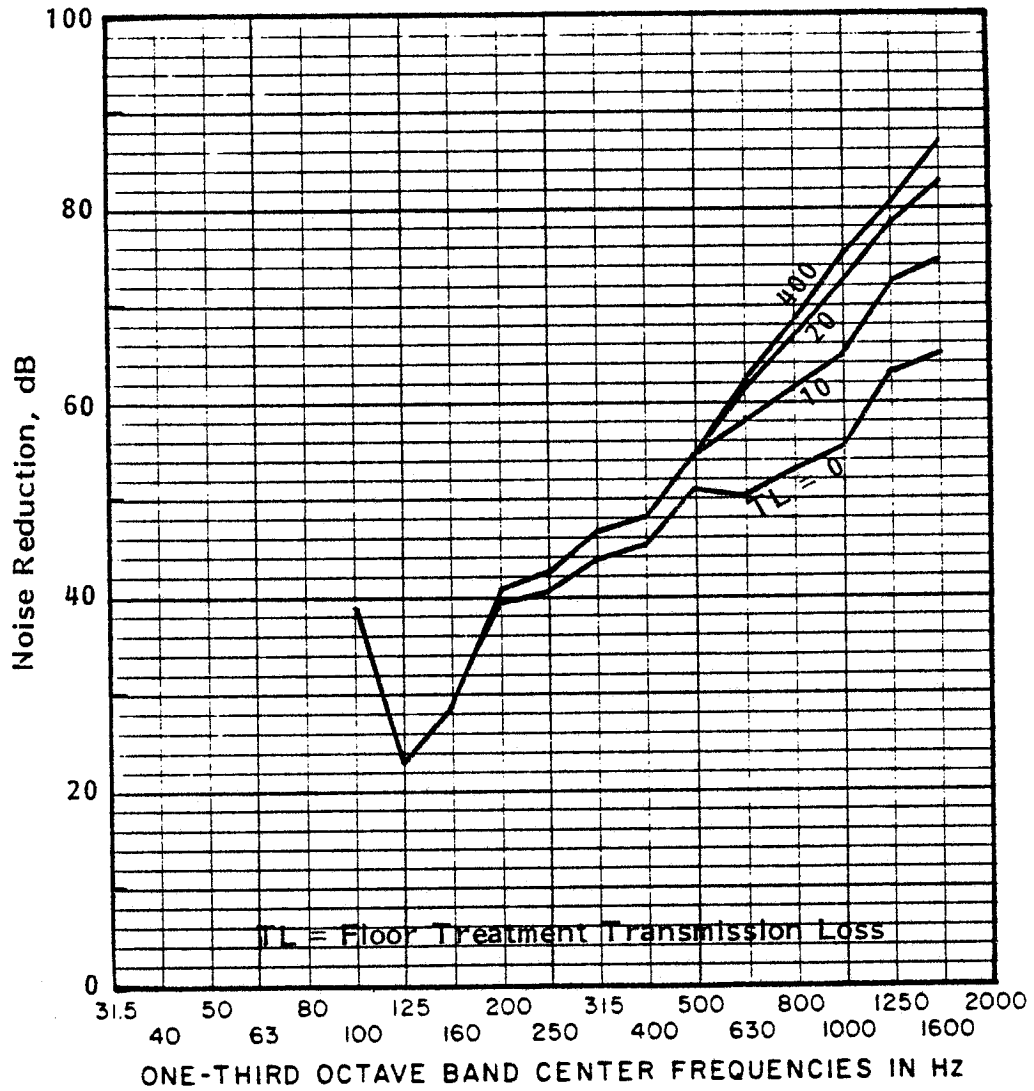
FIGURE 27. PREDICTED NOISE REDUCTIONS FOR TYPICAL GENERAL
AVIATION AIRPLANE BOUNDARY LAYER EXCITATION
(METRO II TEST FUSELAGE CONFIGURATION #1)

(a) Floor TL = 0 dB

Excitation:
——— G.A.Propeller
—··— Simulated Propeller (Electropneumatic Source)
—·—·— G.A.Airplane Boundary Layer
———— ATP Airplane Boundary Layer

(b) Floor TL = 20 dB
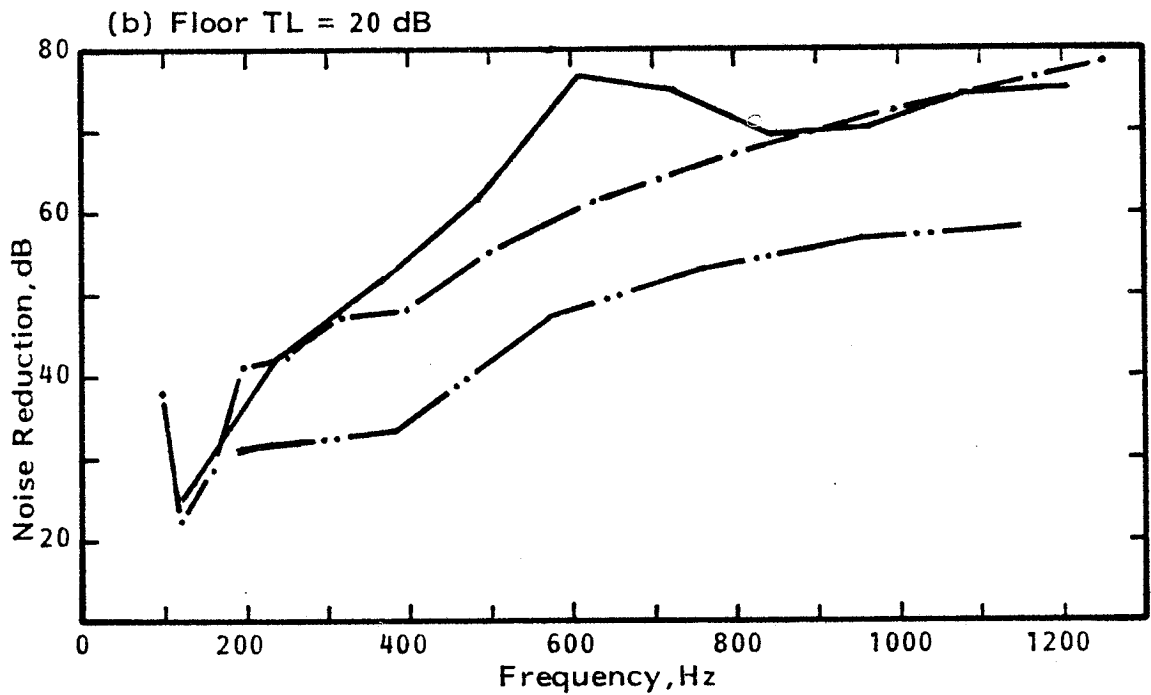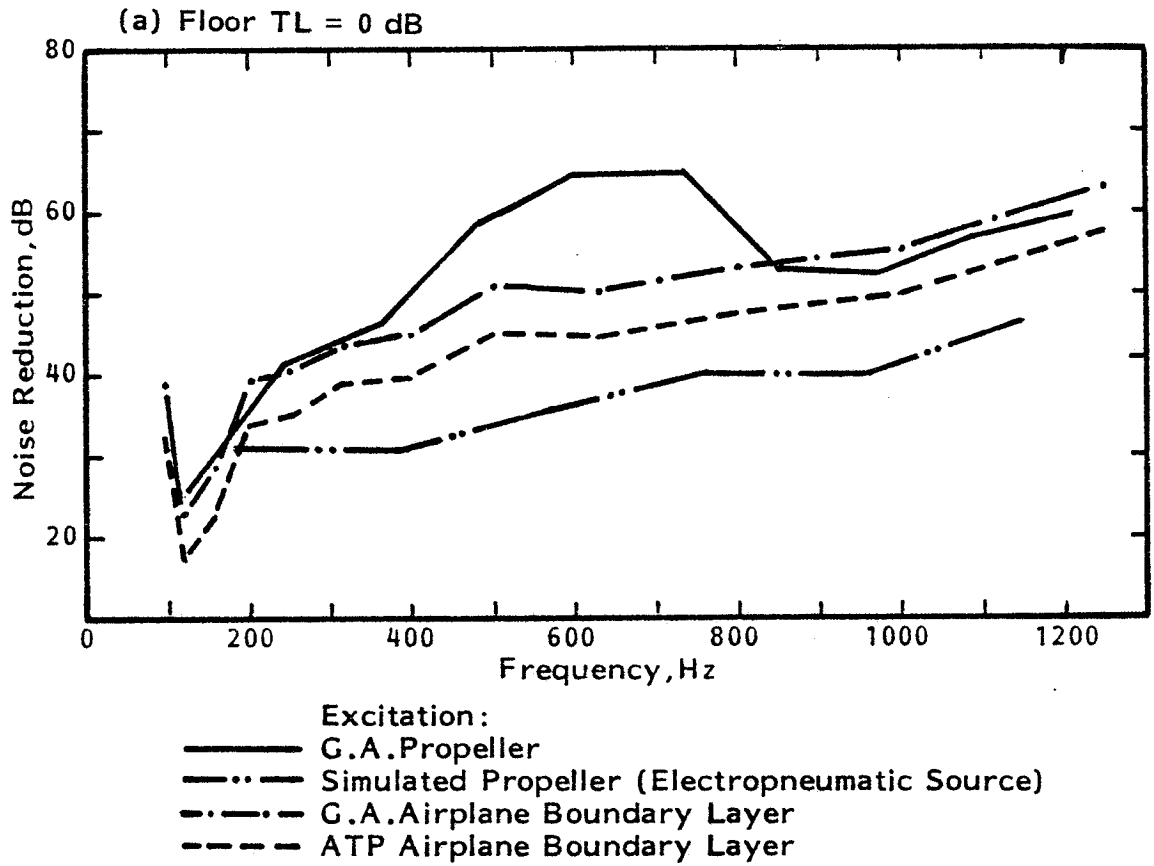
FIGURE 28. COMPARISON OF PREDICTED NOISE REDUCTIONS FOR DIFFERENT EXCITATION PRESSURE FIELDS (METRO II TEST FUSELAGE CONFIGURATION 1)

Comparing first the results for GA propeller and simulated propeller (electropneumatic) excitations it is seen that the noise reductions are higher for the propeller than for the electropneumatic source. Two factors, amplitude and phase of the excitation pressure field, are involved. Both of these factors determine the response of the fuselage structure. Pressure phase differences for the two excitations have been discussed in Section 7.1; the pressure amplitude differences are associated with the spatial distribution, particularly in the longitudinal direction. A representative comparison of the longitudinal distribution of harmonic sound levels is given in Figure 29 where it is seen that the propeller noise pressure amplitude decreases more rapidly with distance than does the electropneumatic source sound field. The latter sound field was designed to simulate propfan pressure levels (which it does successfully [16]), so that Figure 29 essentially compares GA and ATP propeller noise levels.

The different excitation characteristics of the excitation fields will result in different structural responses and, hence, noise transmission into the fuselage. In this case, the more rapid the fall-off of the pressure amplitude, the higher the noise reduction. It is interesting to note that Prydz et al [16] have used an associated argument regarding average and peak exterior sound levels to increase predicted noise reductions by 7 dB. (The predictions in that case [16] were computed initially under the assumption of spatially uniform pressure amplitude and then adjusted to account for the spatially-varying amplitude).

Now compare noise reductions for acoustic (propeller and electropneumatic) and aerodynamic (turbulent boundary layer) excitations. It is seen in Figure 28 that the predicted noise reductions associated with boundary layer excitation lie between those for propeller and electropneumatic sources, even when the 6 dB
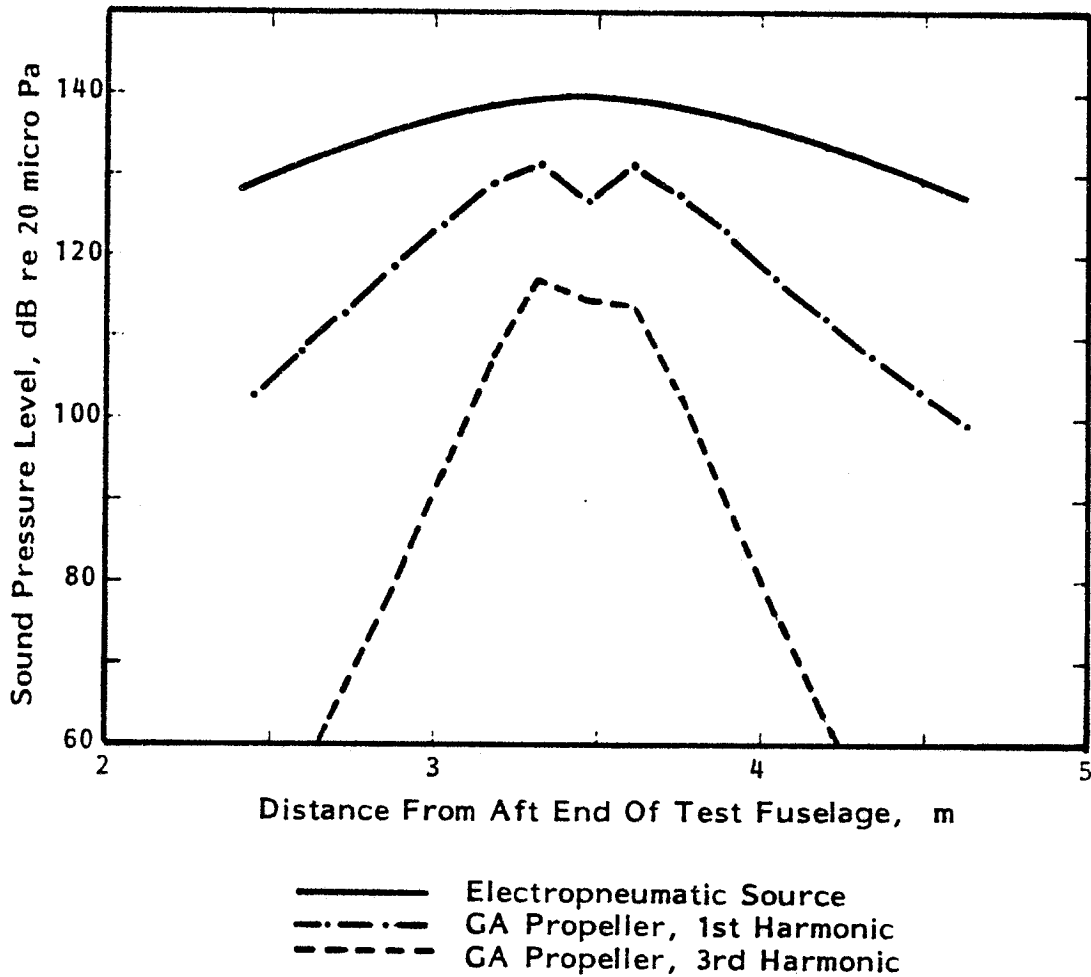
FIGURE 29. TYPICAL LONGITUDINAL DISTRIBUTIONS OF EXCITATION
PRESSURE AMPLITUDE FOR G.A.PROPELLER AND SIMULATED
PROPFAN (ELECTROPNEUMATIC) NOISE SOURCES

adjustment from free field to blocked pressure excitation is applied. As before, excitation pressure amplitude and phase are playing important roles. The boundary layer has a uniformly-distributed pressure amplitude, in contrast to the spatially-varying amplitudes for the propeller and electropneumatic sources. Also the phase characteristics are quite different, the boundary layer pressure field being convected in the longi-tudinal directions and the propeller pressure field circumferen-tially. As the airplane airspeed and pressure field convection velocity increase, the predicted noise reduction decreases and approaches values associated with the electropneumatic source.

7.4 Reverberant Field Excitation

Noise reductions have been predicted for Configuration 1 of the Metro II test fuselage when the excitation was a reverberant acoustic field. The resulting noise reduction spectra are com-pared in Figure 30 for different values of the floor treatment transmission loss. Figure 30 also contains a measured noise reduction spectrum [private communication from R.A. Prydz] measured on the test fuselage when placed in a reverberation chamber. It is seen that the measured and predicted spectra have similar shapes, although the analytical model underpredicts the noise reduction at lower frequencies. It is also observed that the noise reductions predicted for reverberant excitation are lower than those predicted for the other excitations considered in Figure 28. A comparison of predicted noise reductions for reverberant acoustic and boundary layer aerodynamic excitations is contained in Figure 31, where the floor treatment transmission loss is assumed to be zero.
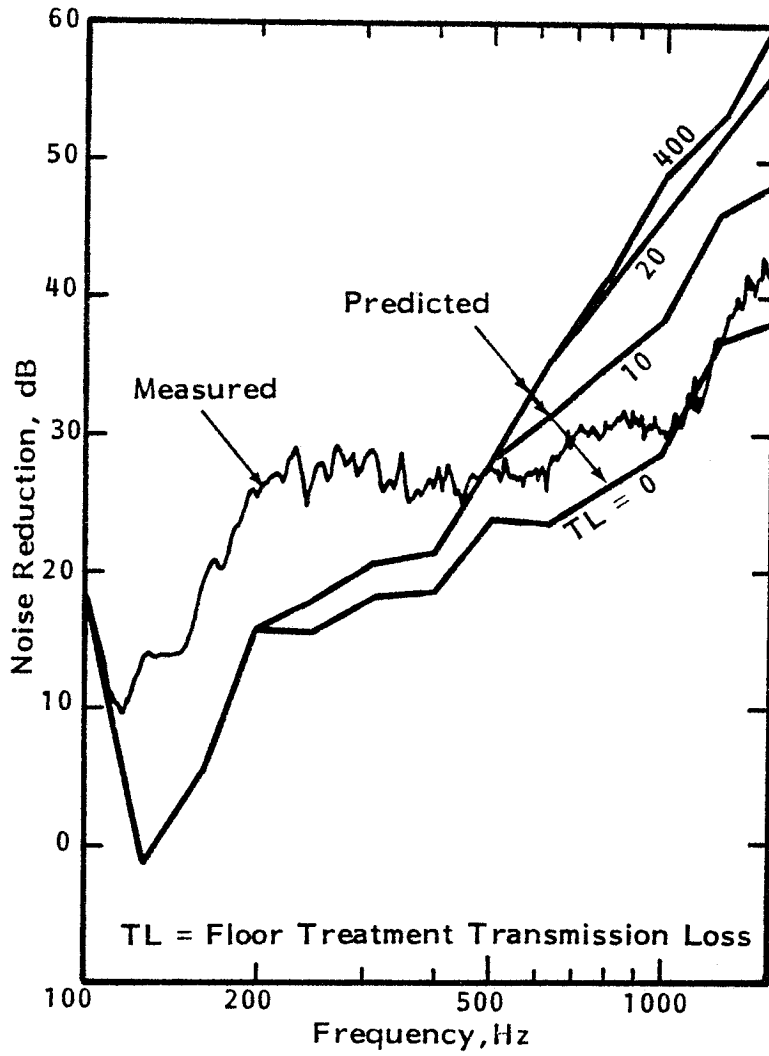
FIGURE 30. COMPARISON OF MEASURED AND PREDICTED NOISE REDUCTION
FOR REVERBERANT FIELD EXCITATION (METRO II TEST
FUSELAGE CONFIGURATION 1)
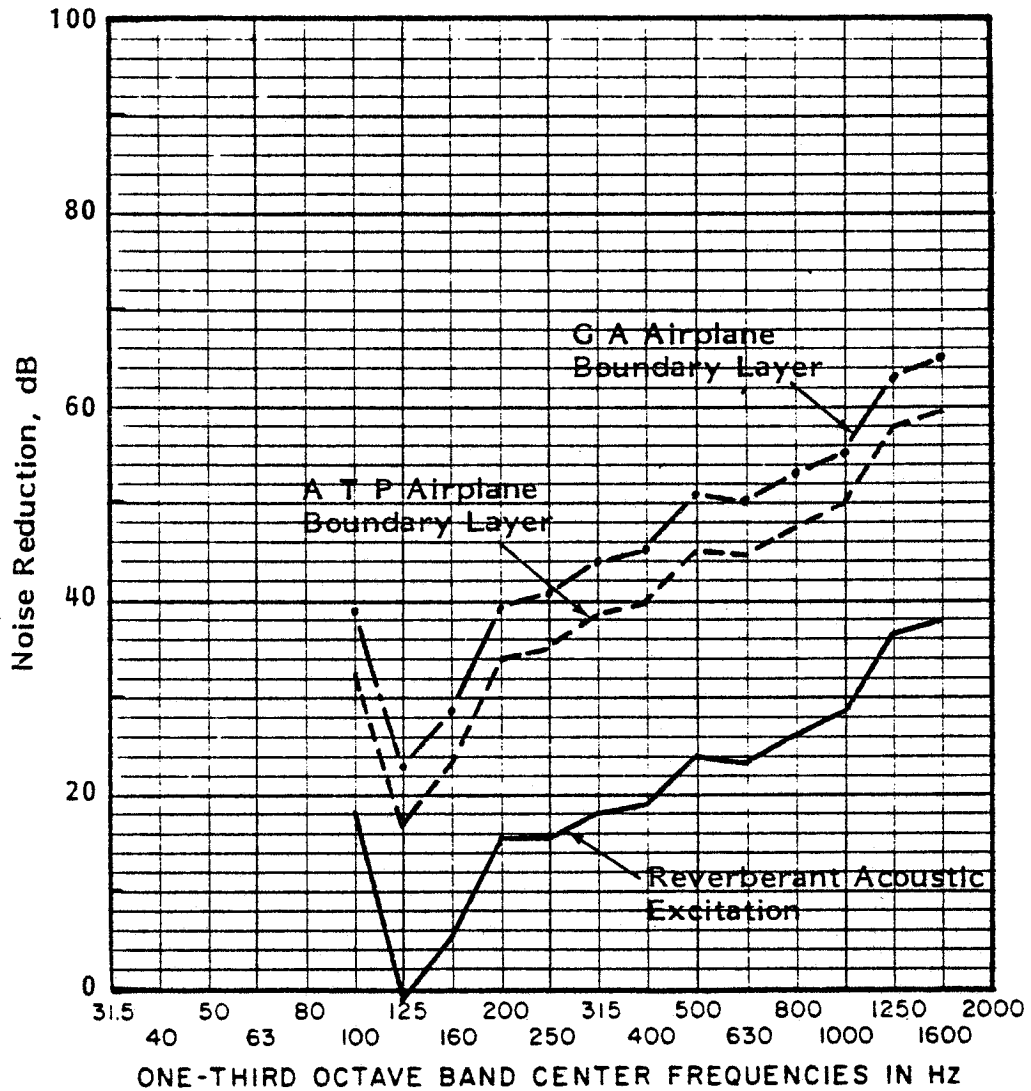
FIGURE 31. COMPARISON OF PREDICTED NOISE REDUCTIONS FOR REVERBERANT ACOUSTIC AND TURBULENT BOUNDARY LAYER EXCITATIONS (METRO II TEST FUSELAGE CONFIGURATION #1, FLOOR TREATMENT TRANSMISSION LOSS = 0 DB)

8.0 DISCUSSION AND CONCLUSIONS

The analytical model developed in Ref.[1] for the prediction of
sound pressure levels in propeller-driven aircraft provides a
representation of the response of the combined fuselage shell
and cabin floor structure. This inclusion of the cabin floor as
an integral part of the analytical model is a significant depar-
ture from earlier analytical models. As a result, a certain
amount of experience has to be gained in the application of the
model to practical structures.

In the comparisons with data from the Metro II noise transmis-
sion tests performed by Prydz et al, it became apparent that
certain changes were required to the way in which the analytical
model [1] represented the floor structure. The analytical
model was modified to incorporate the changes but unfortunately
the particular floor configuration chosen for the Metro II tests
posed a significant problem to the analytical representation.
The floor in the test fuselage did not constitute a structural
member of the fuselage, rather it was a secondary item (albeit
heavy and stiff) introduced to provide a cavity which was geo-
metrically similar to that of a wide-body airplane. The test
floor rested on the structural floor of the Metro II but it did
so via air mounts which would provide some vibration isolation.

Since the analytical model could not handle the test floor
structure without a major change to the structural model, an
alternative approach was adopted whereby a "floor treatment
transmission coefficient" was introduced to represent, among
other things, the vibration isolation provided by the air
mounts. The coefficient could, equally well, represent attenua-
tion provided by any floor coverings, just as the trim transmis-
sion coefficient provides an estimate of the attenuation
provided by the sidewall trim.

Parametric variations of the floor treatment transmission
coefficient allowed the predicted noise reductions to straddle
the measured values. Appropriate values of the coefficient
could be selected to achieve good agreement between measured and
predicted results. While this may appear to be an indirect
approach it can be justified because of the unusual floor con-
figuration in the test fuselage. Furthermore the values of the
floor treatment transmission loss that provide good agreement
between measured and predicted noise reductions are consistent
with the measured reductions in floor vibration attributed to
the use of air mounts (as shown in Figure 24).

It should be noted also that the analytical model assumes that
the sound-absorbing material is distributed uniformly over the
sidewall surface. In the actual test the sidewall treatments
were highly reflective and additional absorptive material was
placed on the floor near the sidewall along the full length of
the cabin. Since the analytical model would not account for
this ad hoc distribution of absorptive material, the appropriate
empirical information was introduced into the computations.

Because of these problems in representing the floor installation
and absorptive material, the validation of the analytical model
was not conclusive. However, the results do show that the
analytical model predicts noise reductions which are consistent
with the measured data.

The capability of the analytical model has been extended to
include turbulent boundary layer pressure fluctuations as an
exterior excitation field. By the same token the model can
represent a convected acoustic pressure field. The model
already had the capability of describing noise transmission from
a reverberant acoustic field. In all these cases the excitation
is broadband and random in character rather than tonal and
deterministic as is the case with propeller noise or simulated
propeller (electropneumatic) noise.

The ability of the analytical model to predict noise reductions for the fuselage structure exposed to various exterior pressure fields has been used to compare propeller and simulated propeller excitation, turbulent boundary layer and reverberant acoustic fields. While the results are probably dependent to some extent on the fuselage structure chosen (Metro II test Configuration #1 in Ref.[5]), the comparisons show certain trends of interest.

Propeller noise (or simulated propeller noise) has the characteristic that the sound pressure level changes markedly with distance away from the plane of rotation of the propeller, but the coherence maintains high values for, at least, the lower order harmonics [17]. In contrast, the boundary layer pressure field has a sound pressure level which is essentially independent of location but a coherence function which decays with increasing separation distance.

It can be shown (see, for example, Eq.(55) of [6]) that the amplitude spatial decay and coherence spatial decay play similar roles in the calculation of panel joint acceptance. Consequently, it might be expected that the noise reductions associated with propeller noise and boundary layer excitation would be similar. This appears to be the case in Figure 28, particularly with respect to the simulated propeller (where the sound pressure level decays relatively slowly with distance) and the higher speed (ATP airplane) boundary layer. As the amplitude spatial decay rate (GA propeller) or the coherence spatial decay rate (GA boundary layer) increases, the predicted noise reduction increases.

Obviously, the results presented in this report represent a limited number of special cases. A more extensive parametric study would define the roles of the different excitations more clearly. Alternatively, calculations should be made for specific airplane configurations of interest.

In conclusion, the analytical model developed in Ref.[1] and extended in this study predicts noise reductions which are consistent with values measured in the Metro II test [5]. However certain configurations peculiar to the test set-up make a definitive validation difficult. Application of the analytical model to different types of excitation show that there can be differences in the predicted noise reductions. For example the predicted noise reductions asssociated with turbulent boundary layer excitation were greater than those for simulated propfan excitation. However, before general conclusions are drawn, calculations should be performed for different fuselage structures with special attention placed on the modeling of the floor.

One further point to be noted is that, because of the unusual distribution of sound-absorbing material in the test cabin, empirical rather than analytical means had to be used to describe the absorption in the cabin. Consequently, it was not possible to make a complete evaluation of the analytical model for the sidewall treatment.

Strictly speaking, the validation of the analytical model has been performed for only one fuselage structure and one excitation. Thus, confidence in the analytical model when applied to other structures and excitation is dependent to some extent on a qualitative judgment of the accuracy of the extrapolation of the model to other conditions. The role played by the floor in a conventional fuselage configuration is of particular interest since it was the modeling of the test floor that posed a major problem in the present study. In spite of these difficulties it seems justifiable to apply the analytical model to airplane configurations such as those discussed in Reference 6 in order to obtain alternative estimates of the treatment weights required to achieve the cabin noise goal. In this manner it should be possible to obtain an indication of the confidence limits for the predictions by the use of different analytical approaches.

REFERENCES

1. Pope, L.D., Wilby, E.G., and Wilby, J.F., "Propeller Aircraft Interior Noise Model", NASA CR-3813, (1984).

2. Pope, L.D., and Wilby, E.G., "Analytical Prediction of the Interior Noise for Cylindrical Models of Aircraft Fuselages for Prescribed Exterior Noise Fields, Phase II: Models for Sidewall Trim, Stiffened Structures, and Cabin Acoustics with Floor Partition", NASA CR-165869, (1982).

3. Pope, L.D., Wilby, E.G., Willis, C.M. and Mayes, W.H., "Aircraft Interior Noise Models: Sidewall Trim, Stiffened Structures, and Cabin Acoustics with Floor Partition," J. Sound and Vib., 89, 3, 371-417 (1983).

4. Pope, L.D., Rennison, D.C., Willis, C.M. and Mayes, W.H., "Development and Validation of Preliminary Analytical Models for Aircraft Interior Noise Prediction," J.Sound and Vib., 82, 4, 541-575 (1982).

5. Prydz, R.A., Revell, J.D., Hayward, J.L. and Balena, F.J., "Evaluation of Advanced Fuselage Design Concepts for Interior Noise Control on High-Speed Propeller-Driven Aircraft," NASA CR 165960, (1982).

6. Rennison, D.C., Wilby, J.F., Marsh, A.H., and Wilby, E.G., "Interior Noise Control Prediction Study for High-Speed Propeller-Driven Aircraft," NASA CR 159200 (1979).

7. Pope, L.D. and Wilby, J.F., "Band-Limited Power Flow into Enclosures," J. Acoust.Soc. Am., 62, 4, 906-911 (1977).

8. Pope, L.D., and Wilby, J.F., "Band-Limited Power Flow into Enclosures, II," J.Acoust.Soc. Am., 67, 3, 823-826 (1980).

9. Beranek, Leo L., Noise and Vibration Control," McGraw-Hill
   Book Company, New York, 1971.

10. White, R.W., "Predicted Vibration Response of Apollo Structure
    and Effects of Pressure Correlation Lengths on Response," Wyle
    Laboratories Report WR67-4, 1967 (Revised March 1968).

11. Abramowitz, M. and Stegun, I.A., Hdbk. of Math. Functions,
    U.S. Dept. of Commerce, Nat'l Bureau of Standards, Amer.Math.
    Series 55. Washington: Govt. Printing Office, 1964.

12. Cockburn, J.A., and Jolly, A.C., "Structural-Acoustic
    Response, Noise Transmission Losses and Interior Noise Levels
    of an Aircraft Fuselage Excited by Random Pressure Fields,"
    AFFDL-TR-68-2, 1968.

13. Mobley, T., Hayden, R., and Wilby, J., "External Tank Aft
    Cargo Carrier Acoustical Protection System," AIAA Paper
    84-0502 (January 1984).

14. Wilby, J.F., "The Response of Simple Panels to Turbulent
    Boundary Layer Excitation," AFFDL-TR-67-70, 1967.

15. Magliozzi, B., "Acoustic Pressures on a Prop-Fan Aircraft
    Fuselage Surface," J.Aircraft, 19, 2, 104-111, (1980).

16. Prydz, R.A., Revell, J.D., Balena, F.J., and Hayward, J.L.,
    "Evaluation of Interior Noise Control Treatments for High-
    Speed Propfan-Powered Aircraft," AIAA Paper 83-0693, (April
    1983).

17. Piersol, A.G., Wilby, E.G., and Wilby, J.F., "Evaluation of
    Aero Commander Propeller Acoustic Data: Taxi Operations,"
    NASA CR-159124 (1979).

APPENDIX A

List of Symbols

This appendix contains the list of symbols used in the equations in Reference [1]. The equations in this report rely heavily on [1] for their development, and the symbols have not been re-defined in the text since the reference will receive wide distribution. The reader should refer to Reference [1] for a detailed presentation of the development of the basic analytical model.

LIST OF SYMBOLS

A   Cylinder surface area

or

A   Interior (cylinder & floor) surface area, used in conjunction with structural/acoustic coupling function f'(n,r)

A'   Transmitting area of cylinder without trim

$\bar{A}$ Exterior cylinder surface area

A_t Transmitting area of cylinder with trim

(A +A')   Total transmitting area of cylinder, floor to floor

A_H^m Amplitude of Fourier component of blocked propeller pressure signature at propeller harmonic H and grid location m ≡ (k,ℓ), see Eq.(43) of [1]

$\bar{A}_H^m$ Amplitude of Fourier component of free field propeller pressure at harmonic H and grid location m≡(k,ℓ)

a   Radius of cylinder

a_H^m Fourier series coeffficient of propeller pressure, for harmonic H at location m; see Eqs.(27),(29)[1]

$a_O^m/2$ Mean propeller pressure amplitude at location m (defined in Eq.(28) of [1])

$\left.\begin{array}{l} \text{arctan}_n \\ \text{arctan}_r \end{array}\right\}$ Functions defined in Section 2.3, Eq.(10), et seq

B   Number of propeller blades

BPF   Propeller blade passage frequency (Hz); BPF = $\frac{NB}{60}$

b_n, b_r Functions defined in Section 2.3, Eq.(10) et seq

b_H^m Fourier series coefficient of propeller pressure for harmonic H at location m; see Eqs.(27),(29)[1]

$C(j)$ Function defined in Eq.(76)[1]

$Cin(z)$ Cosine integral; $Cin(z) = \int_0^z (1-\cos t)dt/t$

$C_{Mn}^{pr} C_{Mn}^{sr}$ Floor and shell generalized coordinates for structural mode $r \equiv (M,N)$; see Eqs.(46)-(49)[1]

$C_{pbl}(\bar{x}|\bar{x}';\omega)$ Cospectral density function of the blocked exterior pressure field

$C_p(\bar{x}|\bar{x}';\omega)$ Cospectral density function of the exterior pressure field

C_W, C_W^R, C_W^I Trim parameter, derived from the trim transfer matrix, Eq.(A.8); $C_W = C_W^R + iC_W^I$

$C_x(\xi,\omega) C_y(\zeta,\omega)$ Cospectral density functions of the exterior pressure field in the axial and transverse directions respectively; see Eq.(60) of [1]

c_0 Speed of sound in air

c_n, c_r Functions defined in Section 2.3, Eq.(10) et seq

c_ω Constant percentage bandwidth parameter, where $\Delta\omega = c_\omega\omega$ [$c_\omega = 0.232$ for one-third octave bands]

LIST OF SYMBOLS
(Continued)

D_{nr} — Function defined in Section 2.3, Eq.(10) et seq

$E[\quad]$ — Expected value of a function

$f'(n,r)$ — Interior structural/acoustic coupling factor; see Eq.(45)

$\bar{f}'(n,r)=\bar{f}'(qi,r)$ Interior structural/acoustic coupling factor including effect of trim factor τ_t and floor treatment factor τ_F, see Eq.(3)

f_1 — Frequency of propeller 1st harmonic; $f_1 = 1/T_o =$ BPF

f_H — Frequency of propeller harmonic H; $f_H = Hf_1$

f_{qm} — Acoustic/structural coupling factor in axial direction; see Eq.(57) of [1]

g_n, g_r — Functions defined in Section 3.2, page 3-11 [1]

H — Propeller harmonic order, used as superscript to denote functions evaluated at frequency ω_H

i — Acoustic mode number counter for fuselage cross-section modes, associated with mode $n \equiv (q,i)$

$I_1 I_2 I_3$ — Integrals defined in Equations (63) and (70)-(73)[1]

j — Circumferential location on fuselage wall, θ_j, a boundary point at which the acoustic eigenvector is evaluated (see Fig.C-2 [1])

$j_M^2(\omega)$ Structural joint acceptance function in axial direction

$j_N^2(\omega)$ Structural joint acceptance function in circumferential direction

$j_r^2(\omega)$ Structural joint acceptance in axial and circumferential directions; $j_r^2(\omega) \equiv j_{MN}^2(\omega)$ $= j_M^2(\omega) \, j_N^2(\omega)$; see Eq.(21)

$j_r^{2\,rev}(\omega)$ Joint acceptance for reverberant/diffuse excitation

$\langle j^2(\omega)\rangle_r^{rev}$ Joint acceptance for reverberant excitation averaged over structural modes resonant in band $\Delta\omega$

k Acoustic wave number, $k = 2\pi/\lambda$

    or

k Axial non-dimensional coordinate for grid point; see Figure 16

L Fuselage structure length

L_p Floor width (wall to wall)

ℓ Circumferential non-dimensional coordinate for grid point; see Figure 16

$\ln_n, \ln_r$ Functions defined in Section 2.3, Eq.(10) et seq

M Number of axial half-wavelengths for structural mode $r \equiv (M,N)$

M_r Generalized modal mass, for structure mode r

$m \equiv (k,\ell)$ Grid point on surface of cylinder used for propeller noise predictions; see Figure 16

     or

m Average surface mass/unit area of cylinder

N Structural mode counter, associated with mode $r \equiv (M,N)$

     or

N Propeller rpm

N_n, N_r Number of acoustic modes or structural modes in frequency band $\Delta\omega$

n Symbolizes acoustic mode $n \equiv (q,i)$

     or

n Number of circumferential wavelengths (or transverse half-wavelengths) in fuselage shell (or floor); see Eqs.(35-36)

n^* Number of terms in displacement series for fuselage shell (or floor)

n_b, n_b' Number of boundary points on the fuselage shell (or floor) at which the acoustic eigenvectors are defined

n_n Modal density of acoustic modes

n_r Modal density of structural modes

LIST OF SYMBOLS
(Continued)

$P(\omega_n)$ Probability distribution function for ω_n in $\Delta\omega$

$p(\omega_n)$ Probability density function for ω_n in $\Delta\omega$

$p_{bl}(\bar{x},t)$ Exterior pressure over the blocked (immobile) fuselage

$\langle p_{bl}^2 \rangle$ Band-limited mean square blocked pressure

$\langle p_i^2(\bar{\xi},\omega) \rangle_t$ Interior mean square pressure at location $\bar{\xi}$

$\langle p_i^2 \rangle_{s,t}$ Space-averaged band-limited mean square interior pressure

$\langle p_e^2 \rangle_{s,t}$ Space-averaged band-limited mean square exterior pressure for a reverberant field

$\langle p_n^2 \rangle_{s,t}$ Space-averaged band-limited mean square modal pressure, for nth mode in interior volume V

Q_H Function defined in Section 3,2, Eq.(12) [1]

q Number of axial half-wavelengths for acoustic mode $n \equiv (q,i)$

r Symbolizes structural mode $r \equiv (M.N)$

r_p Radial distance from center of fuselage cylinder to the axis of rotation of the propeller.

$R_{p_{bl}}(x|x';\omega)$ Average cross correlation of the exterior blocked pressure over the fuselage

S Absorbing surface area of fuselage sidewall

S_e Absorbing surface area on each end surface (bulkhead)

$S_p(\omega)$ Power spectral density of exterior pressure

$S_{p_{bl}}(\omega)$ Power spectral density of exterior blocked pressure

$S_{p_{bl}}(\bar{x}|\bar{x}';\omega)$ Cross spectral density of exterior blocked pressure

$Si(z)$ Sine integral; $Si(z) = \int_o^z \sin t . dt/t$

t time

T Period of rotation of propeller; $T = 60/N$

T_o, T_1 Period of propeller noise signature; $T_o = T_1 = (BPF)^{-1} = T/B$

u In-plane axial displacement of cylinder wall (or floor)

V Volume of cavity

v Circumferential (or transverse) displacement of cylinder wall (or floor)

W_{diss} Power dissipated on the cabin walls

W_{in} — Net power inflow

$W_{rad}^{int}(\omega)$ — Spectral density of power radiated by structure into interior acoustic space

$W_{abs}^{int}(\omega)$ — Spectral density of power absorbed on inner wall of the space from interior acoustic field

w — Cylinder wall (or floor) normal displacement

x — Transverse coordinate; see Figure 19

$\bar{x}$ — Location on exterior surface of fuselage

$\bar{x}_m$ — Location of grid point on exterior surface of fuselage

$x_1 x_2 x_3$ — Local coordinate systems used for PROPFAN propeller noise prediction; see Figure E-6

y — Vertical coordinate, relative to fuselage centerline; see Figure 17

z — Axial coordinate, relative to forward end of the fuselage structure (of length L); see Figure 16

z_k — Axial coordinate for grid point k, see Figure 16

z_p — Location of propeller relative to the forward end of the fuselage structure (of length L); see Figure 17

$\bar{\alpha}$ Band average absorption coefficient

γ Incidence angle between propeller and location $\bar{x}_m$; see Figure 17

$\Delta = \frac{\pi a}{18}$ Grid spacing for propeller noise predictions

$\Delta A = \Delta^2$ Area associated with each grid point; see Figure 16

$\Delta\omega$(radians/sec)   Frequency band of width $\Delta\omega = c_\omega \omega$
         $n{<}\Delta\omega$ symbolizes modes resonant below band
         $n\epsilon\Delta\omega$ symbolizes modes resonant inside band
         $n{>}\Delta\omega$ symbolizes modes resonant above band

$\delta(\ )$ Delta function

$\epsilon_n = V / \int_V \phi_n^2 d\bar{v}$ Acoustic mode normalization factor

ϵ_q Acoustic mode normalizing factor in axial direction (see Eq.C.11 [1])

ζ Transverse coordinate; see Section 3.6 [1]

η_n Acoustic mode loss factor

η_r Structural mode loss factor

η_r' Structural loss factor, including damping due to trim; Eq.(17)

η_r'' Internal radiation loss factor, due to closely coupled structural and acoustic modes; Eq.(83) [1]

$\bar{n}_n$ — Average one-third octave band acoustic mode loss factor

$\bar{n}_r = n_r' + n_r'' + n_{rad}^{ext}$ — Average one-third octave band structural mode loss factor

n_r^{struc} — Average one-third octave band structural loss factor

n_r^{rad} — Average one-third octave band radiation loss factor

$n_{rad}^{int}, n_{rad}^{ext}$ — Average one-third octave band internal and external radiation loss factors defined after Eq.(19) [1]

θ — Angular coordinate, relative to fuselage bottom centerline; see Figure 17

θ_ℓ — Angular coordinate for grid location (k,ℓ)

θ_o — Angle at which fuselage shell/floor joint is located

θ_j — Angle θ for point j on fuselage wall, a boundary point for the acoustic eigenvectors

$\theta_{1j}\theta_{2j}$ — Angles defining mid-points between boundary point j and adjacent boundary points

ξ — Axial coordinate; see Section 3.6 [1]

or

ξ — Conductance for trim on end surface of cylinder interior

$\bar{\xi}$ Interior cavity location

ξ_e Conductance for trim on cylinder (fuselage) sidewall

ρ Density of air inside the cylinder

ρ_o Density of air outside the cylinder

τ Time delay for cross-correlation

     or

τ Acoustic transmission coefficient for diffuse field excitation; $\tau = \tau_f + \tau_R$

τ_f Field incidence transmission coefficient for mass controlled panels; defined in Eq.(20) [1]

$\tau_{mL} = \left(\dfrac{2\rho c_o}{m\omega}\right)^2$ Mass law sound transmission coefficient

τ_t Trim transmission coefficient, defined in Eq.(A.22)[1]

τ_R Resonance transmission coefficient for diffuse field, defined in Eq.(19) [1]

$\psi_G(i)$ Generalized mass for two-dimensional acoustic mode i, defined in Appendix C [1]

ϕ Angular position of propeller hub relative to fuselage bottom centerline; see Figure 17

ϕ_H^m Phase of Fourier component of propeller pressure signature at propeller harmonic H and grid location $m \equiv (k,\ell)$

LIST OF SYMBOLS
(Continued)

$\phi_n(\bar{\xi}) \equiv \phi_{qi}(\bar{\xi})$ Mode shape, or eigenfunction, of the nth mode of the cavity at location $\bar{\xi}$

$\phi_i(\theta_j)$ Mode shape of ith acoustic mode of the fuselage cross-section evaluated on the fuselage wall at location j, angle θ_j

$\Psi_G(r,H)$ Generalized modal forcing function due to propeller noise, mode r at propeller harmonic H; see Section 3.4 [1]

$\psi^r(\bar{x})$ Mode shape, or eigenfunction, of the rth mode of the structure, at location $\bar{x}$

$\psi_p^r(z,x)$ Floor displacement in structure mode r

$\psi_s^r(z,\theta)$ Fuselage shell displacement in structure mode r

ω Angular frequency (rads/sec)

ω_H Angular frequency of propeller harmonic H

ω_n Acoustic mode resonance angular frequency

ω_r Structure mode resonance angular frequency

$< \quad >_{s,t}$ Band-limited, space-averaged and time-averaged value

1. Report No. NASA CR-172384	2. Government Accession No.	3. Recipient's Catalog No.
4. Title and Subtitle Application of Stiffened Cylinder Analysis to ATP Interior Noise Studies		5. Report Date AUGUST 1984
		6. Performing Organization Code
7. Author(s) E.G.Wilby, J.F. Wilby		8. Performing Organization Report No. 5552
9. Performing Organization Name and Address BOLT BERANEK AND NEWMAN INC. 21120 Vanowen Street Canoga Park, CA 91303		10. Work Unit No.
		11. Contract or Grant No. NAS1-16521
		13. Type of Report and Period Covered Contractor Final Report
12. Sponsoring Agency Name and Address National Aeronautics & Space Administration Washington, DC 20546		
		14. Sponsoring Agency Code 535-03-12-01

15. Supplementary Notes

Task 11, Contract NAS1-16521
Langley Technical Monitor: Dr. John S. Mixson

16. Abstract

An analytical model developed to predict the interior noise of propeller-driven aircraft has been applied to experimental configurations for a Fairchild Swearingen Metro II fuselage exposed to simulated propeller excitation. The floor structure of the test fuselage was of unusual construction in that it was mounted on air springs. As a consequence, the analytical model was extended to include a floor treatment transmission coefficient which could be used to describe vibration attenuation through the mounts. Good agreement was obtained between measured and predicted noise reductions when the floor treatment transmission loss was about 20 dB -- a value which is consistent with the vibration attenuation provided by the mounts. The analytical model was also adapted to allow the prediction of noise reductions associated with boundary layer excitation as well as propeller and reverberant noise.

17. Key Words (Selected by Author(s)) Aircraft Interior Noise Noise Reduction Propeller Noise Comparison with Test Data Boundary Layer Excitation	18. Distribution Statement Unclassified - Unlimited Subject Category 71		
19. Security Classif. (of this report) Unclassified	20. Security Classif. (of this page) Unclassified	21. No. of Pages 130	22. Price*